OptoCoil

Design and characterization of a wireless power transfer system for optogenetic ambulatory defibrillation

B.L. den Ouden

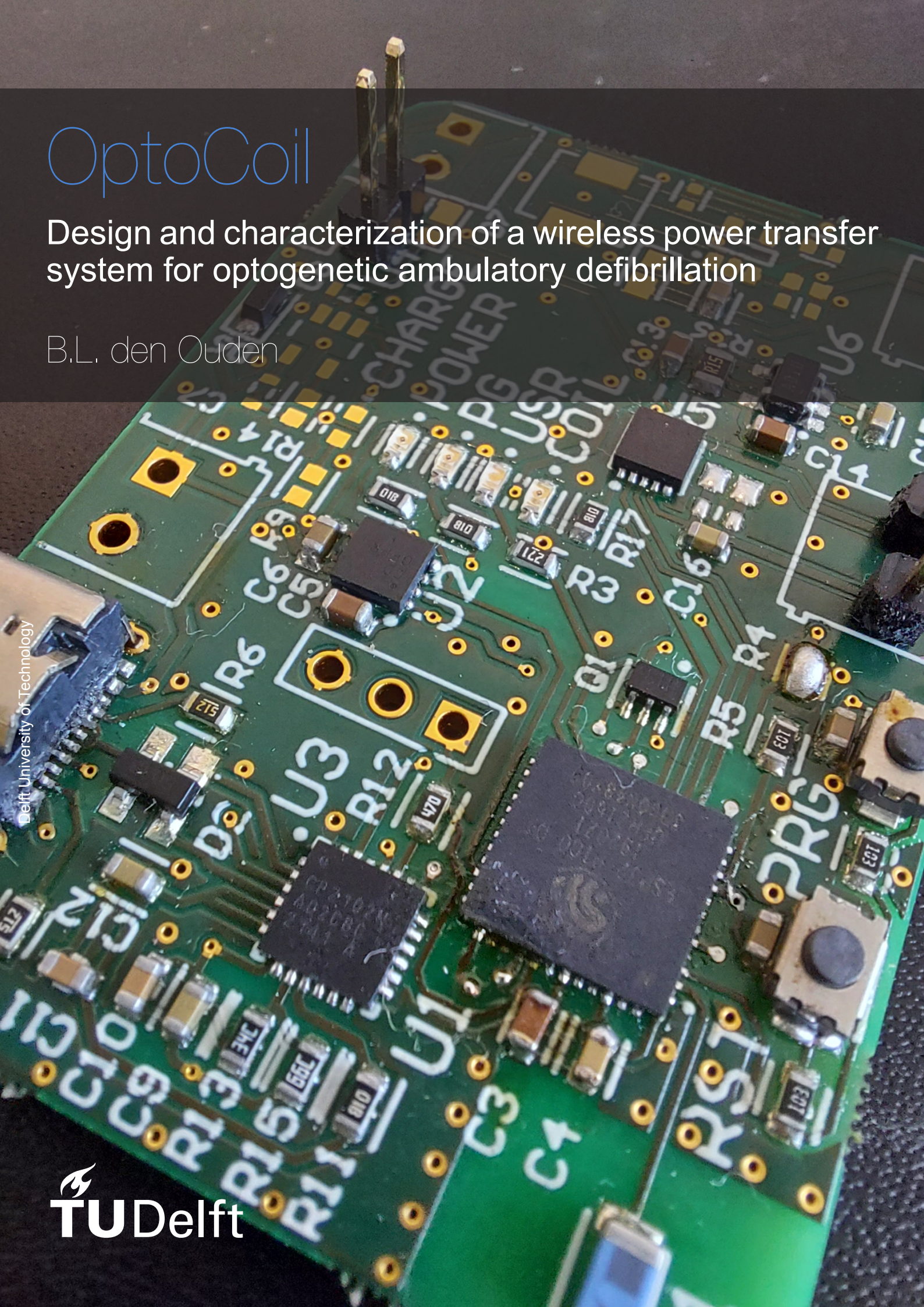

Delft University of Technology

TU Delft

OptoCoil

Design and characterization of a wireless power transfer system for optogenetic ambulatory defibrillation

by

B.L. den Ouden

This thesis is submitted to the Delft University of Technology in partial fulfillment of the requirements for the degree of master of science.
To be publicly defended on the 9th of September 2022

Student number:	4472993
Institution:	Delft University of Technology
Department:	Microelectronics
Group:	Electronic Components, Technology and Materials
Supervisor:	GuoQi Zhang
Daily supervisor:	Shanliang Deng
Thesis committee:	GuoQi Zhang, Willem van Driel, Daniël Pijnappels, Shanliang Deng

Cover Image: OptoCoil Transmitter V2

TU Delft

Acknowledgement

During this project I was introduced into the world of biomedical design and got to work together with experts from Leiden University Medical Center (LUMC) as well as experienced electrical engineers from the Electronic Components, Technology and Materials (ECTM) group from Delft University of Technology.
I'd like to extend my gratitude to all my colleagues, both in LUMC and ECTM, you've all contributed to an extremely welcoming and knowledgeable environment. There are some people I'd like to specifically thank. First and foremost: my daily supervisor Shanliang Deng. Your attitude of being to the point but very creative and open to ideas has been amazing. Any ideas that were suggested during this project have been considered. Even if we expected a different outcome you would be open to trying a newly suggested approach. Your way of supervising me has been a great example I hope to follow if I get in a supervising position one day. It's been an honor and a pleasure being your student.
One of the experts without whom this project would not have been as fun as it was is Lord Vincent Portero. Your positive, fun and at the same time professional attitude is another great example to follow. Long days of experiments with you and Shanliang only left me more motivated to work on this project, both of you have taught me many things about how I should conduct science and at the same time have fun.
When talking about long experiments I would also like to thank Cindy Bart whose expertise helped us get the most out of the in vivo experiments.
Furthermore I would like to express my gratitude to Lord Balazs Ördög and Tim de Coster for the many fruitful discussion, advice and feedback to better understand the genetic side of this research.
Most of the above mentioned people were from the Laboratory of Experimental Cardiology of which Daniël Pijnappels is the head whom I would like to thank for welcoming me into his group.
The final person I would like to thank is my supervisor, GuoQi Zhang, as I would never have been involved in this project without his engaging lecture during the packaging course.
Thank you all for accepting me into your groups and allowing me to enjoy this project as much as I have.

Bram den Ouden
Delft, August 2022

Abstract

Atrial fibrillation is the predominant cardiac arrhythmia with a lifetime risk of 25% Its symptoms range from feeling unwell to clot forming and death by stroke or infarcts. Limited treatment options are available ranging from permanent medication to hospitalized intervention. A surgical solution is the implantable cardioverter-defibrillator, a device which can restore the heart to a normal sinus rhythm by using painful electrical shocks.
Optogenetics is an experimental method where light sensitive channels called optotools are added to the cell membranes. Exposing these optotools using a specific wavelength of light will stimulate or inhibit these cells, allowing control their electrical activity. Optogenetics have been used in cardiac research for over a decade with many different custom designed light sources. Few of these devices were able of terminating atrial fibrillation, none of those were suitable for ambulatory experiments.
This report focuses on the design and characterisation of a wirelessly powered cardiac implantable cardioverter-defibrillator for pain free termination of atrial fibrillation using optogenetics, a system named OptoCoil.
The Optocoil system consists of an implantable passive receiver capable of obtaining a light intensity of 300mW/cm^2 when wirelessly powered. A maximum local temperature increase of 1.6°C was observed with cumulative equivalent minutes at 43°C of 0.0011. 90% of the maximum light intensity is reached within 300μs, making this system capable of fast stimulation protocols.
The OptoCoil has proven capable of 100% ex vivo optical termination of atrial fibrillation upon sufficient expression of the optotool and demonstrated electrical response as a result of optical stimulation during in vivo experiments.

Contents

Nomenclature

Abbreviations

Abbreviation	Definition
3D	three-dimensional
AC	Alternating Current
ADC	Analog to Digital Converter
AF	Atrial Fibrillation
AP	Access point
AV	Atrioventricular
AV-junction	Atrioventricular junction
AV-node	Atrioventricular Node
AVRT	Atria-Ventricular Re-entry Tachycardia
BLE	Bluetooth Low Energy
BMS	Battery Management System
BPM	Beats per minute
BT	Bluetooth
CEM43°C	Cumulative Equivalent Einutes at 43°C
CAD	Computer-aided design
CI	Confidence interval
CVD	Chemical Vapor Deposition
DAC	Digital to Analog Converter
DC	Direct Current
ECG	Electrocardiogram
EMF	Electromotive force
FAT	Focal atrial tachycardia
F-wave	Fibrillatory wave
GPIO	General Purpose Input Output pin
GUI	Graphical User Interface
IC	Integrated Circuit
ICD	Implantable Cardioverter-Defibrillator
IO	Input Output
IPA	isopropylalcohol
LDO	Low Drop Out regulator
LED	Light Emitting Diode
MAT	Multi-focal Atrial tachycardia
MOSFET	metal–oxide–semiconductor field-effect transistor
NIR	Near Infrared
OTA	Over The Air
PCB	Printed Circuit Board
PDMS	Polydimethylsiloxane
PET	polyethylene terephthalate
PG	Power Good
PIB	Polyisobutylene
PLA	Polylactic acid
PWM	Pulse Width Modulation
RPM	Revolutions Per Minute
RX	Receiver
SVT	Supraventriclar tachycardia

Abbreviation	Definition
TdP	torsades de pointes
TX	Transmitter
UART	universal asynchronous receiver-transmitter
UI	User Interface
USB	Universal Serial Bus
VF	Ventricular fibrillation
VT	Ventricle tachycardia
WPC	Wireless Power Consortium
WPT	Wireless power transfer

Tools

Tool	Definition
Altium	Software for designing PCBs
Coil64/Coil32	Software used to calculate inductance of RF coils [1]
LabChart 8	Biomedical data acquisition software
LTSpice	SPICE simulator
MC Stimulus II	Software to control the STG series stimulus generators
PlanarTx	Script for Altium used to generate spiral inductors
Solidworks	Software for CAD modelling
Agilent 4294A	Imedance meter
Fluke 117	Handheld digital multimeter
Keithley 2450	Sourcemeter with labview interface
MultiChannel STG4002	2-channel general-purpose stimulus generator
Powerlab 15T	2-channel data acquisition system
RSDS1000CML+	Benchtop oscilloscope
RSDM3055	5.5 digit benchtop multimeter
RS Pro RPE	4 channel digital benchtop power supply
RS Pro AFG-21000	Benchtop funtion generator
Thorlabs LEDD18	Current mode driver for LEDs
Thorlabs M470L3-C4	470nm wavelength blue light source
Thorlabs PM100D	Light intensity measurement device
Thorlabs S130C	Light intensity sensor
TPS TUJR-CE	Compact temperature test chambers

List of Figures

List of Tables

1

Introduction

The human heart consists of four large chambers which collect and pump the blood throughout the body shown in figure 1.1. The upper two chambers are the right and left atria. The right atrium receives the low-oxygen blood, indicated in blue, which has returned from its trip throughout the body. The left atrium receives the oxygen-rich blood, indicated in red, from the lungs.
The atria are connected via valves to two larger chambers below them: the ventricles. Blood is pumped from the atria into the ventricles. The right ventricle then pumps the low-oxygen blood received from the right atrium through the lungs to re-oxygenate it. This oxygen-rich blood arrives in the left atrium and is pumped into the left ventricle. The left ventricle pumps the blood through the aorta into the rest of the body.

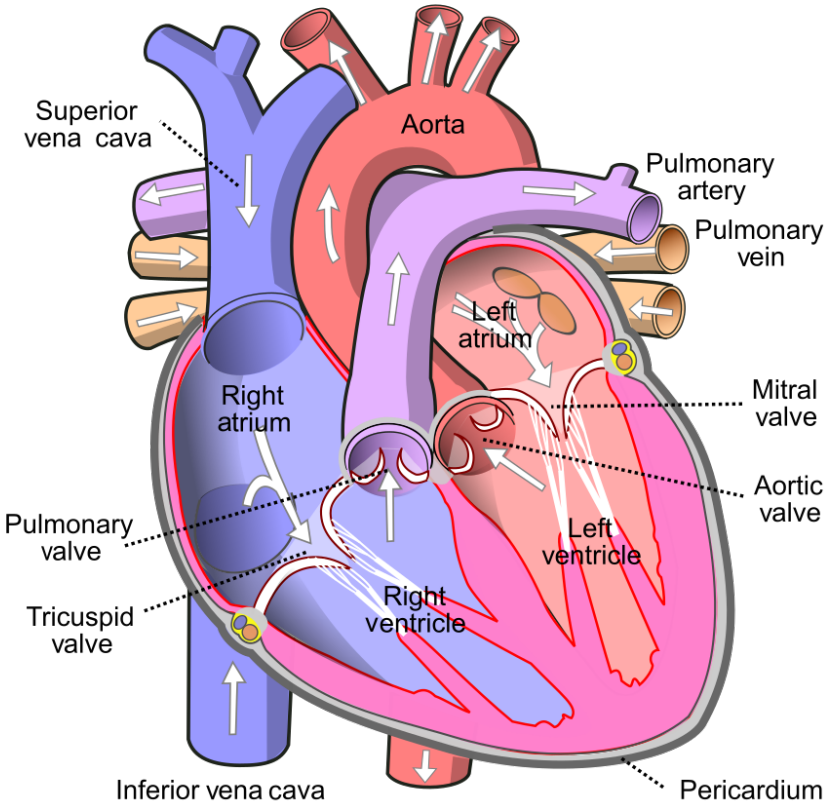

Figure 1.1: A diagram of the human heart, as seen by a coronal section [2].

1.1. Arrhythmias

A cardiac arrhythmia is an irregularity in the electrical signals of the heart affecting the speed of contractions and the efficiency at which blood is pumped through the body. Although some arrhythmias barely have any symptoms, others can be deadly: 10-15% of all deaths are caused by cardiac arrhythmias [3]. Cardiac arrhythmias can be divided in two categories based on the speed of the heart rate while resting:

- Bradycardia means the heart rate is below 60 beats per minute (BPM).
- Tachycardia are arrhythmias where the heart rate is greater than 100 BPM.

1.1.1. Sinus rhythm

The top line in figure 1.2 shows the electrocardiogram (ECG) of a regular sinus rhythm where the most distinguishable waves are highlighted using letters. In chronological order, the first wave of a heartbeat is the P wave. This P wave represents the depolarization and contraction of the atria and is followed by the PR interval which allows the blood from the atria to flow into the ventricles. The PR interval normally takes between 120 and 200ms. The Q, R and S wave follow each other in rapid succession and represent the depolarization and contraction of the ventricles. This is called the QRS complex and represents the blood being pumped from the right ventricles to the lungs and the left ventricle throughout the body. Immediately after the QRS complex, the ST interval starts which represents the beginning of repolarization of the ventricles. The T wave represents the end of the ventricular repolarization. The interval between each R peak, the RR interval, is regular and the line is flat. A regular heartbeat in rest should be between 60 and 100 BPM.

1.1.2. Bradycardia

During episodes of bradycardia the heartbeat falls below 60 BPM. The danger of a low heart beat is that the organs don't get enough oxygen which could damage them. Bradycardia is not always a problem, young or well trained people can have a low heart rate without any negative effects.
The two version of bradycardia are sinus bradycardia and atrioventricular (AV) block. Sinus bradycardia doesn't alter the shape of the heartbeat but can cause an irregular but increased interval between heartbeats. During an AV-block the electrical signals traveling from the sinus node via the AV node to the ventricles are blocked by the AV node. This causes an increase in the interval between contractions of the ventricles. AV-block exists in 3 different degrees with increasing severity: First degree AV-block will pass the electrical signal though the AV node at a low speed. It is mostly innocent and can occur in well trained or young people. Second degree AV-block will allow some but not all electrical signals to pass or takes a long time to pass them. This can be a more serious arrhythmia since the cardiac output is irregular. The most serious third degree AV-block completely blocks communication between the atria and the ventricles. The relation between P waves and a QRS complex is broken while the RR interval is increased. A replacement rhythm may occur which is slower than a normal rhythm, causing dizziness and fainting [4].
Causes of bradycardia can be age-related due to normal wear and tear of heart tissue. Underlying heart diseases, damage from previous surgeries or medication to counter tachycardias can also increase the risk of bradycardia.

1.1.3. Ventricular tachycardia

Ventricular arrhythmias originate, as the name suggest, from the lower two chambers of the heart. These chambers are responsible for pumping the blood throughout the body and irregularities here can have life-threatening effects.
Ventricular tachycardias come in 4 types[5]:

- Supraventricular tachycardia (SVT) describes arrhythmias which start above the ventricles. Symptoms include a very fast heartbeat, pounding in the chest (palpitations), chest pain, shortness of breath, fainting and feeling weak or tired. SVT appears in episodes where the heart rate is between 150 and 220 BPM.
- Ventricular tachycardia (VT) is an arrhythmia where the heart rate is very fast but regular. The rapid contraction of the ventricles prevents them from completely filling which can be dangerous if it becomes sustained (>30 s). Symptoms might not be noticeable if the VT remains for short

periods of times or could be comparable with those of SVT. A dangerous side effect of VT is that it may degenerate into ventricular fibrillation (VF) or cardiac arrest.

- Ventricular fibrillation (VF) occurs when the ventricles are quivering instead of contracting due to chaotic electrical signals. Blood can no longer be pumped through the body causing loss of consciousness and, without immediate intervention, cardiac arrest and death [6].
- Torsades de pointes (TdP) is an arrhythmia which can lead to sudden death. During short episodes palpitations, dizziness and lightheadedness can be experienced. Although TdP may suddenly revert to a normal sinus rhythm, sustained episodes include fainting and can lead to sudden cardiac death without intervention.

SVT can sometimes be resolved with medication, lifestyle changes or cardiac catheterization with ablation.

1.1.4. Atrial tachycardia

Atrial tachycardia (AT) is a type of SVT that does not require ventricular tissue or the AV junction to initiate or maintain the arrhythmia. There are three types of atrial tachycardia: focal, multifocal and re-entrant atrial tachycardia.
Focal and multifocal atrial tachycardia are tachycardia where electrical activity besides those from the sinus node originate from and are contained within the atria [7]. In case of focal atrial tachycardia (FAT) the electrical impulses originate from a single ectopic focus whereas multifocal atrial tachycardia (MAT) has multiple of these foci. The underlying mechanism of FAT can be micro-reentrant circuits or increased automaticity. MAT is also called chaotic atrial tachycardia and can be caused by increased spontaneous activity or an enlarged right atrium.
Re-entrant tachycardia refer to tachycardia caused by the presence of a re-entrant circuit, an electrical pathway through which repeated excitation can occur [8]. Regions where this can occur are called rotors and they result in an increased electrical activity in the atria, causing atrial fibrillation (AF) and flutter, or around the AV-node in which case they're called atrioventricular re-entry tachycardia (AVRT).

Atrial flutter & atrial fibrillation

Atrial flutter is an arrhythmia where irregular electrical activity in the atria causes the heart to beat much faster. Atrial fibrillation has the same increased heart rate as atrial flutter but adds an irregular interval between heartbeats. These rapid contractions of the atria make each contraction an inefficient one: the atrium doesn't fully contract which limits the blood flow into the ventricles and causes blood stasis. Blood stasis means that the blood is not in movement or circulating as well as it could to some or all parts of the body, this causes clots to form. If these clots break loose they can be transported through other parts of the body where they can become stuck and cause strokes, cardiac infarcts or even death [9]. Besides these possible life threatening outcomes, AF or flutter can cause an anxious or uneasy feeling combined with dizziness and shortness of breath. AF and flutter are the most common sustained cardiac arrhythmia with a lifetime risk of 25% [10].
AF or flutter are age related arrhythmias which rarely occur below the age of 50 although prior cardiac surgery can be a risk factor. If AF or flutter occur in younger people it's usually a persistent condition for which treatment is required.

Diagnosis and Treatment

AF is diagnosed based on a distinct ECG pattern as seen in the bottom line of figure 1.2. The QRS complex is unchanged but the interval between them is irregular and on average shorter. The P and T waves are not clearly distinguishable and are replaced by an F-wave (fibrillatory wave) which are caused by the additional electrical activity from the rotors. Since AF can spontaneously occur and revert back to a normal sinus rhythm, a portable ECG recorder called a Holter monitor can be used to record the ECG over longer periods of time.
Recurring atrial fibrillation has to be treated using medicine which slows the heartbeat and reduces the clotting of the blood. This medication has to be re-evaluated on a yearly basis [12] and most patients have to take this medication for the rest of their lives.

A different treatment consists of giving the patient an electrical impulse called a cardioversion. During this cardioversion the sedated patient receives a shock of 50-200 joules which is synchronized with the

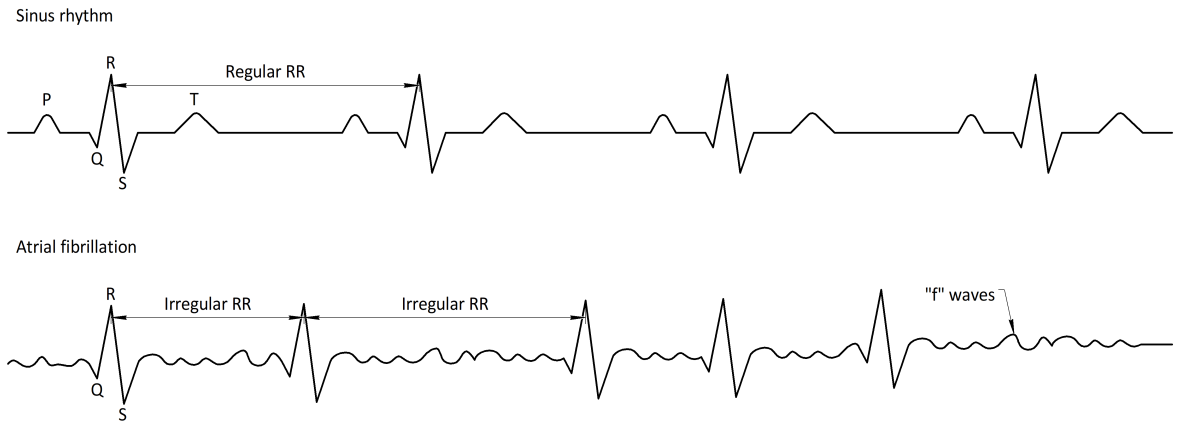

Figure 1.2: Regular heart rhythm (top) and Atrial fibrillation (bottom). X axis is time, Y axis represents voltage [11].

QRS rhythm. This shock overpowers the existing electrical signals in the heart 'resetting' it to a sinus rhythm. Although this procedure uses the same equipment as defibrillation of VF, a cardioversion uses significantly less energy (50-200J vs 200-360J). In both cases the patient unconscious, the difference is that a cardioversion is a scheduled procedure and the administered sedatives help you sleep against the pain whereas defibrillation of VF requires immediate action to avoid cardiac death, the patient is unconscious due to lack of circulation. The electrical pulse used during a cardioversion is synchronised to the QRS complex whereas this is not possible with VF because there is not QRS complex present. Before a cardioversion is performed measures will be taken to prevent blood clots to break loose and possibly cause life-threatening issues. Some patients receive an implantable cardioverter-defibrillator (ICD) which performs the same function as a cardioversion but is surgically implanted in the chest.
A final drastic treatment of persistent AF can be ablation of the atrioventricular node (AV-node) or atrial tissue. Ablation is the process of destroying tissue using very high or very low temperatures. If the AV-node is ablated it permanently stops conduction from the atria to the ventricles. After such a treatment a pacemaker is permanently required to activate the ventricles. Ablation of atrial tissue can interrupt fluttering by preventing continuous electrical re-excitation of the same area, an effect called rotors[8], [13].

1.2. Goal

The goal of this project is to create a battery-free defibrillator which depends on optogenetics to terminate fibrillation of the right atrium. The current solution to AF is, as discussed earlier, either going to the hospital for a cardioversion or having an ICD surgically implanted. Shocks from a cardioversion are scheduled and performed while sedated, shocks from an ICD are often unexpected and feel like a hard punch on the chest or shoulders [14]. An optogenetic defibrillator would eventually replace the existing ICDs and allow people to quickly and painlessly resolve any discomfort caused by the AF themselves without the need to undergo a painful cardioversion.
This optogenetic defibrillation system is named OptoCoil and consist of two parts:

- An implantable device capable of sufficient illumination of the right atrium to terminate atrial fibrillation. This device must be wirelessly powered and may not rely on a battery for long term operation.
- An external device capable of wirelessly supplying power to the implant. This device must also be able to detect AF and alert the wearer when AF occurs so that they can take action to defibrillate themselves.

State of the art smartwatches are capable of detecting AF [15]–[19] and wireless power transfer, making them an ideal basis for the external part of OptoCoil. In addition, they have been widely adopted and are visible in daily life which would allow wearers of OptoCoil to hide their medical condition from public display.
The implantable device should be able to receive power wirelessly and illuminate the atria with sufficient

intensity and area to terminate AF. Figure 1.3 demonstrates how the final device could be used. A person previously diagnosed with reoccurring AF has had the OptoCoil implant surgically implanted and is wearing the external device (1). When AF spontaneously occurs (2), the person is notified (3) and aligns the external device with the subcutaneous implant (4). The external device triggers the implanted light source, successfully terminating the arrhythmia (5).

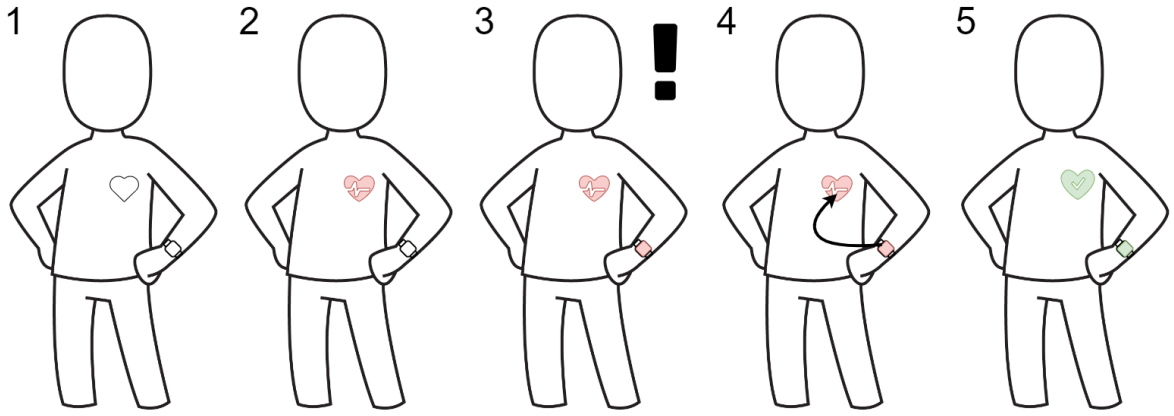

Figure 1.3: Usage of the device. Initially a normal sinus rhythm is present (1) until spontaneously AF occurs (2). A smartwatch device detects the AF and alerts the wearer (3) who then places the watch on his chest, aligned with the implant (4). The watch will trigger the implant, restoring the AF to a normal sinus rhythm (5). Image of person source: `www.iheartcraftythings.com/man-drawing.html`

1.2.1. Thesis outline

The goal of this thesis is to make a first version of the OptoCoil which can be used during in vivo ambulatory experiments with rats. Both the implantable and external devices will be used on rats which have been genetically modified to express optotools which will be further discussed in section 1.3. During in vivo ambulatory experiments the rat, which has had the OptoCoil implanted, will wake up and move around. Upon the occurrence of AF, OptoCoil can be activated to terminate the arrhythmia as described before.
A large difference between rats and humans is the physical size: the right atrium of a rat is significantly smaller than that of a human, adjusting the requirements for the size of a light source to a much smaller one. Since not only the right atrium of a rat is smaller but the rest of the body as well, the maximum size of the implant and the transmitter is also limited.
AF detection and notification is outside the scope of this thesis although an interface must be available to activate the light source based on external measurements.
OptoCoil will be introduced, designed, validated and reflected upon based on the following outline:

1. Introduction: The first chapter introduces the project, the basics of optogenetics and the theory behind wireless power transfer.
2. Existing devices: Cardiac optogenetics have been around for over a decade. This chapter will discuss the devices which have previously been made for cardiac optogenetic applications.
3. Design: The design chapter will specify requirements of the devices and describe simulations and considerations which were made during the design phase.
4. Validation: The validation chapter contains the measurements to determine if the created devices match the criteria from chapter 3.
5. Application: This chapter describes how OptoCoil was used during in- and ex vivo experiments.
6. Conclusion & Future work: This thesis will be concluded by evaluating if the goal described in this chapter has been met and reflect on the design by identifying points of improvement for future work.

1.3. Optogenetics

Optogenetics is an experimental method where cells can be stimulated using light. To allow optical response of nerves or cardiomyocytes they must be made light sensitive [20], [21].
The proteins which add this light sensitive behaviour are opsins but are often referred to as optotools. Optotools are channels or pumps which, when added to the cell membrane, allow ionic currents to flow upon illumination with sufficient intensity of the correct wavelength of light. The direction of this ionic current causes either depolarization or hyperpolarization and thus results in excitation or inhibition of the cell [22]. The amount of illumination required is based on the degree of expression of the optotool in the cell membrane and its intrinsic light sensitivity.
Optogenetics was first applied in 1988 to stimulate oocytes [23], [24] although the term optogenetics did not yet exist at that time. Previous studies were published to demonstrate the light dependent current producing capabilities of cells expressing optotools [25], [26] but Zemelman was first to present a method to control neurons using a protein they named chARGe [27]. Optogenetics has since rapidly been adopted into the neuroscience field [21].
Its first application in the cardiac field followed almost a decade later in 2010 when both Arrenberg and Bruegmann were able to perform in-vitro optogenetic stimulation using cardiomyocytes [28], [29]. Arrenberg used zebrafish cardiomyocytes to create a proof of concept optogenetic pacemaker using channelrhodopsin-2 (ChR2). The cells could be stimulated up to 4.7Hz before starting to skip paces where they were beating at 3.3Hz before stimulation [28]. Bruegmann could stimulate cardiomyocytes of a mouse in-vitro using the ChR2 protein as well [29]. Both experiments were able to demonstrate the precise stimulation in both spatial and temporal domain which optogenetics has to offer. Optogenetics has since been widely adopted into the cardiac research field and many devices have been made and used in both the cardiac and neurological field [21].
A nice demonstration of the capabilities of optogenetics has been provided by Lee [30] who made small fish coated with light sensitive cardiomyocytes. Figure 1.4 demonstrates how these fishes were made and how they were made to swim by exposing them to light in a regulated, alternating pattern.

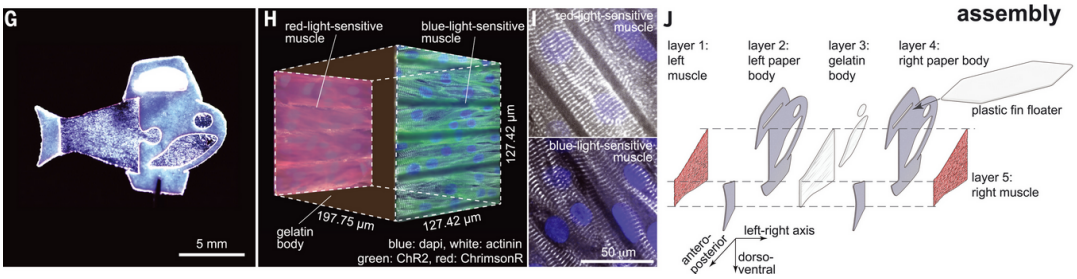

Figure 1.4: [30] figue 1G-J. Lee created fishes coated with light-sensitive cardiomyocytes, allowing them to swim upon illumination from alternating sides.

1.3.1. Optical vs electrical stimulation

Contrary to electrical stimulators, optogenetic stimulators use the current created by the cells themselves to excite them. An advantage of such an approach is that the high-current applications like defibrillation and cardioversion are pain-free when using optogenetics contrary to an electrical solution. In addition, there is no physical contact between the light source and the target tissue required, making optogenetics an excellent way of stimulating moving tissue like the heart. This effect can be leveraged by certain wavelengths of light like near-infrared (NIR) which have tissue penetrating properties allowing stimulating through tissue or membranes [24].

1.4. Wireless power transfer

Wireless power transfer (WPT) is the concept of energy transfer without a physical connection between transmitter and receiver. This transfer is realised by a shared, changing electromagnetic field. Both capacitive and inductive systems exist for wireless power transfer but inductive resonant coupling is the one which most often used.
A simplified model of a WPT system is shown in figure 1.5 of which each box will shortly be discussed.

The 'Supply' box represents the DC power from a power supply unit. The inverter creates a high frequency alternating current from the DC power which then flows through the resonant tank and primary coil. The alternating current flowing through the primary coil creates a rapidly changing electromagnetic field. Since the secondary coil is placed close to the primary coil, they share the same field and thus the same change in their field. This changing magnetic field induces a voltage across the secondary coil which creates a current when connected to a load and thus the transfer of power, a concept which will be mathematically supported in section 3.2.
The resonant tank on the power transmitter side boosts the power transfer capability, the resonant tank on the receiver side increases the efficiency of the power transfer by correcting the phase shift between voltage and current. Both resonant tanks consist of a capacitor in series with the primary/secondary coil and are tuned to have the same resonance frequency.
The rectifier transfers the high frequency AC back to DC which is then transferred to the load.

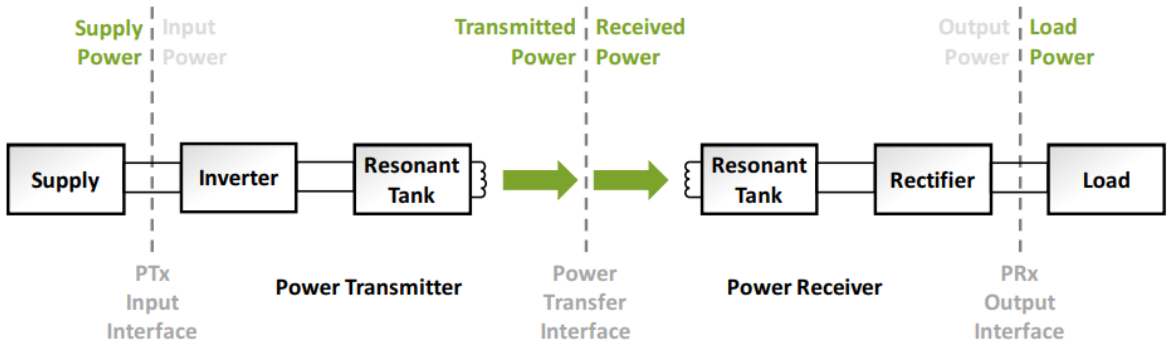

Figure 1.5: Simplified model of a wireless power transfer system [31, power delivery Fig. 2]

1.4.1. QI standard

The Qi standard is an open interface developed by the Wireless Power Consortium (WPC) for inductively coupled wireless power transfer [32]. The standard is intended for small personal electronics and can transfer up to 15W over a distance of up to 4 cm and is used in almost any modern smartphone/smartwatch. The WPC is currently working towards increasing the maximum power transfer up to 60W to allow laptops to charge as well.
Part of the Qi standard is a communication protocol through which the devices can negotiate the power delivery, this also adds safety since power will only be delivered to devices which can authenticate themselves and thus adhere to the QI standard.

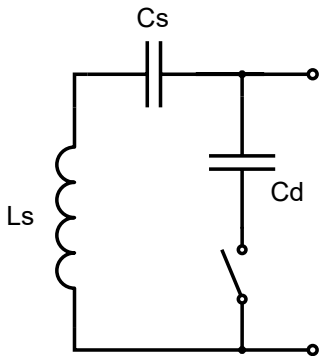

Figure 1.6: Dual resonant circuit of a Power Receiver [31], [32]

A Qi receiver consists of a dual resonant circuit as shown in figure 1.6: C_s is added to optimize the power transfer efficiency whilst C_d allows detection of the receiver position. L_s is the self inductance of the secondary coil without any magnetic material nearby. L'_s is the self-inductance of the secondary coil when aligned to the primary coil, this includes the effect of any magnetic materials nearby which

are part of the power transmitter. The resonance frequency of the power transfer is defined by equation 1.1 and must be around 100kHz (+10%, -5%).

$$F_s = \frac{1}{2\pi * \sqrt{L'_s * C_s}} \tag{1.1}$$

communication takes place by modulation of the current through the primary and secondary coil. This can be done by modulation of a restive or capacitive load.
The quality factor of a coil, Q-factor for short, describes the relation between initial energy stored- and the amount of energy lost in the resonator. The Q-factor for a series LCR circuit such as used in WPT applications can be determined using equation 1.3 where ω_0 is the natural frequency of an LC circuit, L the value of an inductor, C the value of a capacitor and R the sum of any resistance in the circuit including the resistance of the coil and capacitor.

$$\omega_o = \frac{1}{\sqrt{LC}} \tag{1.2}$$

$$Q = \frac{1}{R}\sqrt{\frac{L}{C}} = \frac{\omega_0 L}{R} = \frac{1}{\omega_0 RC} \tag{1.3}$$

Shielding of the coil can be done by placing a conductive sheet behind it. This is important to prevent interference the intended function or overheating due to eddy currents in conductive areas caused by stray.
A well designed QI transmitter contains of a PID algorithm to control the current flowing through the primary coil.
Before a valid power transfer begins, a negation followed by a Power Transfer Contract must occur. To detect if a device is present, the transmitter will 'ping' the receiver every second with a 175KHz pulse. If, following the ping, a negotiation and contract is established the transmitter will gradually lower its frequency whilst keeping a constant voltage. Powering down follows the opposite pattern: The frequency is gradually increased at constant voltage until the maximum voltage has been reached. At this point the voltage will be lowered to complete the power down. The transmitter will at all times maintain a maximum average power which can be drawn from the supply. This is to prevent damage to both the transmitter and the power supply, often a USB charger.

2

Existing devices

Implantable opto-electronic devices for ambulatory optogenetic applications have been made before. Wirelessly powered neurological devices used in ambulatory applications date back as far as 2011 [33]. Designs of opto-electronic devices outside the cardiac field include cochlear implants [34], bladder control [35] and brain activity [33], [36]–[39]. Within the cardiac field there is a separation between cardiac pacemakers [40], [41] and defibrillators [42]–[46]. Before a new design for terminating AF can be added to this list, a comparison between features and shortcomings must be made. This section will compare existing devices to get a clear image of possibilities and limitations in current devices.
Between the different designs which will be discussed a distinction is made between devices which depend on light guides, are partially implanted or fully internal. Devices which use light guides or that are partially implanted are included to provide a reference for devices where power delivery, light intensity and produced heat are removed as a limitation. Internal sources have their light source and power supply inside the body, they can operate while the subject is awake. These sources can again either directly illuminate[1] the targeted area or use light guides to reach the targeted area.

2.1. Light guides

Besides direct illumination of the target area, light guides can be used to direct light from high-powered sources on tissue. Advantages of such an approach in vivo could be to implant the larger parts or parts which generate (moderate) heat away from sensitive tissues or membranes. Commonly used light guides are optical fibres [47], [48] and magnifying setups to focus the light over greater distances [42], [46].
Bruegmann's light source was a mightex GCS-0470-50-A0510 and BLS-13000-1, this is a 470nm 50W 13A 2000mW typical radiant flux light source. This light was focused to a specific area of illumination using a MVX10 microscope in both a langendorff setup and open-chest in vivo experiments. His study showed first evidence of optogenetic AF termination in mice.
Nyns used a thorlabs M470L3-C4 torch which can supply up to 310mw of radiant power when supplied with 1A of current powered by an externally triggered T-cube driver for light emitting diodes (LEDs). They focused the light on a 125mm^2 area using compatible collimators for use with ex vivo experiments. Nyns's study demonstrated optogenetic VT termination in ex vivo rat hearts.
Although both these setups provide an enormous amount of illumination and are able to terminate arrhythmias in all tested cases, its size and power requirements are too high to allow it to be used in ambulatory experiments.

2.2. Partially implantable devices

Partially implanted devices cannot directly be used for ambulatory experiments but can emulate scenarios where there are no limitations on required power, processing power or heat generated by external devices. Heat produces by the light source must be taken into account since this part will be inside of the body.

[1] Direct illumination is defined as less than 5mm between the light source and the targeted tissue

The device which is closest to the target application of this thesis is created by Nyns in 2019 [43]. Nyns created an implantable light source capable of atrial defibrillation. This device combined defibrillation with an automatic AF detection to have a closed loop system for atrial defibrillation as shown in figure 2.1a. Although the size of the power source and control logic currently limit the device from being implanted, this system contains all the logic required to allow it to autonomously replace the current solution to this problem, an implantable cardioverter-defibrillator (ICD). The light source has a power consumption of 0.5W and a physical size of 6x1,5mm making it sufficiently scaled for ambulatory in vivo experiments.
Nyns published a different device in the following years, this time targeting the ventricles instead of the atria [44], [49]. Their cup-like device contains 4 LEDs glued to the apex of the ventricles, see figure 2.1b, which they used to terminate VT. Out of the 4 LEDs, the center one can be controlled individually to allow testing illumination with different surfaces. The current controller they used is the Thorlabs LEDD1B which allowed them to adjust both brightness and power consumption of the device up to 2.85W for the 567nm wavelength and 2.25W for the 617nm wavelength. The ECG based on which is determined if VT occurs is acquired using an existing external device. This study included measurements of temperature increase of the cardiac tissue using the cumulative equivalent minutes at 43°C (CEM43) model. This device targets the ventricles and can not directly be applied to the atria due to the physical size of the device. The multi-LED approach is however something to consider for increased intensity over a larger area while also spreading the heat across a larger area.

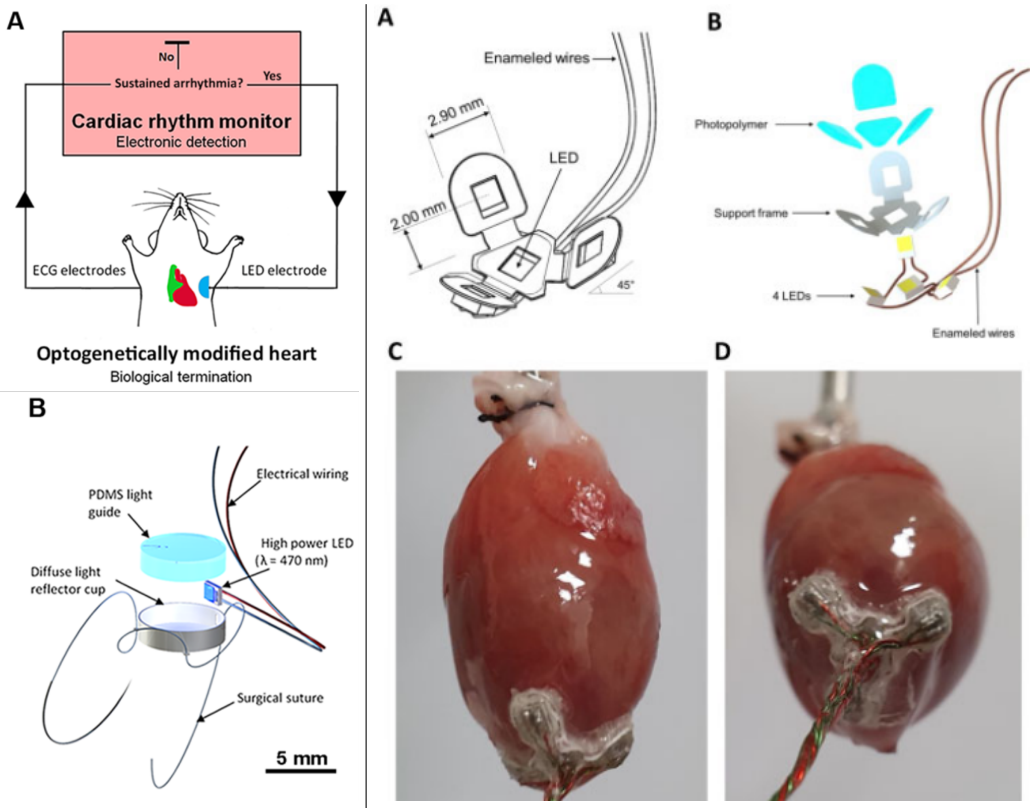

(a) [43, Fig. 4a, b] **(b)** [44, Fig. 4a-d]

Figure 2.1: (a) Optical stimulation using implantable light source. **(b)** Schematic design (top) and application of the apex cup (bottom) to the heart. The apex cup contains 4 LEDs

A more extreme version of a multi-LED approach is created by Hong [45] who demonstrates a flexible grid of LEDs which wraps around the heart allowing multisite stimulation of the ventricles. The LEDs can be individually activated by a controller after receiving measurements from a custom made negative coefficient strain gauge sensor. This approach allows a closed loop system between measuring and termination of VT. Despite the device encapsulating the complete heart, they claim no negative effect due to the strain added to the mechanical function of the heart. Figure Figure 2.2 demonstrates their array of LEDs surrounding a human heart, upon detection of an irregularity the device can automatically

turn on some of the 565nm wavelength LEDs to locally terminate the arrhythmia. Comparing this design to that of Nyns, the largest difference from a technical perspective is the density of the LED array and the required amount of channels to control each LED individually. Hong seems to control each LED individually and although no exact number is mentioned, based on figure [45, Fig. 4e] at least 16 LEDs are used, significantly increasing the required controller.

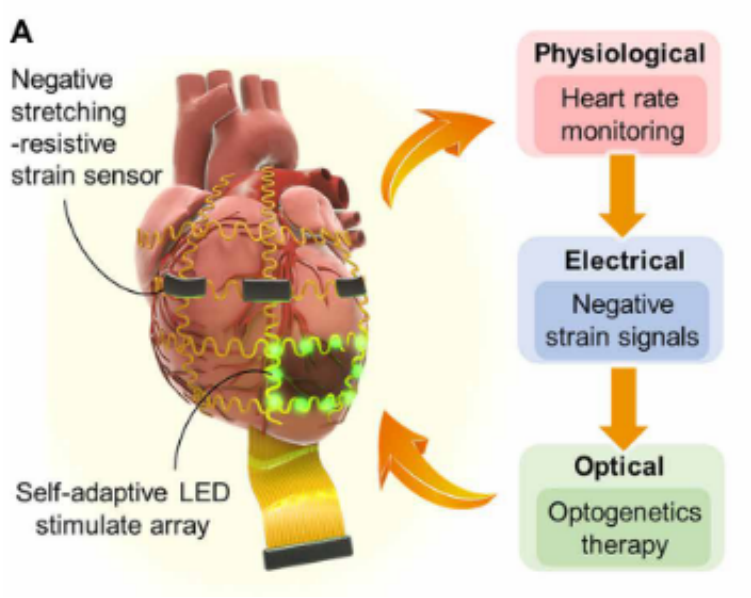

Figure 2.2: [45, Fig. 1a]. A self-adaptive implantable cardiac optogenetics system based on a negative stretching-resistive strain sensor

Tokuda's [38, page 585-600] and Rajalinghams [39] devices use high density LED arrays to illuminate complex patterns on the brain or uniform illumination over larger areas. Tokuda created a CMOS-based opto-electronic neural stimulator capable of not only optogenetically stimulating but also provide feedback using a CMOS image sensor [38, page 585-600]. The physical size of this device (LED array of 1.8x1.9mm) in which 80 LEDs are located. For cardiac applications on humans this much too small to cover the atrium but for animal experiments such an array with feedback could be very useful.
Rajalingham's device, shown in figure 2.3b, is called the Opto-Array. The Opto-Array is a microLED array of 5x5 pixels (24 LEDs and 1 thermal sensor) used to stimulate the brain over an area of 7x7mm. Thermal monitoring of the tissue during stimulation could prove beneficial for fine tuning an optogenetic defibrillation protocol. The higher light output of this device which is comparable to the requirements of [43] might allow for use in cardiac applications in medium sized animals.

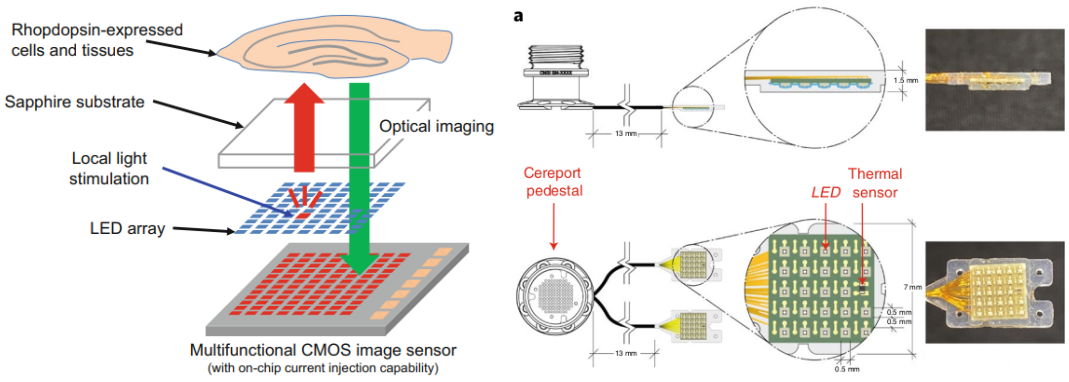

(a) [38, page 585-600, Fig. 41.4] **(b)** [39, Fig. 1a]

Figure 2.3: **(a)** Concept of an implantable CMOS-based opto-electronic neural stimulator for optogenetics. **(b)** Schematic of the Opto-Array design

2.3. Fully implantable devices

Burton [36], Gutruf [40] Samineni [50] and Choi [51] all created a fully implantable wirelessly powered battery-free device. Burtons device measures and stimulates base on optogenetic signals, Choi uses electricity for these tasks, Gutruf and Samineni can only stimulate. Gutruf is able to stimulate either electrically or optogenetic while Samineni can only optically stimulate.
Gutruf, Samineni and Burton receive power from transmitters which are embedded in the cage of the animal whereas Choi created a patch which sticks to the skin and provides the wireless power for the implant. Besides the wireless power transmitter, this patch contains a battery, ECG measurement and a power receiver to charge its internal battery. It has been designed in such a way that removal of the patch is only required at the end of the treatment period.
Burtons design is aimed at long term recording and stimulation of brain activity. Their light source sits right next to a photodetector which provides a feedback mechanism. The processor they used (attiny84 [52]) is connected to an infrared (IR) LED to communicate with a base station. The wireless power transmitter is embedded in the cage of the animal.

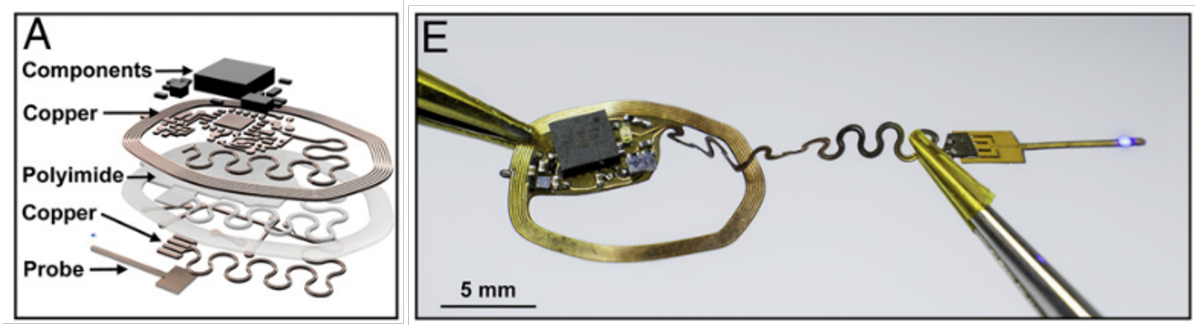

Figure 2.4: [36, Fig. 1a, e]. Exploded view and picture of Burtons wireless, battery-free subdermally implantable photometry system for chronic recording of neural dynamics

Samineni [50] designed a completely passive implant: an optogenetic spinal stimulator shown in figure 2.5. Its electrical design is simple allowing for ease of use and high reliability based on its low complexity. Disadvantages are the lack of regulation of light intensity and feedback which makes the efficiency of the device highly dependent on the position of the transmitter relative to the receiver coil. With a physical size of only 10x5x0.2mm this is the thinnest device in this review. Its small size allows shaping the coil to the tissue and skin, minimizing impact of the implant.

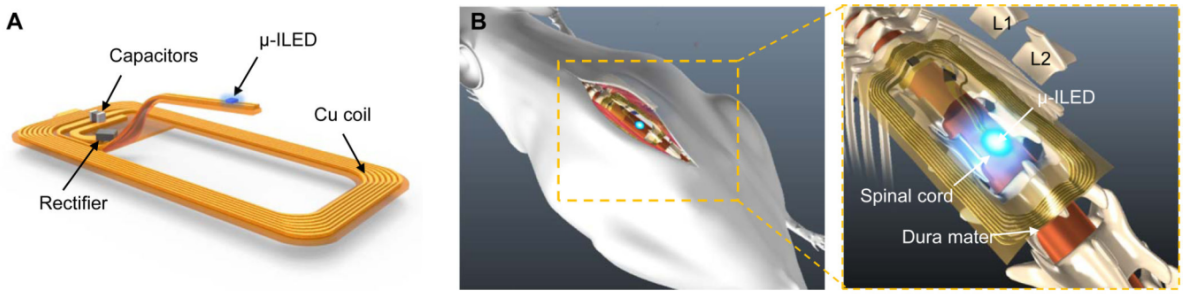

Figure 2.5: [50, Fig. 1a, b]. Design of Samineni's wirelessly powered spinal optogenetic stimulator

Choi's design relies on an external patch to supply power and measure the ECG based on which the pacemaker will be activated. Contrary to other devices on this comparison, Choi uses only electrical pacing. Their design was included since it strongly represents a commonly used layout of a coil implant which is placed subcutaneously but close to the skin with a transmitter on the outside. In addition, Choi's implant is completely passive but linked to an external device which provides the closed loop feedback, matching the goal of this research. A comparable device had been explored earlier as a leadless pacemaker by Das [53]. A significant difference between the two devices is the bioresorbability of Choi's design as well as the integration into an multisensor healtcare application.

Gutrufs pacemaker contains optrodes: A combination between an electrode and optogenetic stimulation. These optrodes are controlled by the attiny84 microprocessor which limits the maximum current draw of the LED or electrode to 30mA [52, Table 22-1] per pin. The voltage used to pace is limited by external components to 2.2V. Multiple of these optrodes can be connected to the processor to allow multisite pacing. The processor can modulate the power transmission to communicate with the power transmitter. A similar design had earlier that year been published with its application in measuring and controlling bladder function [35] demonstrating the capability to add sensors to the optrodes.

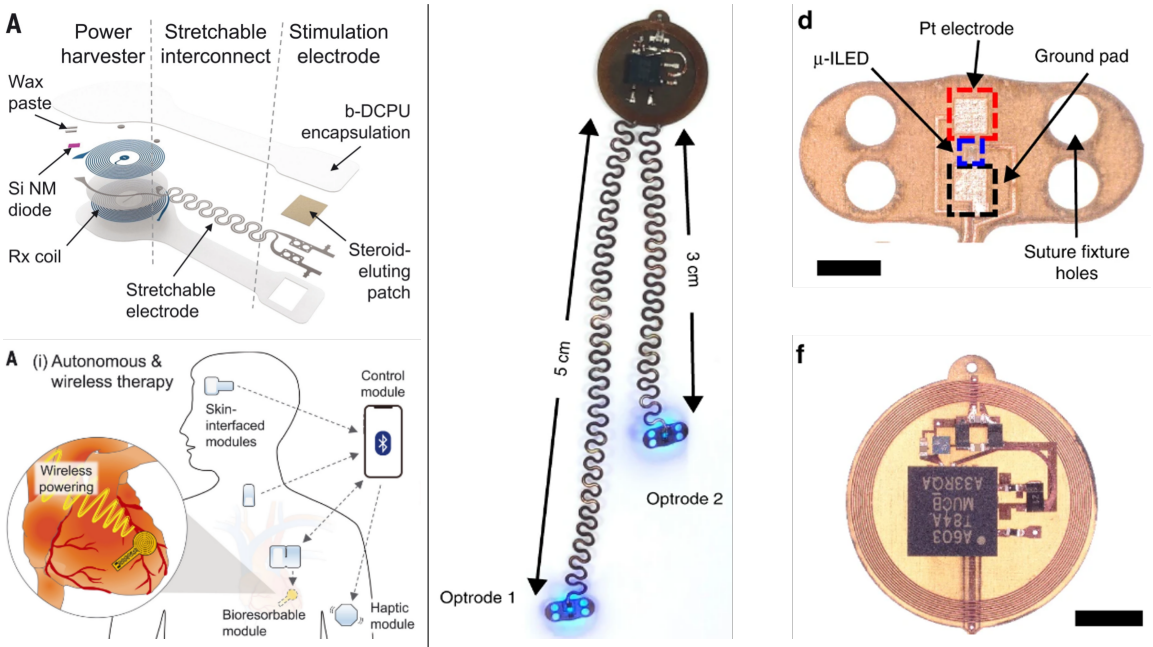

(a) [51, figure 2a(T), 1a(B)] **(b)** [40, Fig. 3a, 1d, f fltr]

Figure 2.6: **(a)** wirelessly powered cardiac electrical pacemaker designed by Choi [51]. **(b)** Wirelessly powered multimodal and multisite cardiac pacemaker created by Gutruf [40]

3

Design

This chapter describes the designs of the coils, transmitter and receiver which have been made as part of this project. Each of these designs will represent one or multiple blocks shown in figure 1.5.
The transmitter section 3.4 implements the ”Power Transmitter” part of figure 1.5 and includes inverter and part of the resonant tank. A microprocessor is added to control the frequency of the inverter and add a user interface for different stimulation patterns. It’s design will be discussed in section 3.4.
The receiver implements the ”power receiver” part of figure 1.5. This part contains part of the resonant tank, a full bridge rectifier and the load which consists of the LED for optogenetic stimulation and a current regulator, this design will be further discussed in section 3.3.
The transmitter and receiver are linked by the coils. These receiver coil should be small and flexible, the transmitter coil must be capable of handling relative large currents and fit on the thorax of a rat. To test and optimize these coils and the combination of transmitter/receiver coil, multiple different designs will be made out of polyimide laminated copper. The details of this design will be further discussed in section 3.2.

3.1. Limitations and requirements

The far future goal of this project is creating an implanted atrial defibrillator for clinical applications. Before any device is ready for clinical applications, it must be tested and proven to be reliable on a smaller scale. The initial in vivo experiments will be conducted using rats, which are significantly smaller than humans. The advantage of the smaller animals is that the atria is also smaller and a single LED can cover it completely which limits the complexity of the device. Downside of such a small animal is that the design is subject to strict limitations in terms of physical size. In addition, the animal cannot be told to not touch certain wires or lay still for example. A device must be made in such a way that it won’t interfere with the well-being of the animal, including no restrictions on allowed movements. As a result the design must be completely implanted inside of the body without any wires passing through the skin, hurting the animal and limiting its movement. A list of requirements has been made to allow validation of the device during and after the design phase. This list contains 4 limitations and subsequent requirements following from them regarding the receiver:

1. **Location of the device**
   The device will be implanted subcutaneously on the thorax. This location has been chosen over the belly or back since it won’t limit the animal curling up whilst they are sleeping. Placing the receiver coil as close to the skin as possible increases the coupling between the transmitter and receiver coil which in turn increases the maximum amount of power that can be transferred as well as efficiency.

   (a) The device must be subcutaneous
   (b) The power receiver coil must be placed on the thorax

2. **Biocompatibility**
   Since the device will be fully implanted, it will make contact with tissue on all sides. This brings

up 3 requirements related to electronic devices inside a body, first of which is a biocompatible coating. A biocompatible coating is required to isolate the metals, moulding compounds of the components and sharp corners from damaging the surrounding tissue. The second and third requirement are related to heat production: Powered electronics will always produce heat, which must be dissipated into the surroundings, in this case the tissue surrounding the device. The limitations set to cardiomyocytes are that they become inexcitable after exceeding 48 °C [54] or after exceeding 128 cumulative equivalent minutes at 43 °C (CEM43°C) [55].

(a) The device must be covered in a biocompatible coating
(b) Local temperature must stay below 48 °C
(c) The CEM43°Cmust stay below 128 minutes

3. **Maximum physical size**
Requirement 1b specifies that the device must be implanted on the thorax. This location determines the maximum physical size of the device. Figure 3.1 shows that the absolute maximum dimensions on the thorax are 50x33x3 mm for a rat of approximately 230 grams. A large or thick device will be more difficult to implant which is why a smaller size is preferred.

(a) The size of the receiver must be within 50x33x3mm

4. **Light source control**
The brightness of the light source must be controllable since this will make experiments repeatable and also adds predictability to them. Although the intensity must be controllable, that does not mean it needs to be adjustable during the experiments. The light source will be used not only to defibrillate but also to pace the heart to validate an optoresponse. Pacing is the highest frequency to which the device must be able to respond and will typically be performed around 7Hz with a 50ms light-on time.

(a) The light source must emit a reproducible, known light intensity
(b) Response time must be sufficient to pace above 7Hz

3.1.1. Transmitter requirements

The transmitter has been omitted from the list of requirements since it should functionally work but its final specifications will be defined as the biomedical experts work with the device. As discussed earlier the aim is to use a smart watch for human applications but such a watch for a rat is not realistic. It's likely that either a large coil embedded in the cage is used for the first ambulatory experiment or that a small device which can be carried by the animal is created or externally sourced in a later stage. Part of this portable transmitter would be the ability to record ECG signals, a battery management system, a coil driver and a processor capable of a wireless communication protocol and sufficient processing power to analyse analog readings for ECG processing purposes. For now, the requirements for the

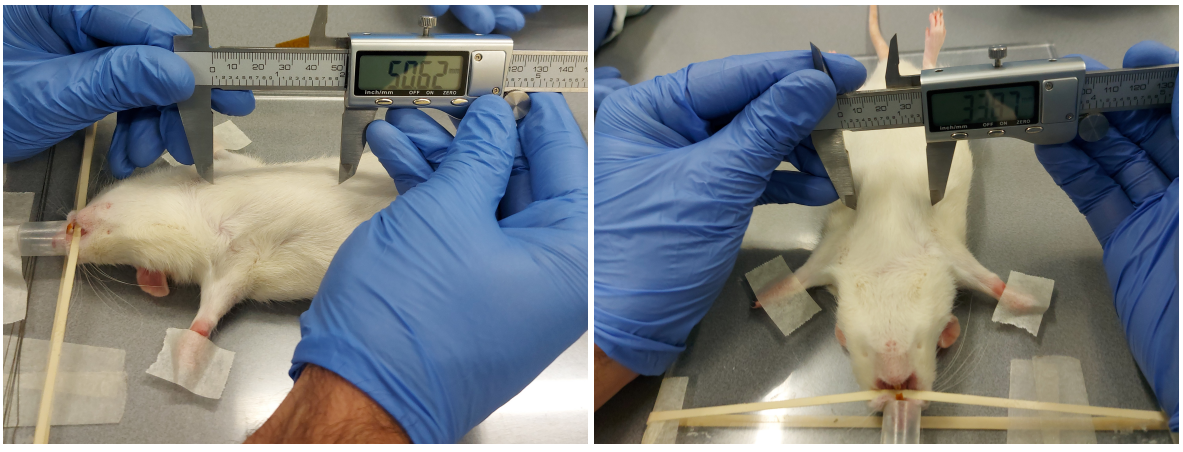

Figure 3.1: Length and width of a rats thorax

transmitter will be limited to being able to drive the transmitter coil with a controllable frequency at sufficient current to satisfy receiver requirement 4a.

3.1.2. External limitations

This system was designed and created during a global chip shortage. As such, most components have been chosen with a generic footprint to allow the use of different components when the original ones are out of stock. Unfortunately this was not possible with all components. Components which don't have pin-compatible alternatives available are called 'critical components'. If these components are unavailable, the device will not work and cannot easily be fixed without redesign of the PCB. These critical components were still used in the design because of their unique features and since they are newly designed chips, pin-compatible alternatives are likely to become available over time. A list of critical components will be supplied at the end of each design description.

3.2. Coil design

The basis of wireless power transfer are coils inside of the resonant tanks in figure 1.5. These coils will form an air coupled transformer where their magnetic flux (Φ_B) is shared. The magnetic flux is defined as the surface integral of the total magnetic field (B) passing through a defined surface (S) and is calculated as shown in equation 3.1. Equation 3.2 shows how the change of the flux over time results in electromotive force (ε, emf) where N is the number of turns of the inductor. The emf is expressed in units of Volt which, when the leads of the inductor are connected by a load, creates a current. This conversion between a changing magnetic field through a surface and the voltage this induces is how wireless power transfer is realised.

$$\Phi_B = \iint_S B \cdot dS \tag{3.1}$$

$$\varepsilon = -N\frac{d\Phi_B}{dt} \tag{3.2}$$

For the purpose of this research these coils have to be able to transmit a few Watts of power for short periods of time whilst the receiver is small enough to fit into a rats chest. The design approach for the coils follows these steps:

1. Determine manufacturing capabilities of the chosen supplier
2. Determine the inductance of a coil with N turns in which satisfies requirement 3.
3. Use the obtained inductance in an LTspice simulation to determine power transfer. This step will also be considered a feasibility study: If the outer limits of the requirements cannot result in a feasible device, a different approach must be considered.
4. Evaluate if the obtained coil is possible to implant into the test subject, if not, back to step 2.

Manufacturing Capabilities

The manufacturing capabilities determine what parameters can be used during the design process in order to obtain a design which is actually meaningful. The chosen manufacturer, PCBWay, lists their capabilities on the website [56]. The most critical ones are the amount of copper layers(1-6), the dielectric (polyimide), thickness of the finished product (0.1mm - 0.3mm), minimum spacing between tracks (0.06mm) and the thickness of the copper layer(17.4 - 69.6 μm). The thickness and the amount of the copper layers influences the thickness of the finished product which in turn influences the flexibility. Less copper layers are therefore preferred as well as thin layers. The downside of thin copper layers is that the resistance will increase, wider traces will mitigate this issue. Equation 3.3 demonstrates the relation between length (L), width (W) and thickness (T) of a conductor versus its resistance (R) at a temperature (t). α is the temperature coefficient and ρ denotes the resistivity which are both values defined by the material of the conductor. For copper this results in a resistance increase of 0.393% per °C above 25°C. The minimal trace width (0.2mm) was decided based on the recommendations and capabilities of the manufacturer.

$$R = \frac{\rho * l}{W * T} * \Big[1 + \alpha(t - 25)\Big] \tag{3.3}$$

Coil characteristics
Initial dimensions for coils were evaluated using an online printed circuit board (PCB) coil calculator[57]. This resulted in a set of circular and square planar inductors which were 25x25mm wide, see table 3.1. The inductance shown in this table is a range of which the lower and upper bounds have been defined using a monomial fit and a modified wheeler expression respectively [58]. These results show that square inductors provide an increased inductance of 9-16% compared to circular inductors with the same size.

Table 3.1: Inductance of circular and square coils

shape	turns	inductance (μH)
Circular	20	10.890 - 11.761
	10	4.366 - 4.528
Square	20	12.257 - 13.647
	10	4.795 - 5.038

The increase in inductance between circular and square coils suggests that rectangular coils could have an even higher inductance without exceeding the size of the rats thorax.
Unfortunately there is no tool yet which implements rectangular PCB coils. Coil64 [1] however does support coils formed around a rectangular former, which can be used as an approximation for the relative increase in inductance. Based on experiments with the coil64 calculator shown in figure 3.2 the expected inductance of rectangular coils will be higher than the calculated values by approximately 41% for multi layer coils and 46% for single layer coils. The relative increase in inductance has been calculated using coils with the same outer dimensions for both the square inductors and the rectangular inductor of 25x40mm.
The first coil is a square coil of which the number of turns has been adjusted to match the inductance calculated for a square inductor with the same size, trace width and isolation width. Based on the determined thickness a rectangular version with outer dimensions 40x25mm was made to obtain a change in inductance. Using the same number of turns, a square and rectangular version was made of a 2 layer coil to again determine the relative increase in inductance. The lower four coils all have 20 turns and outer dimensions of 25x25mm and 25x40mm.
The reference for all dimensions which are used in the calculator are shown in figure 3.2. For all calculations a wire diameter of 0.2mm (parameter d) and a value for the wire + insulator diameter (parameter k) of 0.26mm was used to match the minimal spacing which is within the capabilities of the manufacturer. Since the wire including insulator has a diameter of 0.26mm a value for parameter 'l' of 0.26mm represents 1 layer, 0.52mm represents 2 layers, etc. Parameter c is the width of the windings and equals the number of turns times the wire + insulator diameter.
The thickness of the final PCB will likely be around 0.1-0.2mm. Since this calculator uses a circular conductor in its calculations, the wire + insulation diameter of 0.26mm will also be used to determine the vertical distance between the inductors. This means 0.06mm will be in between the conductive layers which is about twice as large as in the 2 layer pcb stackup from PCBWay [59]. This means the effective self-inductance will be slightly higher in the manufactured version compared to the calculations.
The coil64 calculator obtains a slightly different results compared to the formulas from [58] when using the same set of parameters. To compensate for these differences two approaches were used: The first approach adjusts the amount of turns to achieve a similar inductance as a single layer square coil from table 3.1. The obtained amount of turns will then be used in both the single and double layer designs to obtain a relative difference between square and rectangular inductors.
The second approach uses the same 20 turns as used before and will thus obtain a higher inductance. These turns will be used to determine again the inductance of single- and double layered coils. The relative change in inductance will be calculated and compared to the results from the first approach.

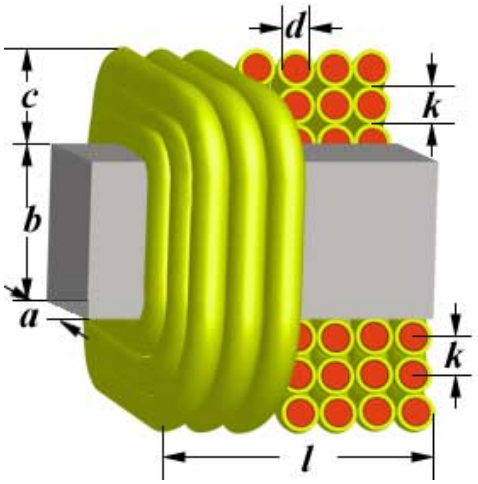

Figure 3.2: Coil64 dimensions for rectangular former. Source: [1]

Table 3.2: Relative increase of inductance for single- vs multi layer inductors when moving from a square to a rectangular layout

inner dimensions a (mm)	b (mm)	thickness c (mm)	winding length l (mm)	outer dimensions A (mm)	B (mm)	inductance (μH)	relative increase of inductance
16	16	4.5	0.26	25	25	13.048	
31	16	4.5	0.26	40	25	18.967	45.36%
20.5	20.5	2.25	0.52	25	25	15.805	
35.5	20.5	2.25	0.52	40	25	22.228	40.64%
14.6	14.6	5.2	0.26	25	25	14.699	
29.6	14.6	5.2	0.26	40	25	21.677	47.47%
19.8	19.8	2.6	0.52	25	25	18.755	
34.8	19.8	2.6	0.52	40	25	26.553	41.58%

The coils created for this design version are listed in table 3.3. The 9 different designs all vary in their combination of shape, number of turns, number of used layers and trace width. The spacing between the turns is 0.06mm which is the minimum spacing the manufacturer could produce. The inductance of the rectangular coils has been calculated as a square inductor using the PCB coil calculator tool and then increased by either 41 or 46% depending on the amount of layers.

Table 3.3: Coils designed for the wireless power transfer based on a copper thickness of 12μm and a temperature of 25°C.

Coil	Size (mm)	Shape	Trace (mm)	Turns	Layers	Inductance (μH)	$R_{t=25}$ (Ω)
P1	40x25	Rect.	0.2	20	2	17.28 - 19.25	16.60
P2	25x25	Circ.	0.2	20	2	10.89 - 11.76	10.15
P3	40x25	Rect.	0.5	20	2	6.37 - 7.16	5.96
P4	40x25	Rect.	0.2	20	1	17.90 - 19.93	14.88
P5	25x25	Circ.	0.2	20	1	10.89 - 11.76	9.06
P6	40x25	Rect.	0.5	20	1	6.60 - 7.42	4.35
P7	40x25	Rect.	0.2	10	1	7.01 - 7.36	8.27
P8	25x25	Circ.	0.2	10	1	4.37 - 4.53	5.16
P9	40x25	Rect.	1.0	20	2	4.72 - 5.39	2.40

LTSpice simulations
LTspice is a SPICE-based simulation tool for analog circuits. The software can be used to analyse behaviour at different frequencies as well as transient or DC sweep analysis. To determine the feasibility and estimate the efficiency of the power transfer, a simplified WPT circuit was created in LTSpice to determine the AC-AC behaviour. Figure 3.3 shows the simulation as well as the circuits used for the transmitter (right, top) and receiver (right, bottom). The circuit had its resonance frequency for both the transmitter and receiver resonant tank set to 117KHz, capacitive values were determined by using equation 1.1. The top left plot demonstrate the efficiency of the power transfer as function of the WPT frequency, the absolute power transfer is shown in the middle plot where the blue line is the input power, green the power delivered to the load R_3. The lower left plot shows the current which through the coil and the receiver load. Since the resonance frequency of the LC tank has been set, this plot only shows how the efficiency of the power transfer using this specific coil and capacitor.
This simulation was used to determine the amplitude of the coil power supply to deliver sufficient power to the load, an estimation of 6V has been made.

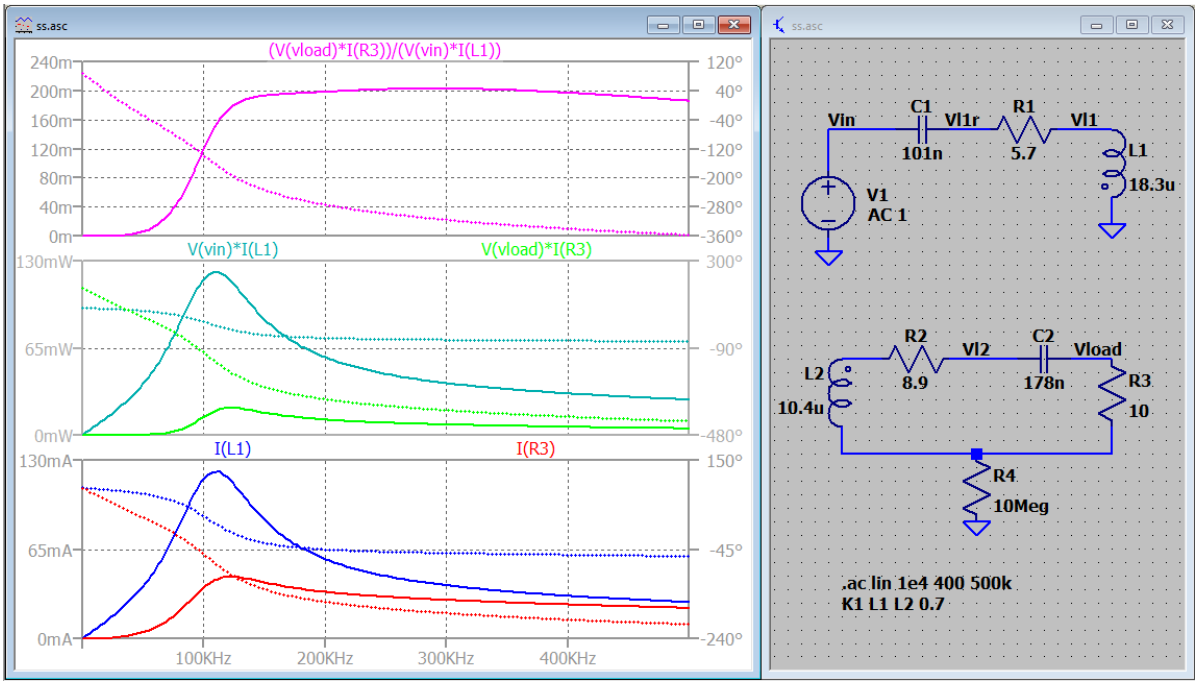

Figure 3.3: top: Efficiency of power transfer , mid: Power consumption of the transmitter coil (blue) and receiver coil (green), bottom: Current through primary coil(blue) and the receiver load (red)

PCB design
The coils will be made out of flexible PCBs. A flexible PCB is consists of copper layers which are isolated using thin polyimide (PI) or polyethylene terephthalate (PET) layers. Their applications vary from connectors for displays to flexible capacitive sensors or actuators. In order to easily test, swap and combine coils, all 9 coils are designed separate from any other components.
The basic shape of the coils is created using the open source add-on for Altium called PlanarTx. This shape was then slightly modified by adding connectors and pads to turn it into an exchangeable component. Each coil was then added to a library to allow reusing the exact coils which will be characterized using this design in future designs. Figure 3.4 shows the schematic design, the coils were combined into a larger panel which is shown in appendix A.

3.3. Receiver

The receiver is the implantable part of the OptoCoil. Its function is to receive the power wirelessly and regulate the current which is used to turn on the LED. The shape of the device allows the coil with all electronics except the LED in the center to be placed subcutaneously and close to the skin, minimizing

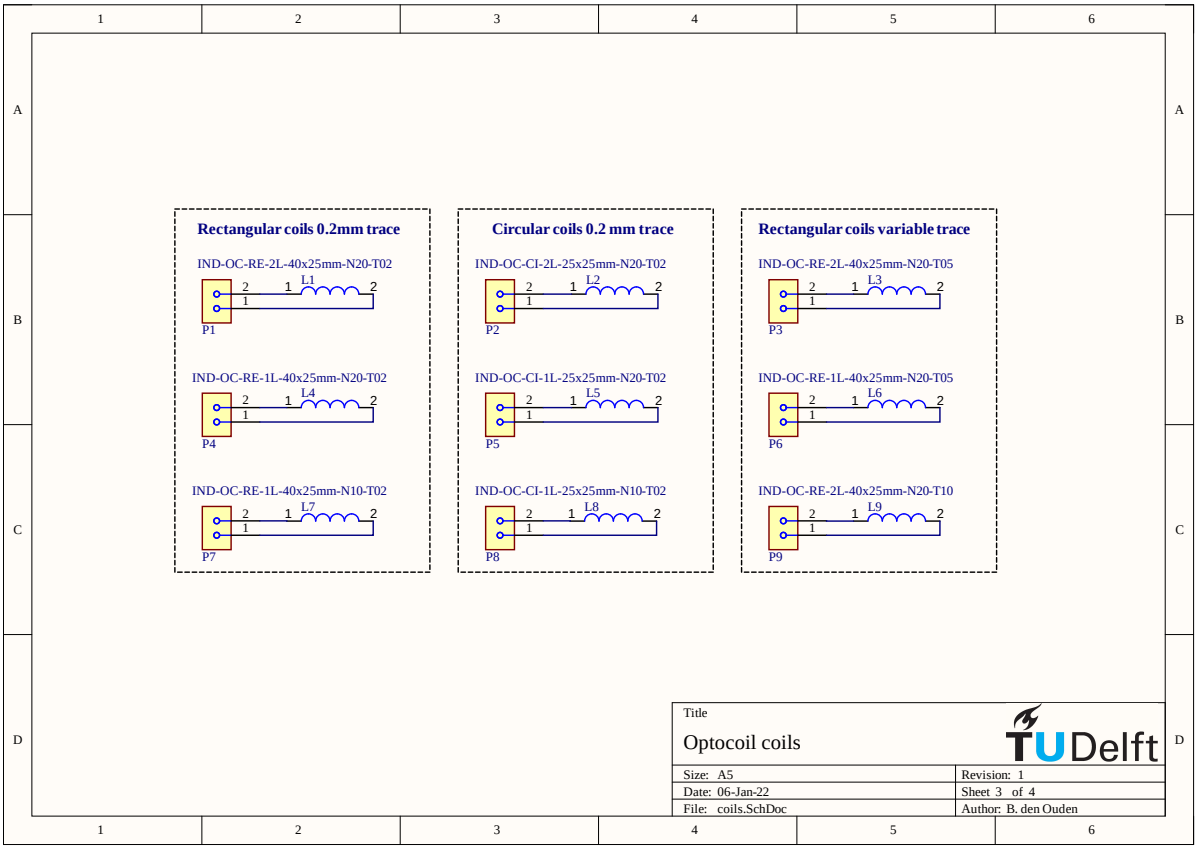

Figure 3.4: Schematic for the different coil designs

the distance between the WPT coils. The LED must be placed on or close to the right atria which requires a flexible connection between the larger coil 'island' and the LED. This flexible connection was realized using a serpentine structure with a width of 1mm of which each loop has a radius of 6mm, dimensions are shown in figure 3.5. Both sides of the structure contained copper traces carrying the current to the LED. At the time of design it was uncertain whether the LED must face the top or bottom layer so both sides have a LED in parallel, only one LED should be connected, the gold pads on the other side should be isolated. The electrical design of the receiver consists of 3 distinguishable blocks:

1. The resonant tank and rectifier are responsible for receiving and rectifying the received power.
2. The power regulation which is responsible generating a stable 3.3V line which powers the on-board logic and LED.
3. The Stimulation LED and logic to control it. The LED itself will be placed close to or on the right atria.

Resonant tank and rectifier

The resonant tank consists of a coil which forms an oscillator together with the capacitor placed in parallel, this is called an LC oscillator after the letters used for these components during shematic design. A full bridge rectifier created from 4 schottky diodes rectifies the voltage to prevent the low dropout regulator (LDO) from getting damaged by reversing its polarity and thereby exceeding its absolute maximum ratings as specified by the datasheet [60]. The used diodes are CDBU0520 [61] schottky diodes capable of a continuous forward current of 500mA and a reverse voltage of 20V. This rectified voltage is called VCC.

Contrary to the schematic shown in figure 1.6, the Cd capacitor was not added to the design. This capacitor is used for load detection, a feature which is not used in a passive design since the switch in series with this capacitor cannot be operated passively. Detection of the receiver by the transmitter is still possible due to change in current draw from the transmitter side.

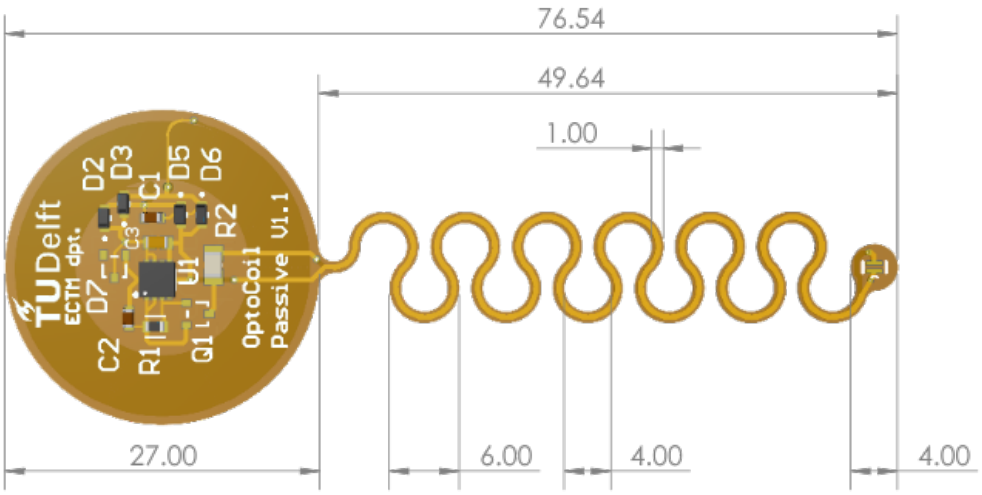

Figure 3.5: Design of the receiver

A first receiver design was to be ordered at the same time as these coils to speed up the process, a coil had to be selected for this purpose. Rectangular or square inductors restrict the orientation in which the receiver can be implanted on the thorax. For the first tests this was undesirable so a round inductor was chosen. Between the three possible round inductors the estimated inductance of P5 and P2 was significantly higher than P8. Out of these two options P5 was chosen since this would allow a 2 layer design to be made which is half the thickness of a 4 layer design [59], increasing the flexibility of the design.
Both the power regulation and the logic to control the LED are placed in the center of the receiver coil to keep the size of the receiver to a minimum.

Power regulation
VCC is then provided to the NCV8187 LDO[60]. This regulator can provide up to 1.2A of current at 3.3V and accepts an input voltage up to max 6 Volts. Its absolute maximum input voltage is 5.5V and to prevent VCC from exceeding this value a 5.3V zener diode was placed across VCC and GND. From this VCC line a 3.3V line is generated to which the stimulation component of the design is connected. Besides the 3.3V line, a power good (PG) line is generated. This is an open collector signal which connects to ground via an internal open-collector circuit when the output voltage exceeds 3V. When the output of the LDO, the 3.3V line, falls below 2.65V the internal transistor controlling the PG line will stop conducting causing PG to be pulled up to the voltage currently on the 3.3V line.

Stimulation LED
The light source used for the stimulation is the lumileds LXZ1-PB01 [62]. This light source has a typical luminous flux rated at 38 lm with a surface of 1mm^2, which translates to approximately 350 mW/cm^2. It is connected to the 3.3V line via a current limiting resistor and a metal–oxide–semiconductor field-effect transistor (MOSFET). The MOSFET will start conducting when the PG pin falls to ground, thus turning on the LED only when the power supply is stable, ensuring a known light intensity.

PCB design
Since most electronics were inside of the inductor, the magnetic field used to power the device will also go through these components. To prevent unintentional heating of components there should not be any inductors or wire loops sharing the same normal vector as the inductor. In addition, large metal planes must be avoided to prevent heating them by eddy currents induces by the same changing flux required for the wireless power transfer.

Critical Components
- NCV8187AMLE330. This is a critical component since it has a power-good pin embedded which is used to ensure the illumination of the LED is at a known value.

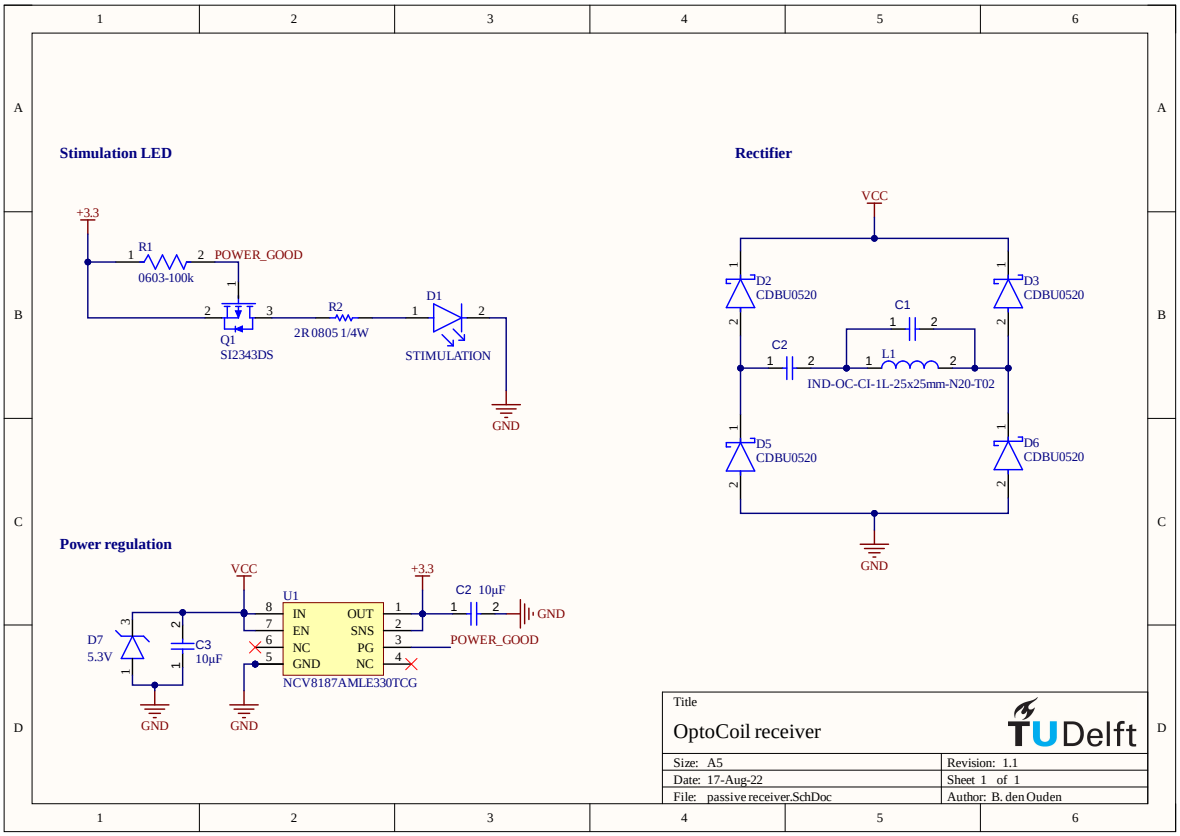

Figure 3.6: Schematic for the passive receiver design

3.4. Transmitter

The transmitter is responsible for the activation of the transmitting coil at a controlled frequency, and represents the inverter and part of the resonant tank from figure 1.5. As described in section 3.1 the final version of the transmitter will likely be a smartwatch, as such this design should be considered a development module. The design is aimed at ease of testing during the in vivo experiments where flexibility between different coils, frequencies and amplitudes of the inverter are required. To allow this broad application of the device, the following four requirements have been identified.

- Variable currents and voltages must be usable by the coil driver.
- The coil current must be measurable.
- An user interface to control the device must be implemented.
- The blocks making up the transmitter must be able to be used individually or connected as a single device.

These requirements will each be discussed below, a three-dimensional (3D) render of the transmitter is shown in figure 3.8, the schematics can be found in appendix A.

3.4.1. Coil driver & current measurement

The transmitter is responsible for alternating the current through the transmitting coil at different frequency values in order to adjust the delivered power to the connected load: the receiver. To generate the alternating current from the DC input, a full H bridge implementation of an inverter has been added using a BD63573NUV [63] integrated circuit (IC) which supports a coil voltage between 2 and 16V and can drive up to 1.2A continuously and 3.2A peak current.
An H-bridge is a configuration where four switches surround the load, in this case the coil, which allows the voltage across and thus the current flow through the load to be reversed. Figure 3.7 demonstrates how the current through the coil can be reversed by closing either S1 and S4 or S2 and S3, creating

an peak-to-peak voltage across the load of $V_{pp} = 2 \cdot V_M$. If S4 remains closed and S1 switches, an alternating current with amplitude of $V_{pp} = V_M$ can be created with variable duty cycle. This same method can be applied to S2 and S3 to create a similar behaviour but at the reversed polarity.

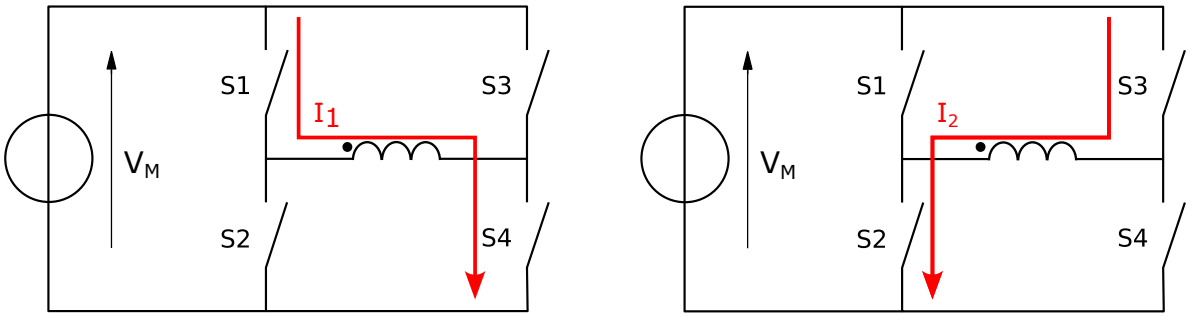

Figure 3.7: Schematic drawing of an H bridge operation. Closing only S1 and S4 applies a positively oriented voltage with amplitude of V_M to the coil, creating current I_1. Closing only S2 and S3 reverses the polarity with the same amplitude V_M creating current I_2.

The current consumption of the H bridge MOSFETs and the coil is measured by a dedicated differential amplifier [64] using a series resistance of 0.15Ω. Since the current is measured before it enters the inverter, the power supply rejection ratio is as high as possible which reduces the noise of the measurement. The analog output of this amplifier is connected to an analog input pin of the microprocessor which allows validation of the coil function as well as a simplified form of load detection by measuring changes in current consumption while the coil is powered.

3.4.2. Power regulation

The microprocessor and logic section of the coil driver are supplied with a 3.3V line generated by the NCV8187 LDO [60]. The power supply for the MOSFETS inside of the coil driver IC is separated from the power supply for the microprocessor by a boost converter which can generate up to 22V with a switch current of up to 1.8A [65]. The input voltage of the boost converter can be between 2.7 and 14V and its current consumption can be brought back to 100 μA by using its shutdown pin, allowing long term battery operation. If external monitoring and control of the coil power supply is required, the boost converter can be left unpopulated in which case the power for the coil driver can be supplied via the screw terminals with the label ”VM”.
Power to the transmitter can either be supplied via the USB-C connector, the 5V or the VCC screw terminals or the battery connector. Any battery which supplies between 3.3 and 5.5V can be used, if a battery is connected when power is also supplied via the 5V screw terminal or the universal serial bus (USB) plug, the charge controller will try to charge the battery. The battery voltage level can be monitored by the microprocessor to alert operators to connect an alternative power source when the battery is almost empty.

3.4.3. Microprocessor

The ’brain’ of the transmitter is the ESP PICO D4 microprocessor which contains two Xtensa 32bit single-core processors and a ultra low power co-processor. The 7x7mm package includes 4MB of SPI ram and an internal 40MHz oscillator in addition to an extensive list of module interfaces such as 18 channels of 12-bit analog-to-digital converters (ADC), 16 channels of dedicated pulse width modulation (PWM) drivers and 34 general purpose input-outputs (GPIO). The processor supports bluetooth 4.2, bluetooth low energy (BLE) and WiFi 2.4GHz connections using and external antenna.
Communication between the processor and external devices like a computer is made possible by the addition of a CP2102N USB to universal asynchronous receiver-transmitter (UART) bridge. This allows the operator to easily upload programs via the USB-C cable but also allows serial data to be exchanged either for monitoring or making changes in the configuration during use, creating the first part of the user interface. Besides the USB connection, one of the previously mentioned wireless interfaces can also be used to communicate or program the device.

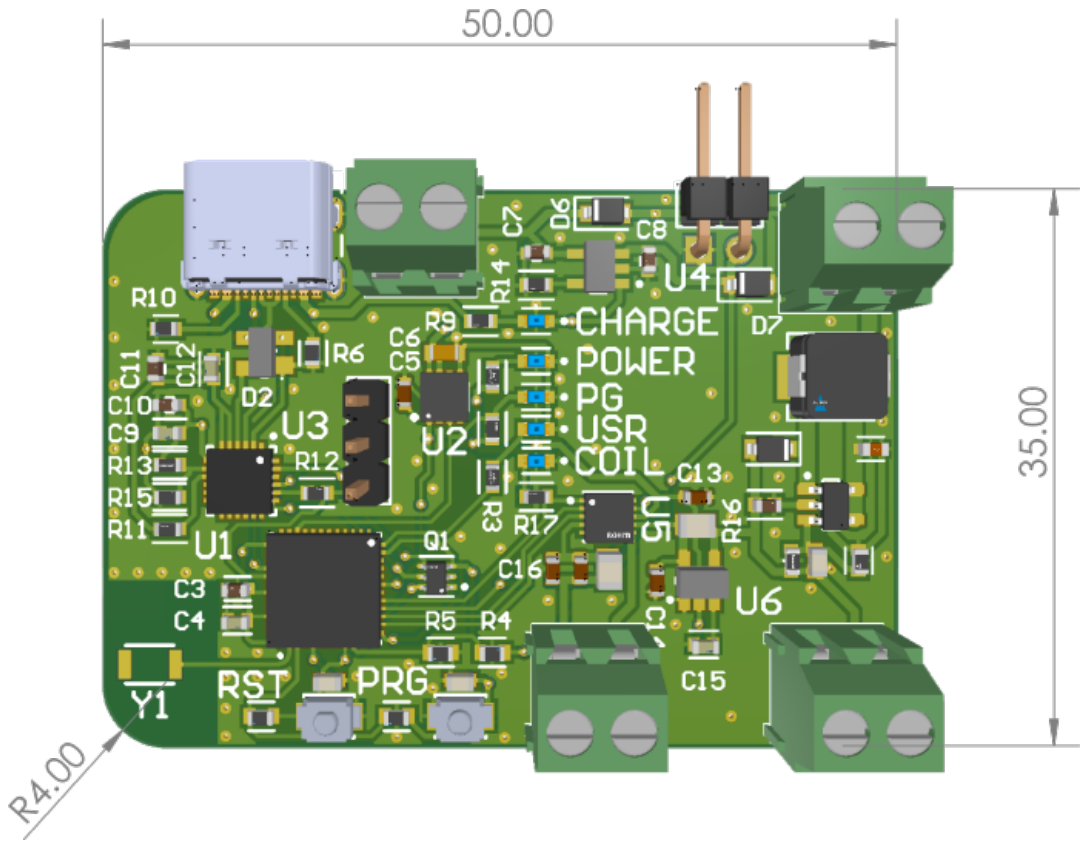

Figure 3.8: Transmitter design

3.4.4. User Interface

The user interface (UI) of the transmitter can be used to configure the stimulation protocol, frequency or plot current consumption of the coil. Communication with the operator can either be via Bluetooth, BLE or WiFi, each requiring a different application on the computer or mobile device.
The advantage of using the WiFi interface is the ability to have multiple devices connected to the same wireless access point (AP) which allows collecting data from multiple transmitters at the same time. Multi-transmitter setups are not likely to occur in the near future but this feature is something very useful to keep in mind for long-term ambulatory experiments. Connecting the transmitter to a WiFi network would also allow monitoring experiments remotely. If no existing AP is available, the microprocessor can host its own network and present data to anyone connected to this network.
Besides the previously mentioned designs which can all be implemented upon request after the transmitter has been fabricated, 5 LEDs have been added to the design as well as a user-defined button connected to GPIO0 shown in figure 3.8. From top to bottom these LEDs convey the following information:

- The CHARGE LED turns on when a battery is connected and is being charged and will otherwise remain off.
- The POWER LED indicates if any power is supplied to the 5V line of the PCB, this LED does not indicate if the voltage is actually 5V.
- The PG LED is connected to the PG output of the LDO and indicates if the 3.3V line is stable and above the minimal threshold. If the POWER LED is on but the PG is not that means either the supplied voltage is below 3V or the PCB is damaged somewhere causing a short or disconnect.
- The USR LED is connected to an output of the microprocessor and can be used to indicate a status to the operator, for example if the battery is empty or a stimulation program is running.
- The COIL LED is connected to the enable pin of the coil driver and the microprocessor. This LED must be on before the coil can be powered.

3.4.5. Critical Components

- The coil driver: BD63573NUV. This is a semi critical device. Although similar chips exist, a re-design would be required.
- The LDO: NCV8187AMLE330. This is a semi-critical device. Although a redesign would be required, it can easily be replaced by any other LDO capable of providing over 800mA since its unique feature, the PG pin, is not used.
- ESP32-PICO-D4, semi critical. although redesign is required, any other chip in the esp32 family could be substituted provided its internal memory is enough for the application.

4

Validation

The designed components must be validated before they can be applied in ex vivo or in vivo experiments. This chapter will discuss the manufactured designs from chapter 3 and their limitations. The designed coils will be matched to the calculated resistance and inductance values from table 3.3, this information can be used to better calculated values for next orders. In addition, the measured values can be used to create an equivalent model which will be used to improve the LTSpice simulations and better estimate and optimise the power transfer.
The receiver will be tested to validate the light intensity and thermal performance of the device since this device will be in physical contact with tissue. The light intensity is tested to see how large possible deviations are and what cause these deviations to occur.
An inverter frequency of 500KHz was used to transfer power in early experiments to determine if the receiver was functioning correctly. Due to the switching losses in the H-bridge the IC heated up significantly and the frequency was lowered to 117KHz. This value of 117KHz will be used as the default value for future experiments unless otherwise stated.
The validation order is based on dependency: The coils are the basis for power transfer, knowing their specifications allows for adjustments to resistor values or supplied voltages. The transmitter and receiver can both be tested individually by using known working power sources or resistive dummy loads. The individual testing of these devices allows for faster debugging of any issues.
When both devices have been tested and are working as expected, they will be combined to test the complete system.
All components are placed either inside or close to a body and must therefore be tested for thermal performance during operation.

4.1. Coil measurements

Up until now the coils have been considered ideal devices containing solely an inductive and series resistance component. Real coils or inductors contain parallel resistance and capacitive components cause by the proximity of the windings to each other and the core material. A non-ideal inductor consists of the four components shown in figure 4.1 and listed below:

- **L** is the inductive component and the most important aspect of an inductor. If the design process is well defined this value will match the previously calculated value in section 3.2.
- **R** This component represents the DC resistance of the inductor. It is a parameter which, just as L, can easily be taken into account when designing the coil.
- **C** The C represents the parasitic capacitance of the inductor, together with the L and RQ components they form a resonant tank which determines the frequency dependent behaviour of a coil.
- **RQ** represents the equivalent core loss parallel resistance. Its value depends on the material of the core and and can be modelled as a parallel resistor.

The resonant frequency and impedance, inductance and Q factor at 117kHz of the coils are measured using an Agilent 4294A impedance meter. To obtain the C and RQ parameters equation 4.1 and 4.2

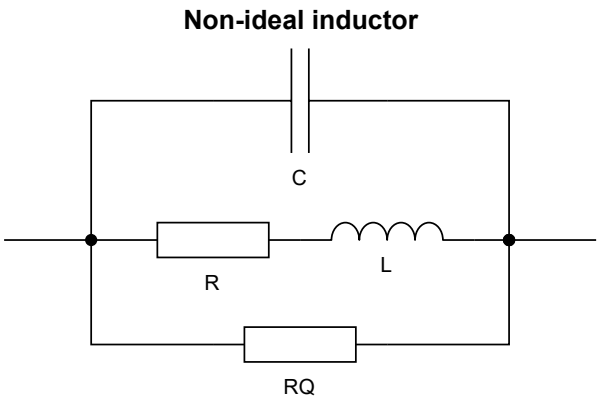

Figure 4.1: Equivalent model of a non-ideal inductor

respectively were used [66]. The characterizing values for each coil have been summarised in table 4.1.

$$C = \frac{1}{(2\pi f_0)^2 L} \tag{4.1}$$

$$RQ = 2\pi f_o L Q \tag{4.2}$$

To validate the calculated parameters the impedance from the equivalent circuit is calculated using equation 4.3 where each part of the denominator sum represents one of the three parallel paths the current can flow through. To determine the Q factor 4.4, where $Z(\omega)$ is substituted by equation 4.3, is plotted over a frequency range from 400Hz up to 15MHz in figure 4.2. Key features such as the impedance and Q factor at the 117KHz frequency have been extracted from this simulation and compared against the measured values to validate and fine-tune the set of parameters from table 4.1.
These values have been used to create a spice model of the created coils allowing better simulation of the wirelessly transferred power, choosing a well-matched transmitter/receiver pair and optimizing the WPT frequency.

$$Z(\omega) = \frac{1}{\frac{1}{RQ} + j\omega C + \frac{1}{R+j\omega L}} \tag{4.3}$$

$$Q(\omega) = \frac{Z(\omega)}{R} \tag{4.4}$$

Table 4.1: Coil characteristics

Coil	F_0 (MHz)	Q_{117}	L_{117} (μH)	R_{117} (Ω)	C (pF)	RQ (Ω)
P1	3.02	1.27	29.80	17.42	93.20	718.14
P2	4.77	1.20	17.32	10.67	64.28	622.91
P3	2.43	2.56	19.59	5.7	219.02	765.55
P4	3.02	1.08	20.71	14.26	134.11	424.41
P5	4.88	1.00	12.02	8.99	88.46	366.85
P6	3.37	1.75	9.48	4.02	235.27	351.28
P7	3.02	0.69	7.50	8.01	370.31	98.48
P8	4.87	0.65	4.39	5.02	243.29	87.45
P9	2.77	3.54	10.78	2.26	306.24	664.17

4.1.1. Coil combination

As discusses in section 3.3 the coil P5 is currently the receiver coil of the device. This coil was chosen in part due to its round shape, of which the only competitors were P8 and P2. P2 has a larger Q factor

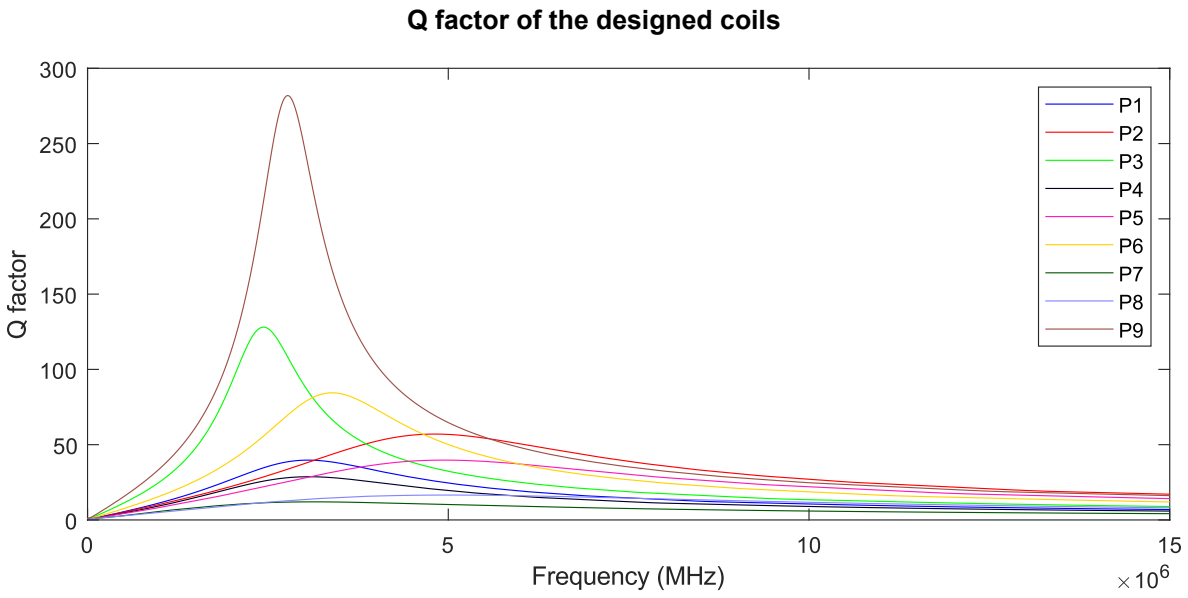

Figure 4.2: Q factor of the designed coil calculated based on measurements of the resonance frequency, DC resistance and Q factor at 117KHz of the coils

than the chosen P3 at the oscillating frequency of 117KHz which mean this would have been a slightly better choice in terms of power transfer. The reason P5 was chosen over P2 was the simplification of the design to a 2 layer process which also made the device less thick (0.1mm vs 0.2mm [59]) and therefore more flexible. P8 has a significantly lower Q factor, about half of P2, which is expected since it shares the same dimensions but has only half the turns. As a transmitter coil either P3 or P9 could be used since they both have a relatively high Q factor at 117KHz, P3 was chosen since its inductance was twice as high as P5 which would result in a relation which increases the current in P5 instead of an increased voltage.
based on table 4.1 the combination of P3 and P5 is a good combination, especially since it boosts the current to the receiver coil due to the difference in inductance. A good alternative could be using P9 instead of P3 as a transmitter coil since the Q factor at this value is very high.
Literature discussed in chapter 2 often uses a WPT frequency of 13.56MHz, which is another standard band for IoT or medical devices [67]. Although table 4.2 suggests that the Q factor of the coil might be higher at this frequency, using an inductor above its resonance frequency is highly discouraged since the parasitic capacitance dominates the behaviour, defeating the purpose of inductive resonant coupling. Table 4.1 lists the resonance frequencies of all coils, none are above 13.56MHz so the coils should not be used at this frequency. An explanation for why the existing devices are able to use this frequency can be found in the lower physical size of the coils allowing a lower flux and thus less energy transferred following equations 3.1 and 3.2.
Simulating the power transfer in LTspice using the new equivalent coil model yields no significant changes compared to the simulations from section 3.2.

4.2. Receiver

Electrical validation of the receiver can be done by manually inspecting the PCB, soldering the components in place, validating the connections using a continuity measurement and then placing it above a QI compatible wireless charger. If the receiver has been assembled well, the LED will start blinking at 1Hz due to the polling of the charger.
With the electrical design working the details about illumination, thermal performance and reliability must be evaluated. The sections which will make up the validation are:

- **Power transfer efficiency** where the efficiency of the DC to DC power transfer will be evaluated.
- **Light intensity** allows predicting the effectiveness of the OptoCoil during experiments and if the light source is stable and controllable as specified in requirement 4a and 4.

- The **thermal performance** discusses the thermal increase during operation and if requirement 2c and 2b is met

during these tests the transmitting frequency will be set to 117KHz, which is within the range of the Qi protocol as discussed in section 1.4. This frequency was chosen based on the resonance frequency of the Qi charger at hand and the tolerance of the resonance capacitor which was used.
Finally limitations and future work regarding the receiver will be discussed. The tested and assembled device is shown in figure 4.3.

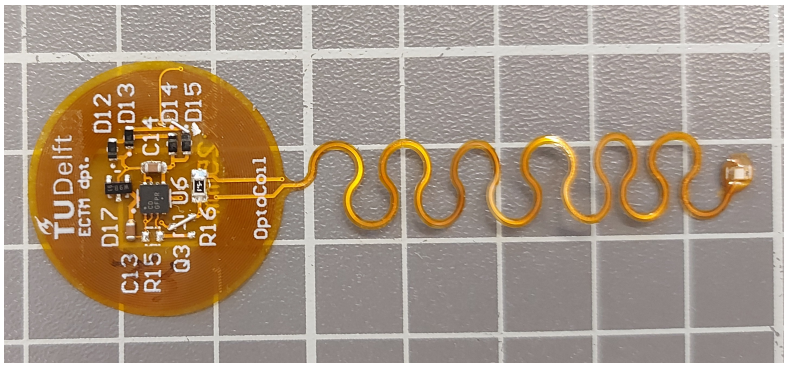

Figure 4.3: Assembled receiver

4.2.1. Power transfer efficiency

The efficiency of the power transfer is defined by the input power divided by the output power. Since for this application the goal is to use a DC power supply from a USB source or battery to light up an LED using a DC power supply, the efficiency will be determined from a DC-DC perspective. This approach will result in a lower efficiency than the AC-AC efficiency since the losses in the inverter and the rectifier are taken into account.
By determining the current through the resistor, the power delivered to the LED can be estimated. In this scenario all losses from the LDO and the rectifier are included as opposed to the estimation made in the design phase.
The coil voltage supply is set to 6.1V and delivers a current of 0.5A when energy is transmitted resulting in a P_{in} of 3.05W. The average current through the 5 ohm resistor and the LED is 52 mA (n=5, 95% CI $\pm$ 368μA), multiplying this by the output of the LDO, 3.3V, results in 172mW delivered to the LED, this is P_{out}. Equation 4.5 shows the relation between P_{in} and P_{out} to obtain the efficiency, η. Using aforementioned P values in equation 4.5 results in an efficiency of 5.6%.
Although this efficiency cannot directly be compared to the previous LTspice simulations due to the unknown value of the losses in the rectifier, it does indicate large losses in the transfer.

$$\eta = \frac{P_{out}}{P_{in}} \tag{4.5}$$

These large losses are to be expected because the transmitter coil gets notably warm when left on for longer periods of time, increasing its resistance (see equation 3.3) and thereby decreasing the efficiency even further. Replacing the transmitter coil with a commercially available Qi receiver coil results in lower heating and significantly higher efficiency, Table B.1. By decreasing the resistance of the receiver coil the efficiency can be increased even further, matching the efficiency obtained by commercially available Qi chargers [31, power-delivery.pdf, table 12].

4.2.2. Light intensity

The light intensity is controlled by a voltage source and a fixed resistor. This creates a smaller design but also adds a temperature dependency to the brightness of the LED since the current to voltage relation of the LED is temperature dependent. The light intensity drops from 2.99 to 2.87 mW/mm^2 during a 3 second pulse, a drop of 4% During a 0.5s pulse the intensity drops from 2.99 to 2.97 mW/mm^2, a decrease of 0.7%. The decrease of light intensity is caused by heating of both the LED and the

transmitter coil. Intensity was measured using a Thorlabs PM100D meter and a S130C light sensor, the data was exported to the SD card.

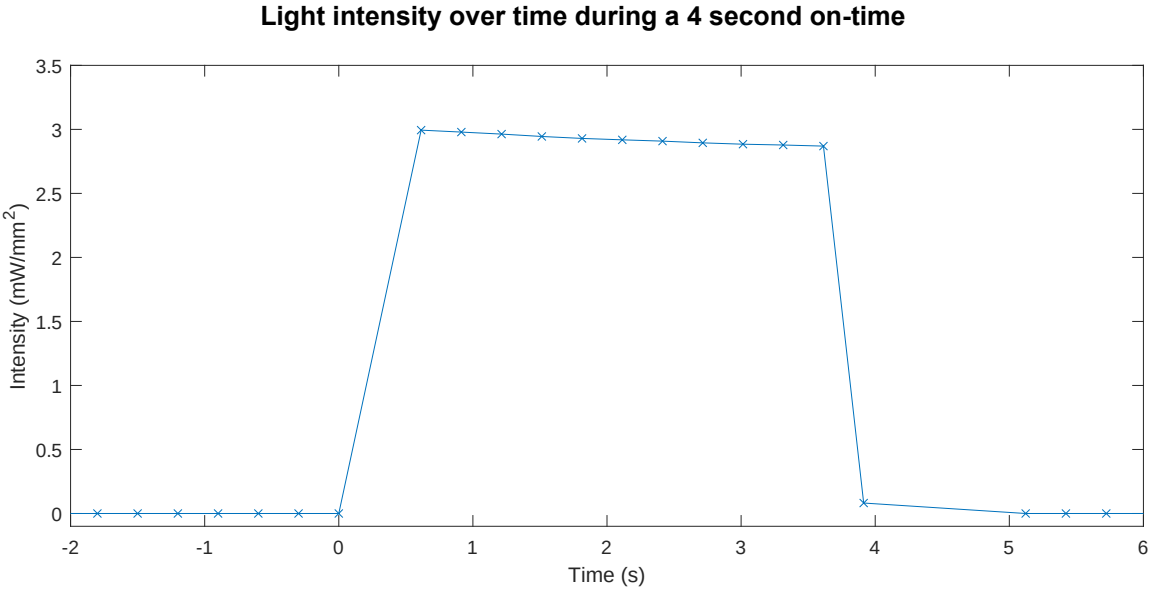

Figure 4.4: Light intensity during a 4 second pulse, measurements are marked with an 'x'

Figure 4.4 indicates a significant rise time of approximately 0.6 seconds, which would disallow short pulses of light required for the defibrillation protocol. Visual validation confirmed that the light did turn on during these pulses, raising the question of the actual rise time. To evaluate this the output of the regulator onboard the receiver was connected to an oscilloscope and 3 separate measurements were performed. These measurements resulted in an average rise time of 0.3ms (2%-90%, n=10), which confirms the receiver can be used for short pulses of illumination.

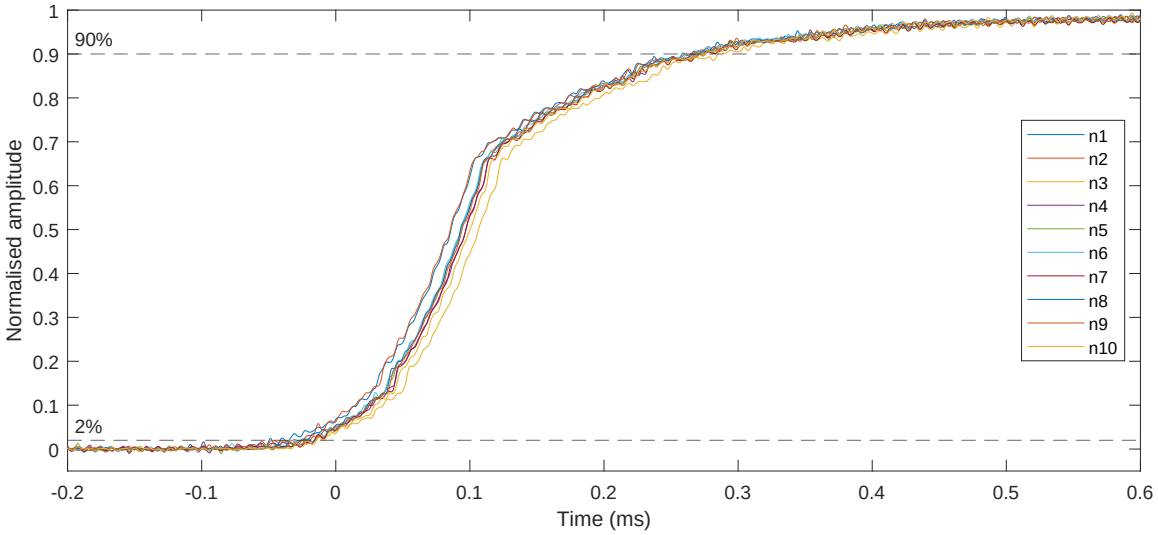

Figure 4.5: Rising edge of the coil, normalised for maximum intensity, n=10. The oscilloscope trigger is set at t=0 ms. The rise time has been defined as the time between 2% and 90% of the maximum value. The 95% confidence interval (CI) for the rise time is between 0.288 and 0.300 ms with an average of 0.294ms.

4.2.3. Thermal performance

Since the receiver is in close contact with the heart tissue, the increase in temperature must be closely monitored. Figure 4.6 shows the infrared images of the passive receiver before and after a 500 ms period of illumination. Since the emissivity, the effectiveness in emitting thermal radiation, is not calibrated perfectly only the relative temperature measurements are accurate. A single pulse of 500ms shows an increase in temperature of 3.2°C at the front of the LED and 1 °C on some parts within the receiver coil. The increase in temperature of the LED is present at the surface of the led but not at the surface of the biocompatible coating covering the LED since this coating is transparent to infrared wavelengths. The biocompatible coating, which will be discussed in section 5.1, will act as a heat spreader lowering the temperature at the interface between the device and the cardiomyocytes. Figure 4.7 demonstrates that the maximum temperature increase at the surface of the LED is below 1.8°C with a 95% confidence interval. The temperature increase of the coil is localised to the traces leading to the diodes of the rectifier, this information should be used in future designs to widen the traces. Behind the receiver coil a rectangular shape becomes visible in figure 4.6b. This is the transmitter coil which heats up significantly faster than the receiver due to the large current flowing through it. For short pulses like the 500ms ones this temperature is negligible since its on the outside of the body, however sufficient time to cool down should be provided before repeated optical stimulation.

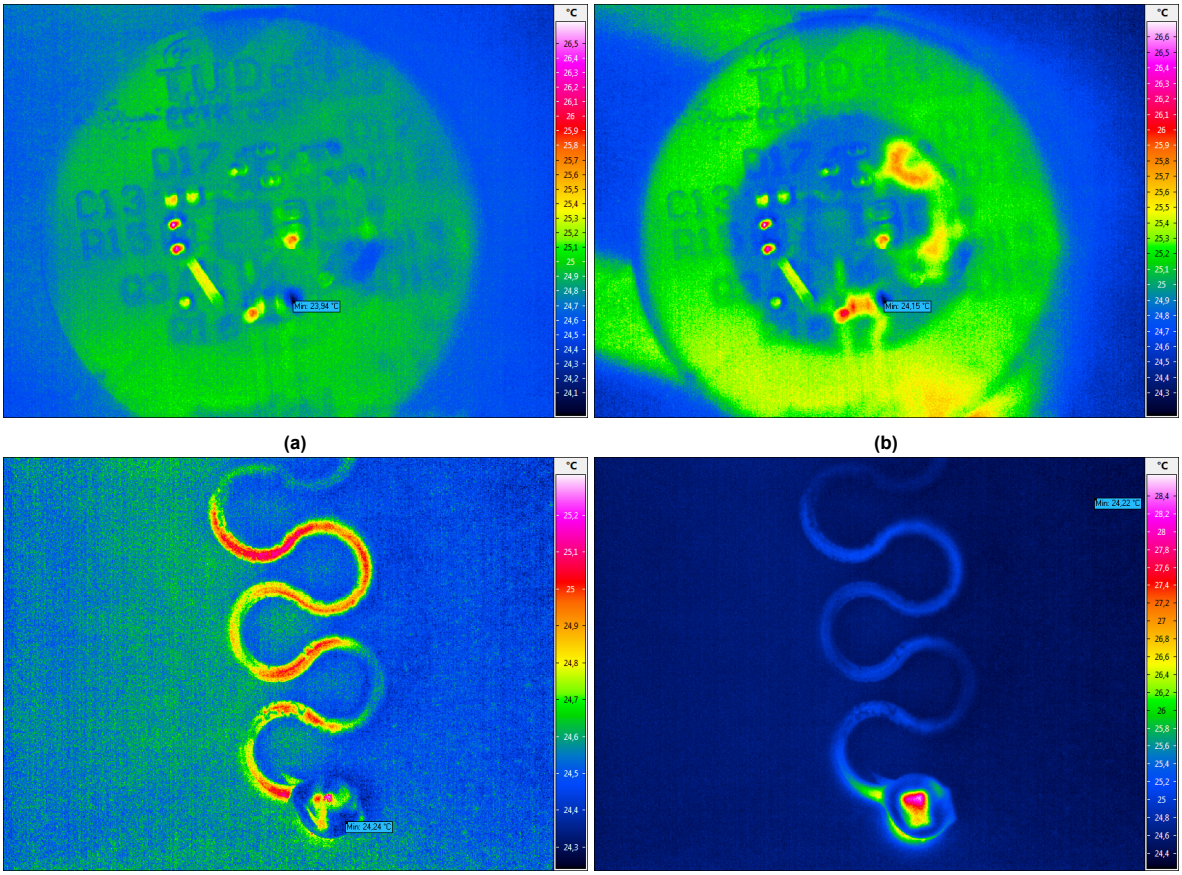

Figure 4.6: **(a)**, **(b)** Infrared images of the coil and **(c)**, **(b)** the LED at t=0 **(a)** and t=0.5s **(c)** and **(b)** and **(d)**. A temperature increase of 1 °C at the coil and 3.2 °C at the LED is measured

CEM43°C

The cumulative equivalent minutes at 43°C (CEM43°C) can be calculated using equation 4.6 [68]. Since the temperature never exceeds 43°C, the value of R is 0.25. The time interval used is 200 seconds, this interval was chosen since this is the time required to return to a 0°Cincrease in temperature as shown in figure 4.7. The average temperature increase over the results from figure 4.7 was calculated using MATLAB where 37°C was used as a baseline. The results of equation 4.6 are a CEM43°C

of 0.00085 minutes when using the average temperature (black line from figure 4.7). A CEM43°C of 0.0011 minutes was achieved when using the upper bound of the 95% confidence interval, concluding the design is well within the 128 minutes of requirement 2c.

$$CEM43 = \sum_{i=1}^{n} t_i \cdot R^{(43-T_i)} \tag{4.6}$$

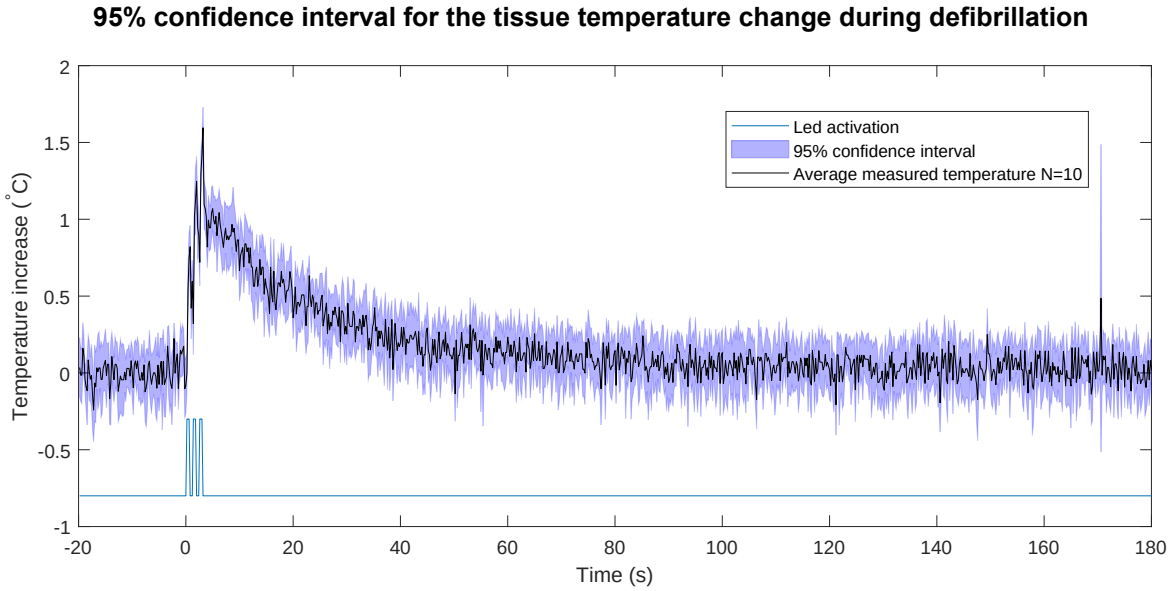

Figure 4.7: Temperature measured using a chicken thigh at 37°C as environment during 3 pulses with a duration of 500ms and a 500ms interval.

4.2.4. Mechanical reliability

In order to evaluate the effect of repeated movement on the meandering structure, a test setup as shown in figure 4.8 was placed inside a temperature chamber and kept at 37°C for a period of 15 days where the serpentine structure was stretched and compressed 600 000 times between 0 and 20 % of its original length. Resistance measurements were taken using a Keithley 2450 SourceMeter which continuously supplied 1mA through the copper wire embedded in the structure. The current used to perform this test is significantly lower than the current used when the device is optically stimulating because the measuring current is constantly applied whereas the activation current is only supplied for very short periods of time with a very large interval between pulses. This measurement is focused on resistance increase caused my metal fatigue instead of degradation due to high currents.
Manual testing showed that permanent deformation occurs beyond a stretch of 20%, this value has thus been defined as the elastic limit of the structure and will be used as a stretch limit for this experiment. The Expected result based on [40, supplementary Fig. 2] was a breakdown around day 6. Figure 4.9 shows that after 600 000 cycles the resistance of the wire has not significantly increased: Outliers are within +1.8% and -0.4% of the median value of 1.095Ω. A slight change of the median values can be observed but no significant increase in resistance is observed.

Limitations and future work

The serpentine structure didn't break in this setup, making this an incomplete experiment. This experiment should thus be repeated with adjusted parameters to say anything definitive about the reliability of this design:

- Same setup but continued until it breaks.
- Increased temperature. This would require making the setup out of a different material than polylactic acid (PLA), which has a glass temperature around 60°C.

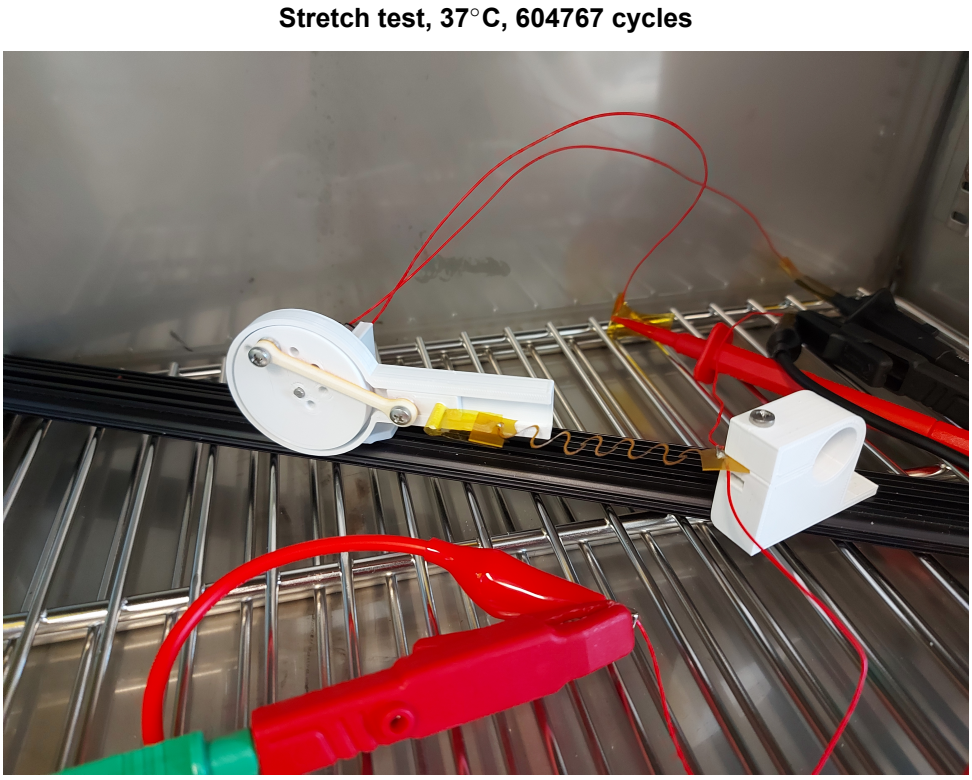

Figure 4.8: Repeated stretch setup using a 30 revolutions per minute (RPM) motor attached to a piston creating a linear movement of $\pm$ 1cm

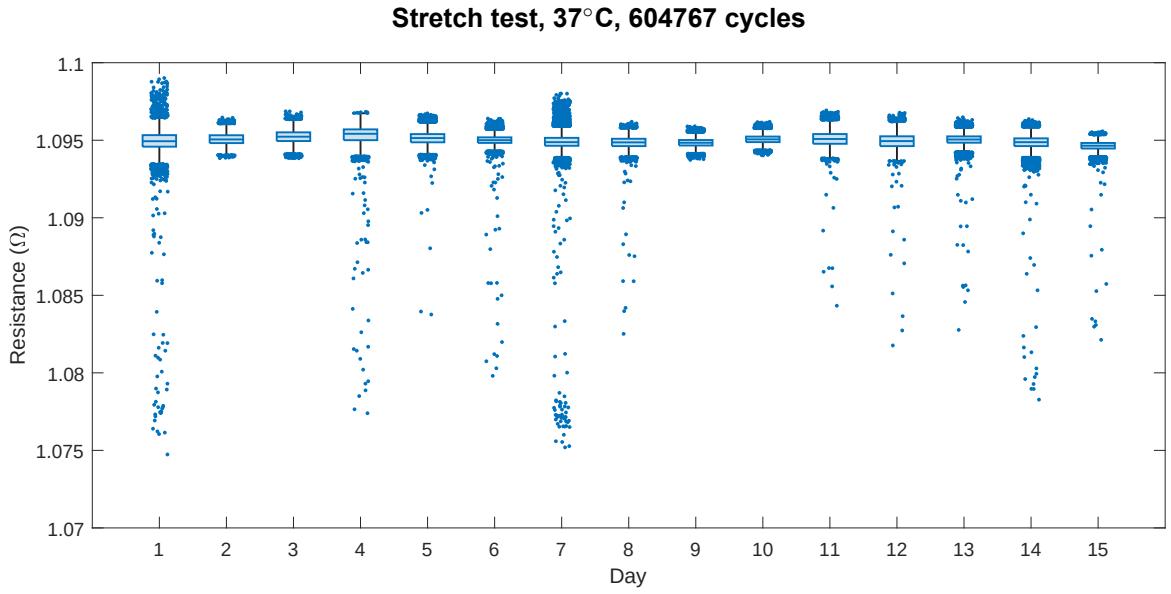

Figure 4.9: Resistance during stretch test per day. measurements per day except day 1 and 15: 76260 ± 20. measurements day 1: 43050, measurements day 15: 32980. Each measurement consists of an average of 5 measurements.

- Increased current/pulsed current. This would heat the serpentine structure and would thus not only be an experiment about metal fatigue anymore. Depending on the magnitude and frequency of the pulses, it could be compared to long-term ambulatory experiments.

Without these changes it can only be concluded that the structure is reliable enough for ambulatory experiments which either don't exceed 600 000 stretches or last a maximum of 2 weeks.

4.2.5. Future work

During the design and manufacturing of the receiver an issue occurred where a piece of copper from the coil was not connected to a trace. This was resolved by manually adding a thin wire between a connected pad the the diodes but sacrificed the resonance capacitor of the receiver. Simulations suggested that this was acceptable since the loss of efficiency would be low, all measurements have been performed with this adjustment. A next iteration should add back this capacitor to increase the distance between the coils before the light output decreases.
The MOSFET controlling the LED was also left out of the design due to an error in the datasheet of the LDO. The datasheet suggested that the function of the PG pin is exactly reversed as opposed to how it actually functions thus turning the LED on only when the voltage output of the regulator was below the threshold.
This was resolved by removing the MOSFET and shorting its drain and source pads using a thin wire. benefit of this approach is that it allows for variable light intensity by adjusting the transmitter coil voltage or distance between the coil.
Future iterations might not require this MOSFET which allows decreasing the size of the receiver coil. The inductance value and Faraday's law of inductance (equation 3.2) must be kept in mind when re-designing a smaller receiver.

4.3. Transmitter

This section describes how the hardware and firmware of the transmitter responds to decide if the requirements are met and if the transmitter is working well enough to be used for actual experiments. For the first experiments, the boost converter and battery charge IC are not required, they will be left unpopulated, requiring a USB power source and an external power supply to energise the coil.
Although the battery connector was not required, the setup used for automated testing at the lab uses MC stimulus II to trigger separate devices which added the requirement for an external trigger. This was realized by using the battery sense connector which was connected to pin 34. R4 and R5 can either be used as a voltage divider to allow an input voltage above 3.3V or as a pull-down since this hardware is not included internally in pin 34. Figure 4.10 shows the transmitter as used during the experiments.

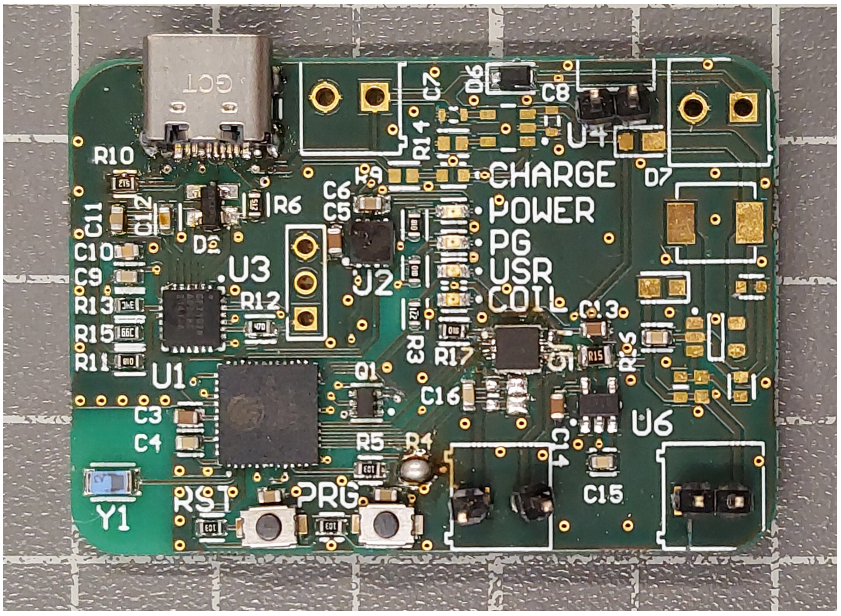

Figure 4.10: Partially assembled transmitter placed on a centimeter grid. The screw headers have been replaced by header pins to allow connecting the transmitter without requiring a screw driver. The boost circuit has not been populated to allow an external power supply to be used for the coil. The battery charging circuit has been repurposed into an external trigger

An initial test of the USB user interface is performed when first connecting the transmitter to a computer to flash the firmware to it. The firmware from appendix C will be used to test the all individual modules

of the transmitter and output the results to the serial monitor during operation. When the coil driver is validated and activates when desired, a coil and power supply for the coil are connected. The maximum voltage and current of the power supply is limited to 6V and 0.8A to prevent overheating, these settings proved able to light up the LED from the passive receiver even at a few millimeters distance. Unless mentioned otherwise, these are the settings used in all further experiments.
Tests include measurements through a dummy load and validating both current, voltage and frequency. If all components are working correctly, wireless power transfer with a dummy load connected to the receiver will be attempted in order to characterize the power transfer.
A higher switching frequency decreases the losses in the magnetic core [69] which is why initially a transmitting frequency of 500KHz was used. At this frequency the coil driver IC noticeably got warm which suggested increased losses in the inverter, therefore decreased efficiency. For this reason the frequency was lowered to 117KHz as described in the introduction of this chapter. Figure 4.11 demonstrates the waveform measured at the output of the transmitter, the interval of 8.54 μs confirms that the set frequency is met.

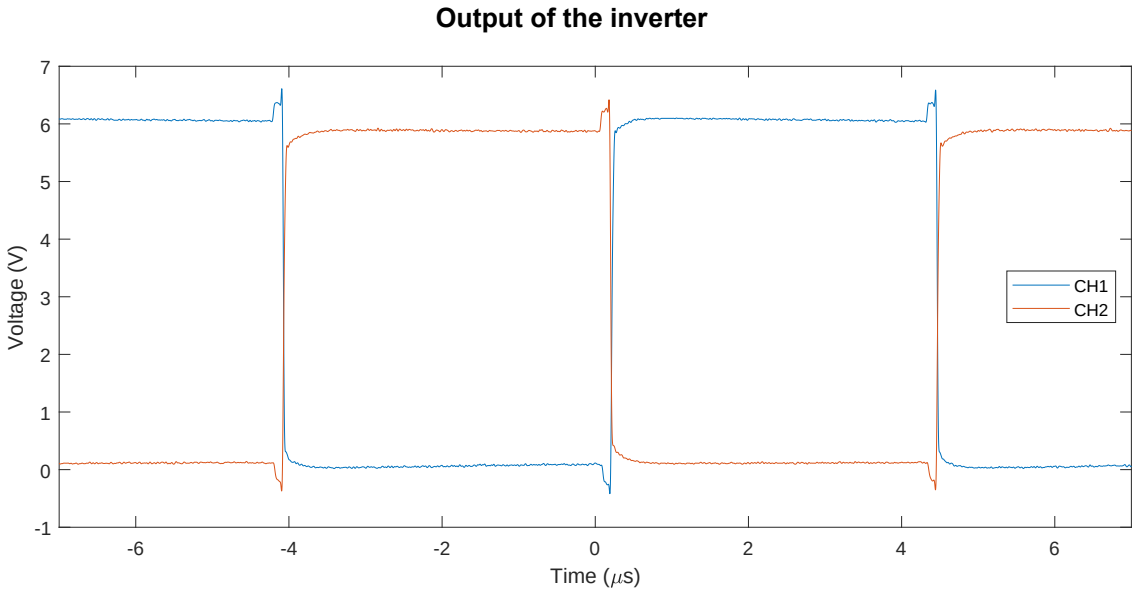

Figure 4.11: Output of the inverter of the coil driver. The coil voltage is set to 6.1V

Future revisions should remove the boost converter and battery charging circuit and instead include a galvanic isolation for the external trigger. Larger buttons would also be a nice addition, mounting holes and an enclosure are also good additions for future revisions.

4.3.1. Future improvements

The current implementation of the external trigger has a very small tolerance since it's directly connected to a GPIO on the microprocessor. Any voltage above 3.5V will permanently damage the microprocessor, any voltages below 2.5V are not registered as a logical high. Future revisions should include a dedicated external trigger which is galvanically isolated using a buffer or an an optocoupler. This would ensures no damage to the processor can occur as a result of an external trigger or large capacitive/inductive leads.
Future versions should not include a battery charger and should instead focus on a controlled battery discharge by adding a Battery management system (BMS). The idea of charging the battery using the same USB port as the serial interface is nice for development modules but will in practice rarely occur.

4.4. Conclusion

The OptoCoil system has been validated and verified to be working correctly. The light intensity obtained from the coil has a time dependent decrease but with a decrease of less than 1% this will not be a significant influence on the experiments, satisfying requirement 4a.

A rising edge of 300 μs has been measured. This rising edge is 0.6% of the 50ms pulses used during pacing which means the response time is high enough to accurately pace and can completely be neglected during defibrillation, satisfying requirement 4b.
Since the receiver has a diameter of 27mm and the tail is flexible enough to pass through the ribs to the heart, requirement 1 and 3 regarding the location and size have also been met. A CEM43°C value of 0.0011 with a 95% confidence interval is well below the limit of 128 minutes and the maximum temperature increase of just under 2°C leaves the cardiac tissue at a safe temperature satisfying requirements 4.6 and 2b. Requirement 2a is yet to be satisfied, this part will be explored in chapter 5.

5 Application

Having a validated system means the OptoCoil can be used in biomedical research and experiments. This receiver is an implant, meaning it will be completely contained within the body and will thus be in contact with both tissue and bodily fluids.
The larger island of the receiver containing the coil will be implanted subcutaneously but as close to the surface of the skin as possible. The serpentine wire, referred to as the tail, will then pass in between the ribs and lungs to the heart. The tail is a springy structure structure and should be fixed to surrounding tissue to prevent it from moving around too much when the LED at the end of the tail is attached to the right atrium. A schematic drawing of the device after implantation is shown in figure 5.1.
Electronics and conductive materials like wet tissue generally don't combine well which is why a coating is added to the electronics to isolate them from the body. From a body perspective this bio-compatible coating is required since the sharp edges of the components and the metal of the solder joints can damage the tissue over time or cause accidental electrical stimulation. A commonly used coating for these applications is polydimethylsiloxane (PDMS). The first section of this chapter will describe the preparations required before the system can be used during in vivo or ex vivo experiments. After the preparations the experiments, their setups and the obtained results will be discussed.

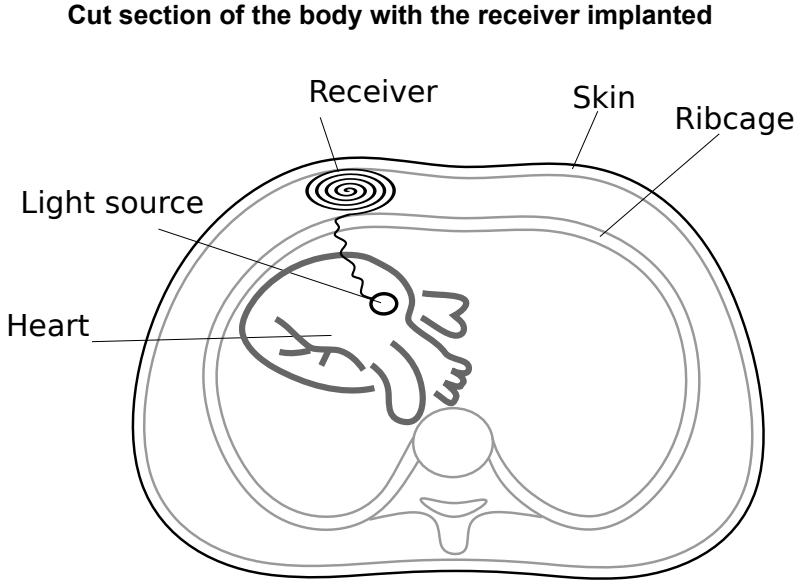

Figure 5.1: Schematic drawing of a cut section of the thorax demonstrating how the device will be implanted

5.1. Biocompatible coating

A biocompatible coating is the interface between the bodily tissue and the electronic implants such as the OptoCoil receiver. This coating is required because, as mentioned in the introduction of this section, electronics can be damaged by bodily fluids but the metals and compounds used in the electronics can also poison or damage the body over time.
Literature shows 4 types of bio-compatible coating for electronics which are often used by themselves or in combination with others on the list[34]–[36], [40], [43], [50], [70], [71]:

- Polydimethylsiloxane (PDMS)
- Parylene C
- EcoFlex
- Polyisobutene (PIB)

Out of these, parylene requires chemical vapor deposition (CVD), all others are a type of silicone. PMDS, specifically Sylgard 184, is the most often used biocompatible coating since it's the easiest to process and will be used to coat the receiver. It consists of two separate components which are mixed in different ratios to obtain a different level of flexibility [72]. To validate if PDMS can create a waterproof seal with the polyimide (PI) substrate of the receiver pieces of PI tape with silicone adhesive on one side (kapton tape) were used. The surface of the PI out of which the receiver is made is smooth and chemically resistant making it difficult to permanently adhere anything to it. Different techniques exist to bond them together [73]–[75] but they require chemical bonding, plasma surface activation or high-intensity lasers or to do so, adding complexity to the coating process. Initial tests will be performed without surface activation since the contour of the coil of the receiver is mostly closed which could allow the PDMS to fully encapsulate the coil and therefore not needing a surface activation.
The LED of the receiver will be coated using the Thorlabs optical UV glue NOA81 which has been cured under a UV light for 10 minutes. This coating will create a solid dome covering both the LED and the solder joints.

5.1.1. PDMS/PI adhesion

This experiment aims to find the optimal mixing ratio between the PDMS base and curing agent where delamination of PDMS from the PI sheet is minimal. The idea is that a higher base to curing agent ration would increase the flexibility and stretchability of the PDMS, making it more difficult to peel off. The materials used for this experiment were:

- Kapton tape, 0.1mm thick
- Temperature chamber, 60 degrees Celcius, 3 hours
- PDMS mixed at a curing agent to base ratio of 1:10, 1:15, 1:20 and 1:25

The PDMS will be mixed, degassed and stored in separate containers. The PI sheets are degreased using isopropyl alcohol (IPA) and afterwards partially submerged in the PDMS mixture. A small part will intentionally be left out of the PDMS to evaluate a transition area between PDMS and PI. This is required because the design of the passive receiver will only have PDMS coverage on the coil and components while the serpentine tail and the LED itself will not be covered in PDMS. The PDMS coated PI sheets will afterwards be cured in an oven at 60 degrees C for 3 hours.
When the PDMS is fully cured, the PI will repeatedly be bend, twisted and rotated to provide an extreme environment.

Results

Due to the low thickness of the PDMS layer, delamination by means of bending does not occur independent of the mixing ratio. Firmly rubbing the PDMS coated PI sheet in between your fingers however removes the PDMS coating in a matter of minutes. The PDMS is not firmly attached to the PI but instead covers it by wrapping around the edges. This is however only true for the side of the PI where no adhesive is present; The adhesive side of the PI cannot be separated from the PDMS without rupturing it.

5.1.2. Liquid ingress

Due to the transition area between PDMS coverage and uncovered PI, there is a risk of liquid ingress between the PDMS and PI sheet. If this happens, the possibility for body fluids and tissue to come in contact with the electronics exists and additional steps are required to properly seal this area. To test the ingress of liquid in between the PDMS and PI, the samples will be submerged in a colored liquid for a longer period of time. Both discoloration of the cured PDMS or ingress of the colored water between PDMS and PI could be cause for further experiments. This experiment will be performed using both newly cured PDMS-PI sheets as well as the sheets used in the bending test before, provided no visible delamination occurred.
As a second step to this test, a dummy receiver with some components present will be used in the same colored liquid. The reason this might yield a different result compared to the kapton tape could be the absence of glue on 1 side or the much smaller opening through which water could get into the coating. Peeling the PDMS off of the dummy coil will likely be more difficult due to the vertical structures (components) soldered to it. Coating was done by dipping the coil into the PDMS while holding the serpentine structure and using this structure to support the coil during the curing process.

Results

The PDMS coated PI pieces were left in a 50-50 mixed liquid of ethanol and DI water over a period of 15 hours. No discoloration of the PDMS or water in between the layers was observed although gently drying the pieces with a piece of paper towel separated the PDMS from the non-adhesive side of the PI tape suggesting that the coating is affected. The glued side stuck again very well to the PDMS and separating the two was not possible. Different effects between previously used pieces of PI or newly coated was not observed.
The dummy PCB did not show any signs of liquid ingress although the PDMS could relatively easily be removed by rubbing the PDMS when a rupture across the perimeter was created. As long as the perimeter was intact, the coating remained in place.

5.1.3. Conclusion

A sufficient coating for short experiments can be achieved by dip-coating the PCB with 2 layers of PDMS while suspending them by the serpentine structure during coating and curing. After dip coating the PCB it is hung by the tail again and cured at 100 °C for 1 hour. The first cured PDMS layer is very thing and cover almost all components, some corners of components are not fully covered, these corners are on the tail side of the PCB. In addition there is a difference in PDMS thickness between the PCB edge which is facing up during curing and the edge which is facing down: The upper edge has a very thin coating which can easily be broken or rubbed off when touching it. The edge facing down has a much thicker coating which cannot easily be removed. Future designs should include short PI arms to hang the coils at different angles during the curing process for a more even coating.
The mixing ratio between base and curing agent effects the flexibility of larger volumes of PDMS but has little to no influence for thin layers like used in this coating.

5.2. Experiments

Throughout this report the term in vivo and ex vivo have been used without actually applying them. In vivo experiments are defined as experiments conducted within the complete body of a living organism. Ex vivo experiments are experiments performed on tissue or organs which have been taken out of the organism and placed in an environment which mimics the natural environment. In vivo experiments are better translatable to clinical applications compared to ex vivo experiments because every aspect of an organism is taken into account. Ethically in vivo experiments require more attention compared to ex vivo experiments since the organism is alive during the procedure, any impact the experiment has will directly be experienced by the organism. For this research rats were used as a model organism. The research is conducted on their hearts meaning that precautions must be made to ensure the animal does not experience any pain during the in vivo procedure. At the end of an in vivo experiment the heart is explanted and used for ex vivo experiments in order to maximise the amount of data that can be obtained from a single organism. The in- and ex vivo experiments are discussed in more detail in sections 5.3 and 5.4 respectively.

5.2.1. Methods

During the experiments there are 2 methods by which both the optoresponse of the heart and the function of the OptoCoil is evaluated:

- Pacing, stimulating the heart at a slightly higher frequency than the normal sinus rhythm. A 50ms pulse followed by a 100ms interval is used.
- Defibrillating, restoring the normal sinus rhythm after atrial fibrillation occurs. The defibrillation protocol consists of 3 500ms pulses with a 500ms interval between them as shown in figure 5.2.

The optoresponse of the heart will be evaluated using the Thorlabs M470L3-C4 light source with a controllable light intensity. The external trigger of the LEDD1B LED current driver is connected to MC Stimulus II to accurately illuminate the heart. The light pulses of the OptoCoil system will be controlled by the external trigger of the transmitter connected to MC Stimulus II. The waveform generated by MC Stimulus is added as a separate channel to each ECG recording to show when the light was on. The amplitude of this pulse is not correlated to the light intensity.
The ECG will be recorded using LabChart 8 connected to an AD PowerLab 15T data acquisition device. For the ex vivo experiments a 2 wire ECG is recorded, for the in vivo experiment this is a 5 wire recording interpreted by the Eindhoven triangle method, resulting in 3 separate traces in the recording.

Atrial fibrillation

To induce AF, electrical burst is used with a 10ms on and 20ms off time which is repeated for 3 seconds. The pure metal probe used to induce is placed on the atria after which MC Stimulus and the Multichannel STG4002 is used to supply the signal. An arrhythmia is considered sustained if it is maintained for over 10 seconds, at this time the defibrillation protocol will be triggered. Auto termination is defined as the restoration of the normal sinus rhythm without external intervention. If the AF auto terminates within 10 seconds the defibrillation is manually canceled. A successful defibrillation means that a normal sinus rhythm is restored within 1 second after the last pulse as shown by the black arrow in figure 5.2. Should the OptoCoil fail to defibrillate after multiple attempts, an electrical defibrillator is used to shock the heart back into sinus rhythm.

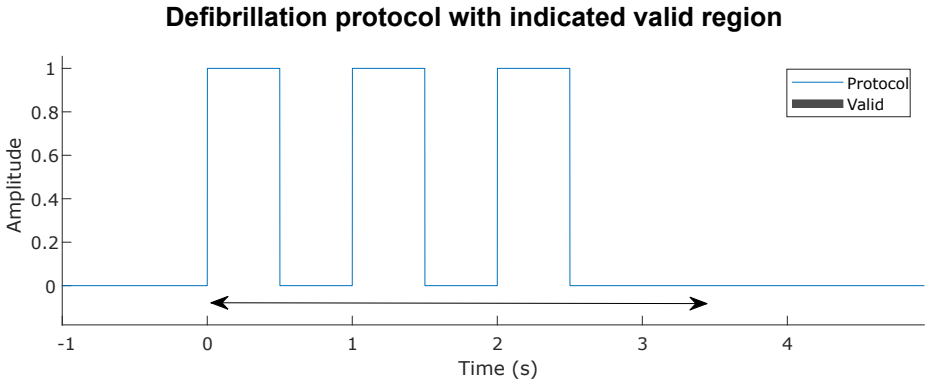

Figure 5.2: Defibrillation protocol. Every termination within the black arrow counts as a successful termination

Pacing

Pacing is the process of artificially creating pulses at a known rate. When pacing the atria, an artificial P wave will proliferate from the atria via the AV node and result in a QRS complex and thus a heartbeat. To distinguish between heartbeats originating from the sinus node and the pacing, a frequency is chosen which is slightly higher than that of the normal sinus rhythm.
To test the optoresponse of the right atrium it will be paced at a frequency slightly higher than the normal sinus rhythm which should show the heartrate increasing to the pacing frequency if an optoresponse is present. The possible outcomes of pacing the right atrium are:

A) Each pacing pulse results in a QRS complex, the heartrate follows the pacing perfectly.
B) Some of the pacing results in a QRS complex, this is called partial following.

C) The heartrate is completely unaffected by the pacing, meaning no optoresponse is present.

The pacing threshold is the minimal required light intensity to have a heart completely follow the light pulses. This threshold is dependent on the expression of the optotool in the right atria since a higher expression will result in a larger current flow upon illumination as demonstrated in figure 5.3

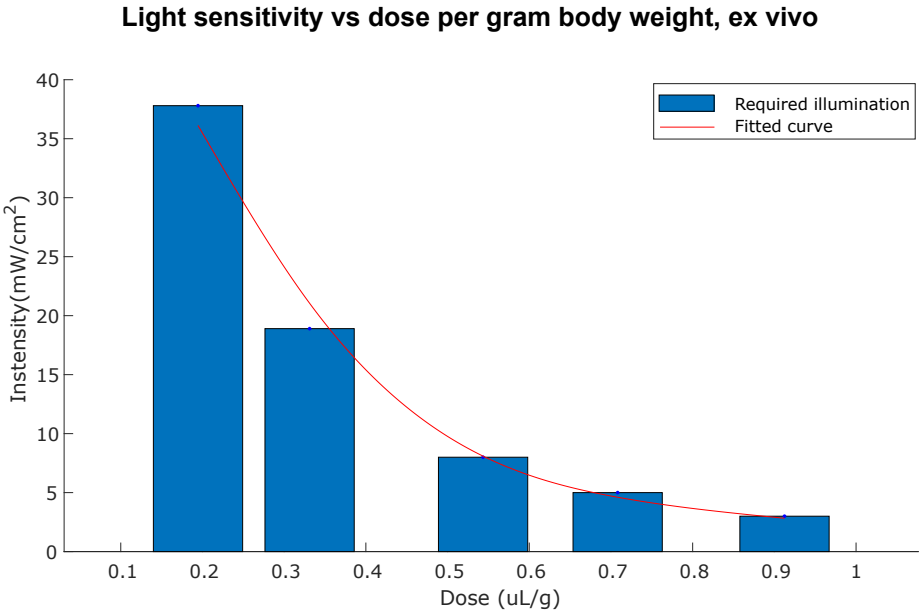

Figure 5.3: Required light intensity for a complete following of pacing. The injected dose has been normalised over the body weight and contains the NPPA promotor

5.3. In vivo

In vivo experiments are experiments where the device will be tested inside of a living organism. Such an experiment is a good comparison to clinical applications since every aspect of a living organism is included. The aim of the experiments is to optically pace and terminate atrial fibrillation using optoCoil. During the in vivo experiments the animal will be under full anesthetic and intubated after which a thoracotomy is performed: Some ribs are cut and the ribcage is then folded open to reveal the lungs. In order to get access to the right atrium of the heart the right lung must be punctured. These actions are incompatible with life and are only performed because this is a terminal experiment.
The experiment setup is shown in figure 5.4. This figure shows the sedated and intubated animal to which two separate ECG measurements are connected:

- A 5 channel ECG used as a reference. This ECG consists of 5 needle probes connected to the leg and neck muscles of the animal. The needle probes are the red, yellow, black, blue and green wires and are used to construct a 3 channel output according to the Eindhoven triangle.
- A custom made subcutaneous ECG measurement which functions as AF detection and trigger for the OptoCoil. The wires connected to this device are the green ones connected to the small green PCB near the tail.

In addition to the ECG measurement devices, figure 5.4 shows the optoCoil transmitter and receiver taped together. The LED of the optoCoil will be manually positioned over the heart to find the spot where, upon illumination, an optoresponse is measured. When this position on the right atria is found, the LED is glued there using Braun Surgical histoacryl glue to prevent it from slipping off due to the movement of the animal.
When pacing the right atria a partial following of is observed. Although the heartrate is influenced, it is not occasionally missing a beat making the RR interval the strongest indicator for the optoresponse. Figure 5.5 shows the ECG recording in the first 3 channels, the light source trigger on the 4th channel

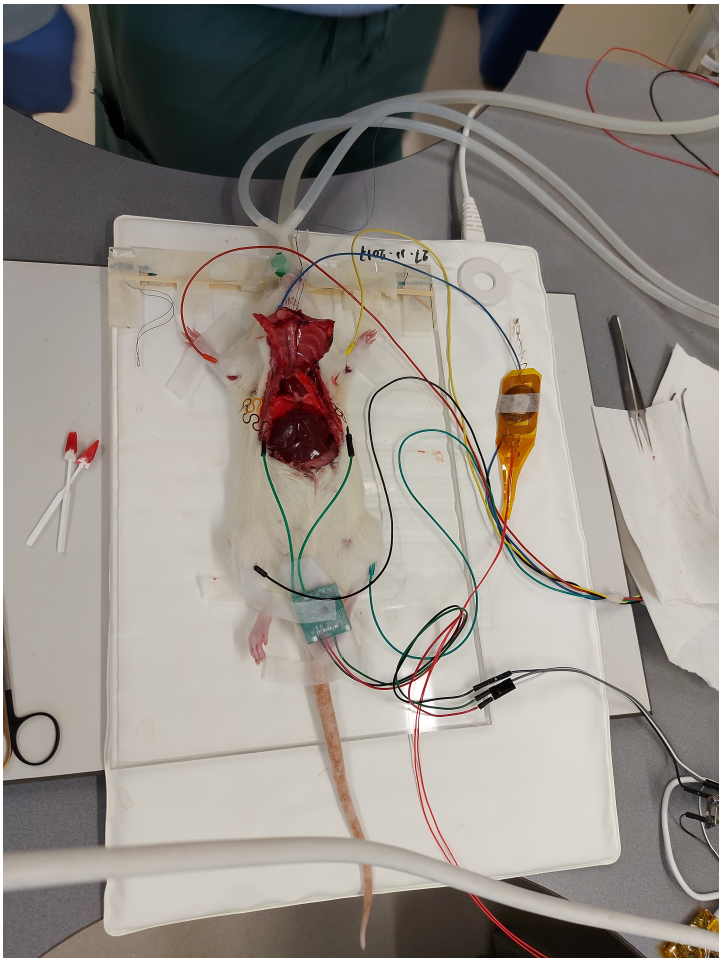

Figure 5.4: In vivo setup with a thoracotomy performed on the intubated, subconscious animal

and the 5th channel shows the RR interval calculated by LabChart based on the detected QRS complexes indicated by the green dots above channel 1. The RR interval is stable around 0.16s before and after pacing while during pacing the interval fluctuates between 0.11 and 0.17.
Using a different promotor expression in the ventricles was achieved as well. Optical pacing resulted in the heartrate perfectly following the pacing as shown in figure 5.6. This experiment shows that the optoresponse is largely dependent on the promotor and, when using one that is sensitive enough, the desired results can be achieved, even in much thicker muscles like the ventricles compared to the atria.

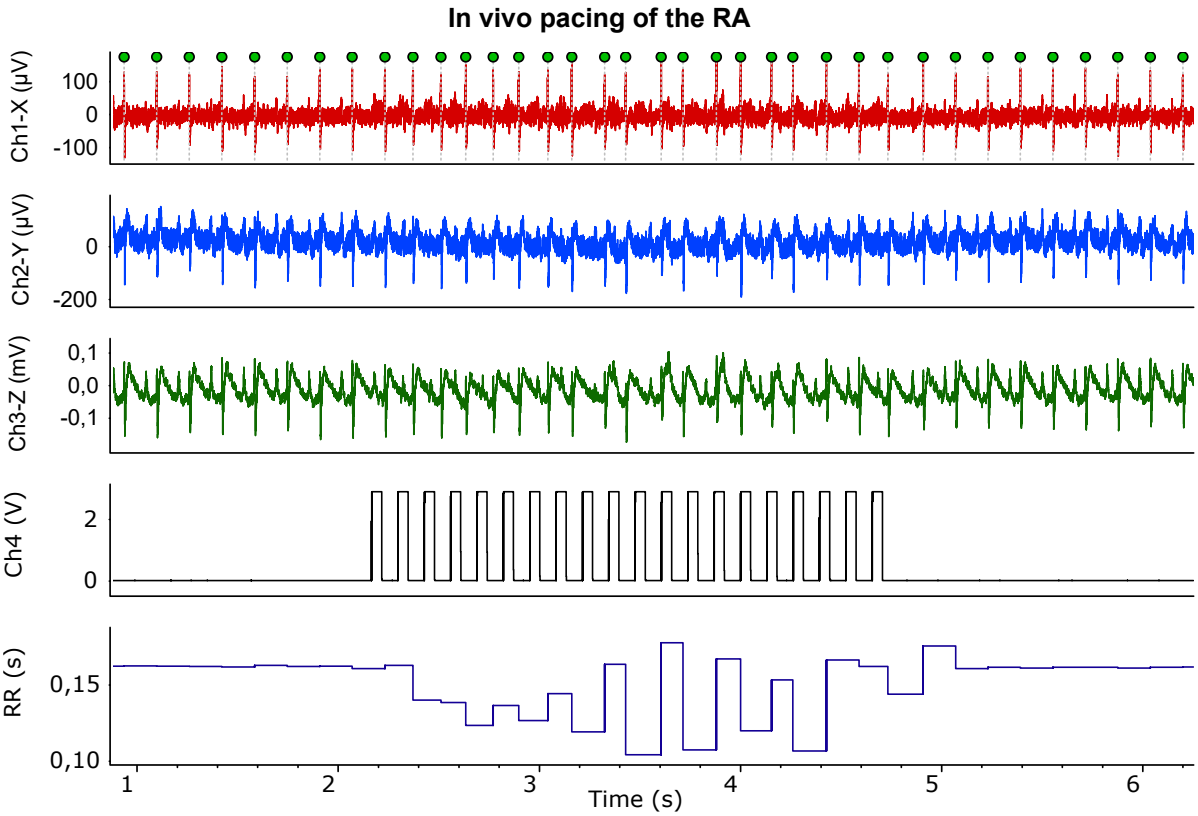

Figure 5.5: In vivo optoresponse of the right atrium. The green dots above channel 1 indicate the detected heartbeats on which the RR interval from the lowest channel is based. Channel 1-3 are the Eindhoven ECG leads, Ch4 is the external trigger of the Thorlabs light source. The rat was injected with 250uL of viral vector containing the NPPA promotor via the tail vein

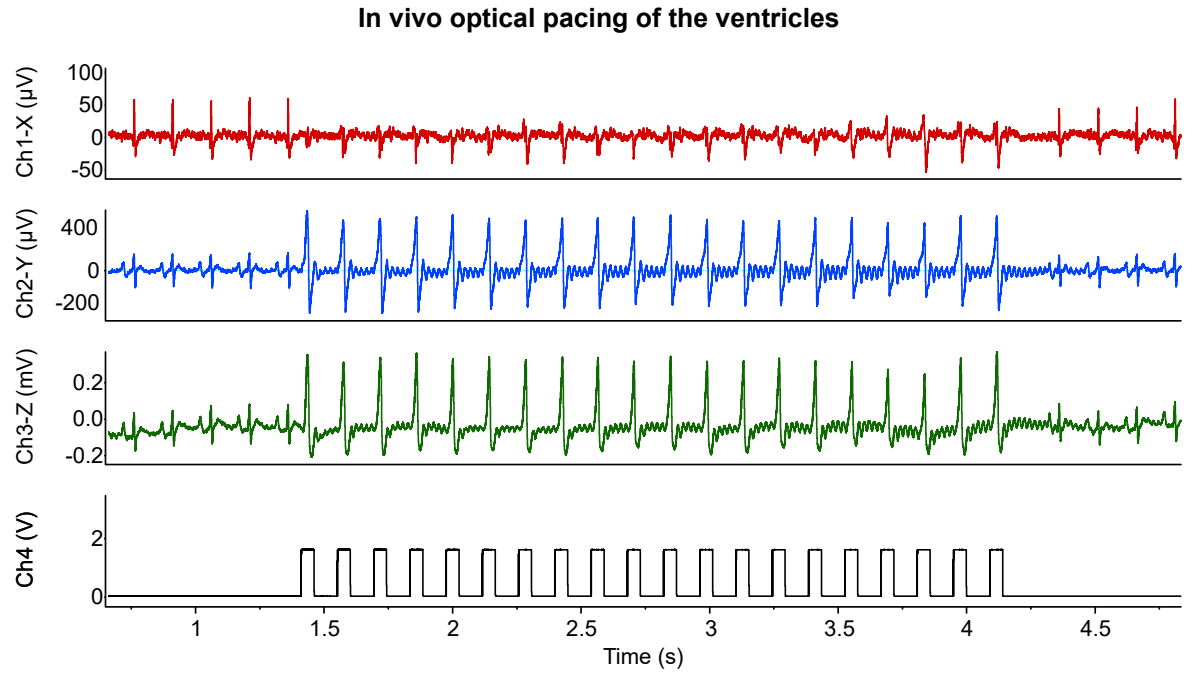

Figure 5.6: Pacing the ventricles in vivo. 250uL of the viral vector containing the myh6 promotor was injected via the tail vein

5.4. Ex Vivo

The heart which was used during the in vivo experiments from section 5.3 is explanted at the end of the in vivo experiment to be used in ex vivo experiments directly after.
A Langendorff heart setup with an explanted heart, OptoCoil receiver and wires to external devices is shown in figure 5.7. In a Langendorff setup the heart is continuously perfused via the aorta using Tyrode's solution allowing it to keep contracting outside of the body for multiple hours. The stimulation LED of the OptoCoil receiver is glued to the right atrium using histoacryl glue. The power receiver coil is taped to the outside of a container in such a way that minimal pressure or torsion is applied to the heart via the serpentine structure, the transmitter coil (not visible in this figure) is aligned over the receiver at varying distances.
The red and green wire in figure 5.7 are needle probes used to measure the ECG which will be used to determine if AF is present. The orange wires are connected to a platinum probe which electrically stimulates the heart to induce arrhythmias.

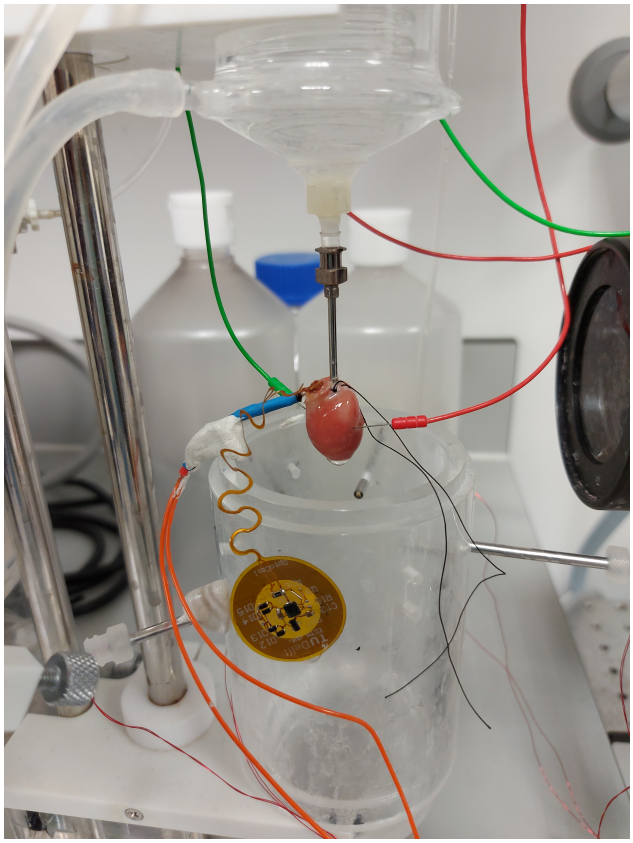

Figure 5.7: Langendorff heart setup with a rat's heart

5.4.1. Pacing

When the heart has been attached to the Langendorff setup and a normal sinus rhythm is observed, a first test is optical pacing using the protocol mentioned before. Optical pacing and the used protocol has been discussed in section 5.2.1, figure 5.8 demonstrates a perfectly following heart. The three contractions before and after the optical pacing are used as a reference for the sinus rhythm before and after pacing and show there is no lasting effect of the pacing. If, like during the in vivo experiment, some of the faster contractions are missing, that is called partial following. The critical pacing thresholds from figure 5.3 has been constructed by pacing with decreased light intensity until one or more contractions were not following the pacing, the last intensity where all paces were followed has been defined as the critical pacing threshold.

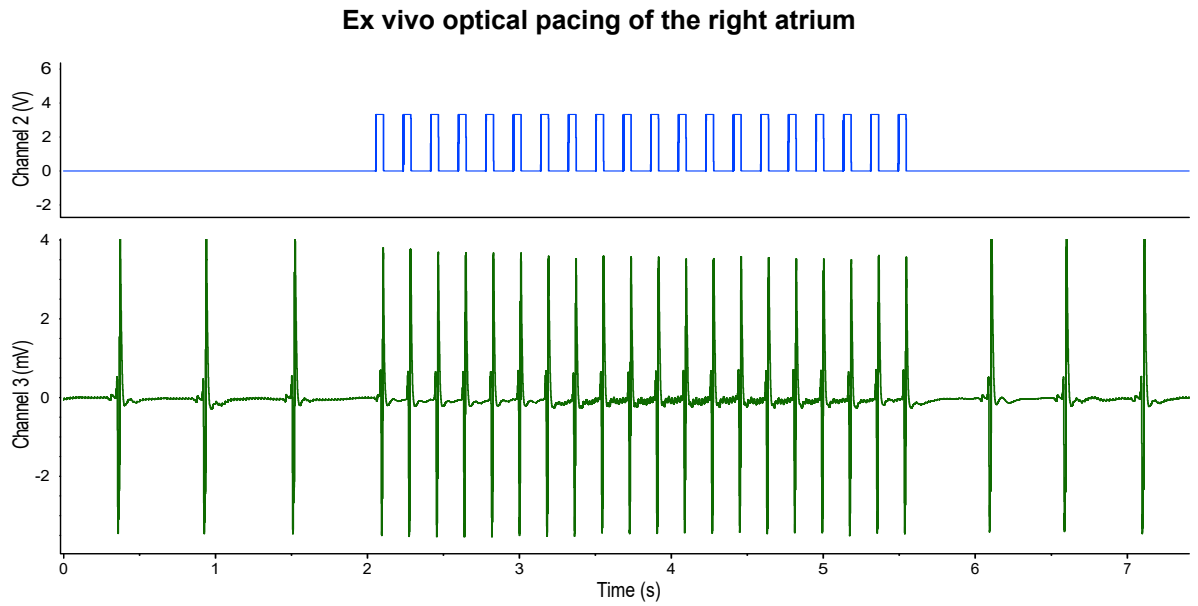

Figure 5.8: Pacing on the right atrium and 100% following of the heart ex vivo. 250uL of the viral vector containing the myh6 promotor was injected via the tail vein

5.4.2. Defibrillation

Figure 5.9 demonstrates how the heart initially has a normal sinus rhythm ($t < 0$). Atrial fibrillation is induced by rapidly stimulating the right atria with an electrode ($0 < t < 3$, region I) causing the electrical signals within the atria to get disrupted which results in AF. Atrial fibrillation is detected by the irregularity of the contractions and the fibrillatory wave of the signal within the RR interval ($3 < t < 13$, region II). Since the AF last for over 10 seconds, it is classified as sustained AF and will be optically terminated ($13 < t < 16.5$, region III). A normal sinus rhythm returns within 1 second after the last light pulse indicating the AF was optically terminated.

To compare the ECG of a single contraction before, during and after the atrial fibrillation, a zoomed in version of the cardiogram is shown in figure 5.10. Figure 5.10a shows the sinus rhythm before AF was induced, subplot 5.10b shows AF: the RR interval is irregular but shorter than before inducing and fibrillatory waves are visible in between the QRS complexes. Figure 5.10c shows the sinus rhythm after defibrillation where the fibrillatory waves are gone.

During the ex vivo experiment of the rat with the highest injected dose, AF was induced 13 times. Every one of these arrhythmias was successfully terminated using the OptoCoil system. To understand the effect auto termination could have on false positives 2 rats without the optoresponse underwent the same procedure. The hearts were suspended in the Langendorff setup and the coil was attached to the atria. After inducing AF and determining it was sustained the OptoCoil turns on and if AF terminated within the limits defined by the protocol, this termination would count as a successfully termination. Figure 5.11 shows 100% termination can be achieved using this device ex vivo, only 1 out of 32 induces arrhythmias auto terminated within the limits of the protocol.

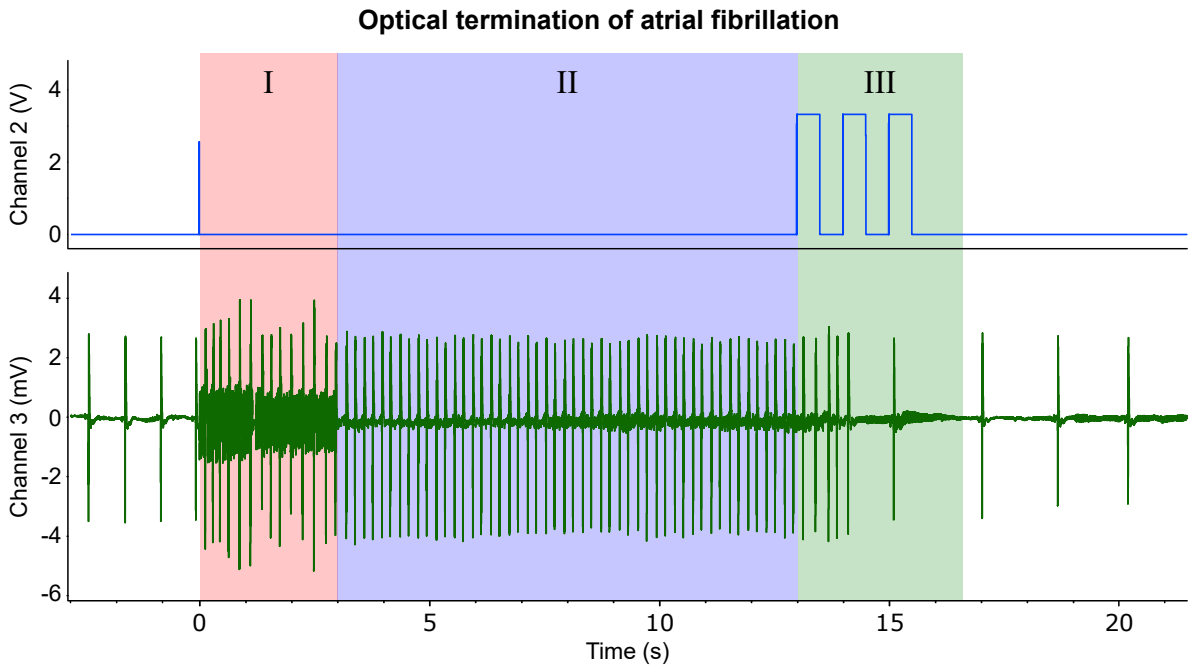

Figure 5.9: ECG optocoil AF termination during an ex vivo experiment. 250uL of the viral vector containing the NPPA promotor was injected via the tail vein

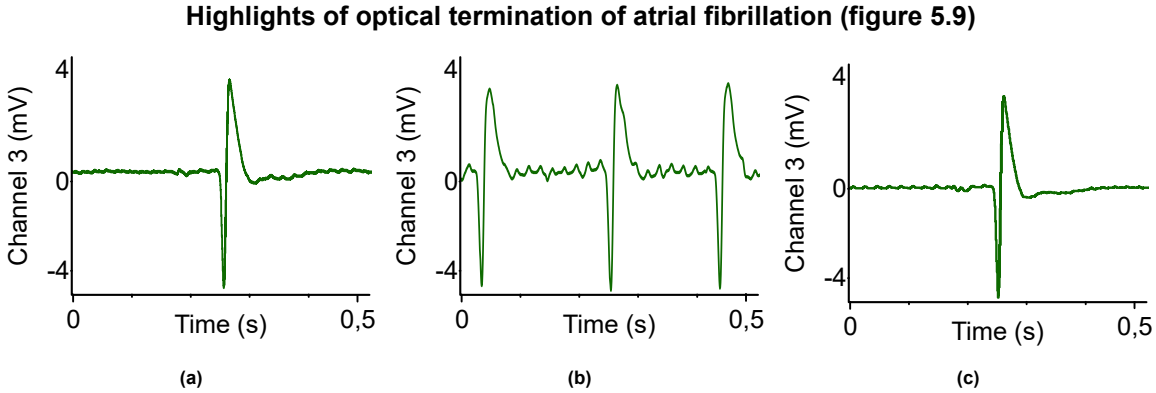

Figure 5.10: Highlights of figure 5.9. Zoomed in section of the ECG **(a)** before inducing AF, **(b)** during AF and **(c)** after AF is terminated.

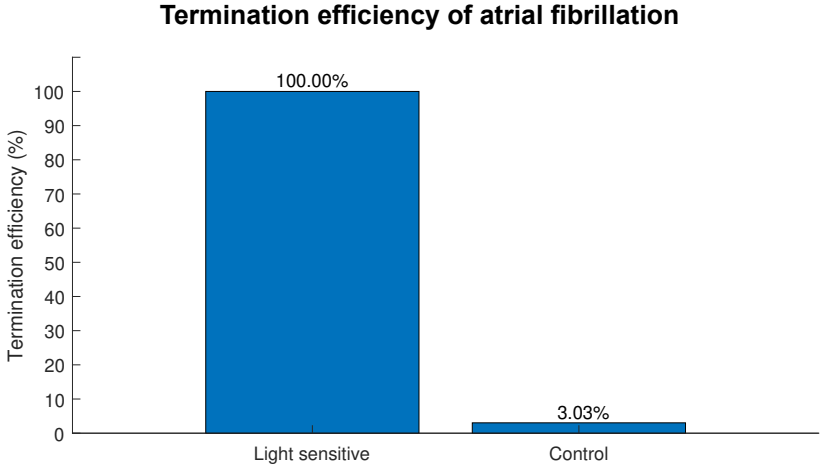

Figure 5.11: Termination efficiency of atrial fibrillation during ex vivo experiments. A light sensitive heart is compared to a non light sensitive control.

6

Conclusion

A first version of the OptoCoil has been designed and validated after which this system has been used during in- and ex vivo experiments. OptoCoil proved capable of termination of AF during ex vivo experiments as shown in figure 5.11. In vivo optical response was achieved using the Thorlabs torch, although the pacing was partially followed. Figure 5.3 demonstrates a correlation between the injected amount of virus carrying the optotool and the required illumination to achieve the desired optoresponse ex vivo. In vivo pacing of the ventricles was possible using a different promotor of the optotool which was not atria specific, demonstrating the dependence of this device on the biomedical engineering. The light sensitivity of the optotool, the injected amount of virus and the expression of the optotool realised by the promotor are significant factors in the effectiveness of OptoCoil. The atria specific promotor allowed 100% termination of AF during ex vivo experiments, suggesting an increased dose would allow in vivo optical response using the current version of OptoCoil. Differences between the in vivo and ex vivo results are likely due to the absence of blood which limits the penetration of the light, future research should be conducted into the penetration of blue light through blood to verify this hypothesis.
Future in vivo experiments should be conducted using hearts which are more light sensitive or future iterations of the OptoCoil which are able to achieve a higher levels of illumination.
Besides a higher illumination a similar illumination over a larger area could also prove to be fruitful since displacements of the LED with respect to the right atria would immediately result in decreased light sensitivity. Enlarging the illuminated area would decrease this dependency and is likely to increase effectiveness during in vivo experiments, especially in anticipation for ambulatory experiments.

6.1. Future Work

Some points of future work have been introduced above, this section will focus on the more long term future work and reliability tests. The future work has been separated into three parts:

- Design, where the physical and electrical components of the system will be subject to future improvements.
- Power transfer efficiency, which will focus on the coils and ways to decrease losses. This is not required for short ambulatory experiments but will be very useful in long term experiments.
- Biocompatible coating will focus on the PDMS and glue covering the receiver. This topic is relevant for ambulatory experiments with a longer duration.

6.1.1. Design

As discussed earlier the transmitter coil heats up during stimulation. To limit the device from operating at high temperatures a nice addition to the transmitter coil would be an embedded temperature sensor. In addition this could be used to monitor the temperature of the animal which can be useful in long running ambulatory experiments.
Recently the option to implant the coil on the back of the rat was reconsidered, this might open up the possibility of larger receiver coils which could transfer more power.

A redesign with smaller diameter meanders and a straight ending containing the LED has been requested. This will increase the flexibility of the serpentine structure while also decreasing its springiness and is part of the ongoing design of the second version of the OptoCoil receiver. The part where the LED is attached to should become a more straight end which would ease attaching it to the atria, possibly by using sutures. A first attempt to suture a PI structure to the atria has been made and demonstrated its feasibility provided the design contains holes to suture through.

During the ambulatory experiments the receiver must not only be capable of defibrillation but also inducing AF. Either a logical circuit or a microprocessor is required for this approach since a distinction must be made between the stimulation sources, in both cases a way of communication to the receiver is required.
Backpack of the rat containing the transmitter and a battery

6.1.2. Power transfer efficiency

The current limitation in power efficiency comes from the winding resistance. This can be solved by using litze wire but this will not fit inside of a rat. When upscaling to larger animals and thus increased requirements for power transfer, both the transmitting and receiving coil should be made out of litze wire.

The receiver currently rectifies the transmitted power by using a full bridge diode configuration, a passive approach which is often used. Active rectification by means of synchronised H bridge is an approach especially well suited for high power applications with limited space or thermal budget available. Advantages of this active rectification can mostly be seen in low voltage high current applications due to the minimised voltage drop of the rectifier. The efficiency could increase by a few percent after implanting such a rectifier.

6.1.3. Biocompatible coating

Recent experiments in PBS demonstrated that the PDMS layer is not water tight after being used in multiple experiments. In addition the optical glue covering the LED has visually been confirmed to be delaminating from the polyimide when bending the serpentine structure close to the rigid coating. Resolving these issues requires future research using parylene C chemical vapor deposition (CVD) which can be done while keeping the receiver at room temperature. Parylene C vs PDMS shows better biocompatibility but the outer layer will likely still have to be PDMS due to the components which contain sharp edges and add some height [76]. A setup with PBS at 37 $^{\circ}$C or higher will be used to evaluate water ingress over longer periods of time to determine the reliability and biocompatibility of the device.

References

[1] Valery Kustarev. *Coil32 - the coil inductance calculator*. 2014. URL: https://coil32.net/.

[2] Wapcaplet. *Diagram of the human heart*. June 2006. URL: https://commons.wikimedia.org/wiki/File:Diagram_of_the_human_heart_(cropped).svg.

[3] Daniel J. Blackwell, Jeffrey Schmeckpeper, and Bjorn C. Knollmann. "Animal Models to Study Cardiac Arrhythmias". In: *Circulation Research* 130.12 (2022), pp. 1926–1964. DOI: 10.1161/CIRCRESAHA.122.320258. eprint: https://www.ahajournals.org/doi/pdf/10.1161/CIRCRESAHA.122.320258. URL: https://www.ahajournals.org/doi/abs/10.1161/CIRCRESAHA.122.320258.

[4] Mayo Clinic staff. *Heart arrhythmia*. Apr. 2022. URL: https://www.mayoclinic.org/diseases-conditions/heart-arrhythmia/symptoms-causes/syc-20350668.

[5] Aksana Baldzizhar, Ekaterina Manuylova, Roman Marchenko, et al. "Ventricular Tachycardias: Characteristics and Management". In: *Critical Care Nursing Clinics of North America* 28.3 (2016). Cardiac Arrhythmias, pp. 317–329. ISSN: 0899-5885. DOI: https://doi.org/10.1016/j.cnc.2016.04.004. URL: https://www.sciencedirect.com/science/article/pii/S0899588516300302.

[6] Emran M. Abu Anas, Soo Y. Lee, and Md K. Hasan. "Sequential algorithm for life threatening cardiac pathologies detection based on mean signal strength and EMD functions". In: *BioMedical Engineering OnLine* 9.1 (Sept. 2010), p. 43. ISSN: 1475-925X. DOI: 10.1186/1475-925X-9-43. URL: https://doi.org/10.1186/1475-925X-9-43.

[7] M. Liwanag and C. Willoughby. *Atrial Tachycardia*. Jan. 2022. URL: https://www.ncbi.nlm.nih.gov/books/NBK542235/ (visited on 08/16/2022).

[8] David E. Krummen, Vijay Swarup, and Sanjiv M. Narayan. "The role of rotors in atrial fibrillation". In: *Journal of Thoracic Disease* 7 (2 Feb. 2015), pp. 142–151. ISSN: 20776624. DOI: 10.3978/j.issn.2072-1439.2014.11.15.

[9] Nicholas A. Bosch, Jonathan Cimini, and Allan J. Walkey. "Atrial Fibrillation in the ICU". In: *Chest* 154 (6 Dec. 2018), pp. 1424–1434. ISSN: 19313543. DOI: 10.1016/j.chest.2018.03.040.

[10] Donald M Lloyd-Jones, Thomas J Wang, Eric P Leip, et al. "Lifetime risk for development of atrial fibrillation: the Framingham Heart Study". en. In: *Circulation* 110.9 (Aug. 2004), pp. 1042–1046.

[11] *AFIB-Detector*. URL: https://www.medicomholter.ru/afib-detector.

[12] Nederlands Huisartsen Genootschap. *Belangrijkste wijziging*. 2017.

[13] Sandeep V. Pandit and José Jalife. "Rotors and the dynamics of cardiac fibrillation". In: *Circulation Research* 112 (5 Mar. 2013), pp. 849–862. ISSN: 00097330. DOI: 10.1161/CIRCRESAHA.111.300158.

[14] Hartstichting. *Alles over DE ICD*. URL: https://www.hartstichting.nl/hart-en-vaatziekten/behandelingen/icd.

[15] Ki H Chon and David D McManus. "Detection of atrial fibrillation using a smartwatch". In: *Nature Reviews Cardiology* 15.11 (Nov. 2018), pp. 657–658.

[16] Patti Shih, Kathleen Prokopovich, Chris Degeling, et al. "Direct-to-consumer detection of atrial fibrillation in a smartwatch electrocardiogram: Medical overuse, medicalisation and the experience of consumers". In: *Social Science & Medicine* 303 (2022), p. 114954. ISSN: 0277-9536. DOI: https://doi.org/10.1016/j.socscimed.2022.114954. URL: https://www.sciencedirect.com/science/article/pii/S027795362200260X.

[17] Po-Cheng Chang, Ming-Shien Wen, Chung-Chuan Chou, et al. “Atrial fibrillation detection using ambulatory smartwatch photoplethysmography and validation with simultaneous holter recording”. In: *American Heart Journal* 247 (2022), pp. 55–62. ISSN: 0002-8703. DOI: https://doi.org/10.1016/j.ahj.2022.02.002. URL: https://www.sciencedirect.com/science/article/pii/S000287032200028X.

[18] Eric Y. Ding, Maira CastañedaAvila, Khanh-Van Tran, et al. “Usability of a smartwatch for atrial fibrillation detection in older adults after stroke”. In: *Cardiovascular Digital Health Journal* 3.3 (2022), pp. 126–135. ISSN: 2666-6936. DOI: https://doi.org/10.1016/j.cvdhj.2022.03.003. URL: https://www.sciencedirect.com/science/article/pii/S2666693622000287.

[19] Christopher Ford, Charis Xuan Xie, Ashlea Low, et al. “Comparison of 2 Smart Watch Algorithms for Detection of Atrial Fibrillation and the Benefit of Clinician Interpretation: SMART WARS Study”. In: *JACC: Clinical Electrophysiology* 8.6 (2022), pp. 782–791. ISSN: 2405-500X. DOI: https://doi.org/10.1016/j.jacep.2022.02.013. URL: https://www.sciencedirect.com/science/article/pii/S2405500X22002201.

[20] Josue D Ordaz, Wei Wu, and Xiao-Ming Xu. “Optogenetics and its application in neural degeneration and regeneration”. en. In: *Neural Regen Res* 12.8 (Aug. 2017), pp. 1197–1209.

[21] Emilia Entcheva and Matthew W. Kay. “Cardiac optogenetics: a decade of enlightenment”. In: *Nature Reviews Cardiology* 18 (5 May 2021), pp. 349–367. ISSN: 17595010. DOI: 10.1038/s41569-020-00478-0.

[22] Emily A Ferenczi, Xiaoqiu Tan, and Christopher L-H Huang. “Principles of optogenetic methods and their application to cardiac experimental systems”. en. In: *Front. Physiol.* 10 (Sept. 2019), p. 1096.

[23] H G Khorana, B E Knox, E Nasi, et al. “Expression of a bovine rhodopsin gene in Xenopus oocytes: demonstration of light-dependent ionic currents”. en. In: *Proc Natl Acad Sci U S A* 85.21 (Nov. 1988), pp. 7917–7921.

[24] Kalyanam Shivkumar. “Cardiac Bioelectric Therapy”. In: ed. by Jacob I. Laughner Igor R. Efimov Fu Siong Ng. springer, 2021. URL: https://link.springer.com/book/10.1007/978-3-030-63355-4.

[25] A Hoffmann, V Hildebrandt, J Heberle, et al. “Photoactive mitochondria: in vivo transfer of a light-driven proton pump into the inner mitochondrial membrane of Schizosaccharomyces pombe.” In: *Proceedings of the National Academy of Sciences* 91.20 (1994), pp. 9367–9371. DOI: 10.1073/pnas.91.20.9367. eprint: https://www.pnas.org/doi/pdf/10.1073/pnas.91.20.9367. URL: https://www.pnas.org/doi/abs/10.1073/pnas.91.20.9367.

[26] G Nagel, B Möckel, G Büldt, et al. “Functional expression of bacteriorhodopsin in oocytes allows direct measurement of voltage dependence of light induced H+ pumping”. en. In: *FEBS Lett* 377.2 (Dec. 1995), pp. 263–266.

[27] Boris V. Zemelman, Georgia A. Lee, Minna Ng, et al. “Selective Photostimulation of Genetically ChARGed Neurons”. In: *Neuron* 33.1 (2002), pp. 15–22. ISSN: 0896-6273. DOI: https://doi.org/10.1016/S0896-6273(01)00574-8. URL: https://www.sciencedirect.com/science/article/pii/S0896627301005748.

[28] Aristides B. Arrenberg, Didier Y. R. Stainier, Herwig Baier, et al. “Optogenetic Control of Cardiac Function”. In: *Science* 330.6006 (2010), pp. 971–974. DOI: 10.1126/science.1195929. eprint: https://www.science.org/doi/pdf/10.1126/science.1195929. URL: https://www.science.org/doi/abs/10.1126/science.1195929.

[29] Tobias Bruegmann, Daniela Malan, Michael Hesse, et al. “Optogenetic control of heart muscle in vitro and in vivo”. In: *Nature Methods* 7.11 (Nov. 2010), pp. 897–900. ISSN: 1548-7105. DOI: 10.1038/nmeth.1512. URL: https://doi.org/10.1038/nmeth.1512.

[30] Keel Yong Lee, Sung-Jin Park, David G. Matthews, et al. “An autonomously swimming biohybrid fish designed with human cardiac biophysics”. In: *Science* 375.6581 (2022), pp. 639–647. DOI: 10.1126/science.abh0474. eprint: https://www.science.org/doi/pdf/10.1126/science.abh0474. URL: https://www.science.org/doi/abs/10.1126/science.abh0474.

[31] *QI Specification*. v1.3. Rev. 1.3. Wireless Power Consortium. Jan. 2021.

[32] *Wireless Power Consortium*. URL: https://www.wirelesspowerconsortium.com/qi/.

[33] Christian T Wentz, Jacob G Bernstein, Patrick Monahan, et al. “A wirelessly powered and controlled device for optical neural control of freely-behaving animals”. en. In: *J Neural Eng* 8.4 (June 2011), p. 10.

[34] Daniel Keppeler, Michael Schwaerzle, Tamas Harczos, et al. “Multichannel optogenetic stimulation of the auditory pathway using microfabricated LED cochlear implants in rodents”. In: *Science Translational Medicine* 12.553 (2020), eabb8086. DOI: 10.1126/scitranslmed.abb8086. eprint: https://www.science.org/doi/pdf/10.1126/scitranslmed.abb8086. URL: https://www.science.org/doi/abs/10.1126/scitranslmed.abb8086.

[35] Aaron D. Mickle, Sang Min Won, Kyung Nim Noh, et al. “A wireless closed-loop system for optogenetic peripheral neuromodulation”. In: *Nature* 565.7739 (Jan. 2019), pp. 361–365. ISSN: 1476-4687. DOI: 10.1038/s41586-018-0823-6. URL: https://doi.org/10.1038/s41586-018-0823-6.

[36] Alex Burton, Sofian N Obaid, Abraham Vázquez-Guardado, et al. “Wireless, battery-free subdermally implantable photometry systems for chronic recording of neural dynamics”. In: *PNAS* 117 (6 Feb. 2020), pp. 2835–2545. DOI: 10.1073/pnas.1920073117/-/DCSupplemental. URL: www.pnas.org/cgi/doi/10.1073/pnas.1920073117.

[37] Choong Yeon Kim, Min Jeong Ku, Raza Qazi, et al. “Soft subdermal implant capable of wireless battery charging and programmable controls for applications in optogenetics”. In: *Nature Communications* 12.1 (Jan. 2021), p. 535. ISSN: 2041-1723. DOI: 10.1038/s41467-020-20803-y. URL: https://doi.org/10.1038/s41467-020-20803-y.

[38] Callum M. Zgierski-Johnston and Franziska Schneider-Warme. “Observing and Manipulating Cell-Specific Cardiac Function with Light”. In: *Optogenetics: Light-Sensing Proteins and Their Applications in Neuroscience and Beyond*. Ed. by Hiromu Yawo, Hideki Kandori, Amane Koizumi, et al. Singapore: Springer Singapore, 2021, pp. 377–388. ISBN: 978-981-15-8763-4. DOI: 10.1007/978-981-15-8763-4_24. URL: https://doi.org/10.1007/978-981-15-8763-4_24.

[39] Rishi Rajalingham, Michael Sorenson, Reza Azadi, et al. “Chronically implantable LED arrays for behavioral optogenetics in primates”. In: *Nature Methods* 18.9 (Sept. 2021), pp. 1112–1116. ISSN: 1548-7105. DOI: 10.1038/s41592-021-01238-9. URL: https://doi.org/10.1038/s41592-021-01238-9.

[40] Philipp Gutruf, Rose T. Yin, K. Benjamin Lee, et al. “Wireless, battery-free, fully implantable multimodal and multisite pacemakers for applications in small animal models”. In: *Nature Communications* 10.1 (Dec. 2019), p. 5742. ISSN: 2041-1723. DOI: 10.1038/s41467-019-13637-w. URL: https://doi.org/10.1038/s41467-019-13637-w.

[41] Aneesh Alex, Airong Li, Rudolph E. Tanzi, et al. “Optogenetic pacing in Drosophila melanogaster”. In: *Science Advances* 1.9 (2015), e1500639. DOI: 10.1126/sciadv.1500639. eprint: https://www.science.org/doi/pdf/10.1126/sciadv.1500639. URL: https://www.science.org/doi/abs/10.1126/sciadv.1500639.

[42] Emile C.A. Nyns, Annemarie Kip, Cindy I. Bart, et al. “Optogenetic termination of ventricular arrhythmias in the whole heart: towards biological cardiac rhythm management”. In: *European Heart Journal* 38.27 (Dec. 2016), pp. 2132–2136. ISSN: 0195-668X. DOI: 10.1093/eurheartj/ehw574. eprint: https://academic.oup.com/eurheartj/article-pdf/38/27/2132/24120456/ehw574.pdf. URL: https://doi.org/10.1093/eurheartj/ehw574.

[43] Emile C. A. Nyns, René H. Poelma, Linda Volkers, et al. “An automated hybrid bioelectronic system for autogenous restoration of sinus rhythm in atrial fibrillation”. In: *Science Translational Medicine* 11.481 (2019), eaau6447. DOI: 10.1126/scitranslmed.aau6447. eprint: https://www.science.org/doi/pdf/10.1126/scitranslmed.aau6447. URL: https://www.science.org/doi/abs/10.1126/scitranslmed.aau6447.

[44] Emile C A Nyns, Tianyi Jin, Magda S Fontes, et al. “Optical ventricular cardioversion by local optogenetic targeting and LED implantation in a cardiomyopathic rat model”. In: *Cardiovascular Research* (Sept. 2021). cvab294. ISSN: 0008-6363. DOI: 10.1093/cvr/cvab294. eprint: https://academic.oup.com/cardiovascres/advance-article-pdf/doi/10.1093/cvr/cvab294/40452750/cvab294.pdf. URL: https://doi.org/10.1093/cvr/cvab294.

[45] Wen Hong, Chunpeng Jiang, Mu Qin, et al. “Self-adaptive cardiac optogenetics device based on negative stretching-resistive strain sensor”. In: *Science Advances* 7.48 (2021), eabj4273. DOI: 10.1126/sciadv.abj4273. eprint: https://www.science.org/doi/pdf/10.1126/sciadv.abj4273. URL: https://www.science.org/doi/abs/10.1126/sciadv.abj4273.

[46] Tobias Bruegmann, Thomas Beiert, Christoph C Vogt, et al. “Optogenetic termination of atrial fibrillation in mice”. In: *Cardiovascular Research* 114.5 (Dec. 2017), pp. 713–723. ISSN: 0008-6363. DOI: 10.1093/cvr/cvx250. eprint: https://academic.oup.com/cardiovascres/article-pdf/114/5/713/24519673/cvx250.pdf. URL: https://doi.org/10.1093/cvr/cvx250.

[47] Tania Zaglia, Nicola Pianca, Giulia Borile, et al. “Optogenetic determination of the myocardial requirements for extrasystoles by cell type-specific targeting of ChannelRhodopsin-2”. In: *Proceedings of the National Academy of Sciences* 112.32 (2015), E4495–E4504. DOI: 10.1073/pnas.1509380112. eprint: https://www.pnas.org/doi/pdf/10.1073/pnas.1509380112. URL: https://www.pnas.org/doi/abs/10.1073/pnas.1509380112.

[48] Panpan Rao, Long Wang, Yue Cheng, et al. “Near-infrared light driven tissue-penetrating cardiac optogenetics via upconversion nanoparticles in vivo”. In: *Biomed. Opt. Express* 11.3 (Mar. 2020), pp. 1401–1416. DOI: 10.1364/BOE.381480. URL: http://opg.optica.org/boe/abstract.cfm?URI=boe-11-3-1401.

[49] Emile C.A. Nyns, Tianyi Jin, Cindy I. Bart, et al. “Ultrasound-Guided Optogenetic Gene Delivery for Shock-Free Ventricular Rhythm Restoration”. In: *Circulation: Arrhythmia and Electrophysiology* 15.1 (Jan. 2022). DOI: 10.1161/circep.121.009886. URL: https://doi.org/10.1161/circep.121.009886.

[50] Vijay K. Samineni, Jangyeol Yoon, Kaitlyn E. Crawford, et al. “Fully implantable, battery-free wireless optoelectronic devices for spinal optogenetics”. eng. In: *Pain* 158.11 (Nov. 2017). 00006396-201711000-00009[PII], pp. 2108–2116. ISSN: 1872-6623. DOI: 10.1097/j.pain.0000000000000968. URL: https://doi.org/10.1097/j.pain.0000000000000968.

[51] Yeon Sik Choi, Hyoyoung Jeong, Rose T. Yin, et al. “A transient, closed-loop network of wireless, body-integrated devices for autonomous electrotherapy”. In: *Science* 376.6596 (2022), pp. 1006–1012. DOI: 10.1126/science.abm1703. eprint: https://www.science.org/doi/pdf/10.1126/science.abm1703. URL: https://www.science.org/doi/abs/10.1126/science.abm1703.

[52] *ATtiny24/44/84*. Attiny84. 7701G–AVR–02/15. Atmel. 2015.

[53] Rupam Das and Hyoungsuk Yoo. “Biotelemetry and Wireless Powering for Leadless Pacemaker Systems”. In: *IEEE Microwave and Wireless Components Letters* 25 (4 Apr. 2015), pp. 262–264. ISSN: 15311309. DOI: 10.1109/LMWC.2015.2400920.

[54] Rupamanjari Majumder, Afnan Nabizath Mohamed Nazer, Alexander V. Panfilov, et al. “Electrophysiological Characterization of Human Atria: The Understated Role of Temperature”. In: *Frontiers in Physiology* 12 (2021). ISSN: 1664-042X. DOI: 10.3389/fphys.2021.639149. URL: https://www.frontiersin.org/articles/10.3389/fphys.2021.639149.

[55] Zhen Tian, Qun Nan, Xiaohui Nie, et al. “The comparison of lesion outline and temperature field determined by different ways in atrial radiofrequency ablation”. en. In: *Biomed Eng Online* 15.Suppl 2 (Dec. 2016), p. 124.

[56] *Capabilities for FPC*. URL: https://www.pcbway.com/pcb_prototype/What_is_Flexible_PCB.html.

[57] *planar spiral coil inductor calculator*. URL: http://www.circuits.dk/calculator_planar_coil_inductor.htm.

[58] Sunderarajan S Mohan, Maria Del Mar Hershenson, Stephen P Boyd, et al. “Simple Accurate Expressions for Planar Spiral Inductances”. In: *IEEE JOURNAL OF SOLID-STATE CIRCUITS* 34 (10 1999), p. 1419.

[59] *Stack-up for FPC*. URL: https://www.pcbway.com/pcb_prototype/Stack_up_for_FPC.html.

[60] *ncv8187: low iq, low dropout, power good output*. Rev. 8. ONSEMI. Aug. 2021.

[61] *SMD Schottky Barrier Diode*. CDBU0520-HF. Rev. A. COMCHIP. URL: https://www.comchiptech.com/admin/files/product/CDBU0520-HF-RevA797161.pdf.

[62] *LUXEON Z Color Line*. LXZ1-PB01. LUMILEDS. 2017.

[63] *bd63573nuv: single h-bridge driver high-speed switching*. Rev. 001. ROHM Semiconductor. Dec. 2015.

[64] *Low-Cost, UCSP/SOT23, Micropower, High-Side Current-Sense Amplifier with Voltage Output*. MAX4372TEUK+T. Rev. 5. Maxim Integrated. 2011.

[65] *LM2731 0.6/1.6-MHz Boost Converters With 22-V Internal FET Switch in SOT-23*. LM2731XMF/NOPB. Rev. 9-2015. Texas Instruments. 2004.

[66] M. O'hara. "Modeling Non-Ideal Inductors in SPICE". In: 1993. URL: http://www.intusoft.com/articles/inductor.pdf.

[67] *System Reference document (SRdoc); Wireless Power Transmission (WPT) systems operating below 30 MHz*. ETSI TR 103 493. V1.1.1. ETSI. Feb. 2019. URL: https://www.etsi.org/deliver/etsi_tr/103400_103499/103493/01.01.01_60/tr_103493v010101p.pdf.

[68] Gerard C van Rhoon, Theodoros Samaras, Pavel S Yarmolenko, et al. "CEM43°C thermal dose thresholds: a potential guide for magnetic resonance radiofrequency exposure levels?" en. In: *Eur Radiol* 23.8 (Apr. 2013), pp. 2215–2227.

[69] Faical Turki, Ralf Wiengarten, Viktor Reising, et al. "Impact of the Working Frequency on Wireless Power Transfer Systems". In: *PCIM Europe 2014; International Exhibition and Conference for Power Electronics, Intelligent Motion, Renewable Energy and Energy Management*. 2014, pp. 1–6.

[70] Kate L. Montgomery, Alexander J. Yeh, John S. Ho, et al. "Wirelessly powered, fully internal optogenetics for brain, spinal and peripheral circuits in mice". In: *Nature Methods* 12 (10 Sept. 2015), pp. 969–974. ISSN: 15487105. DOI: 10.1038/nmeth.3536. URL: https://doi.org/10.1038/nmeth.3536.

[71] Woong Jin Bae, Jin Bong Choi, Kang Sup Kim, et al. "AB168. Evaluation of the biocompatibility of packing materials for a catheter". en. In: *Transl. Androl. Urol.* 4.1 (Aug. 2015), pp. 168–168.

[72] Zhixin Wang, Alex A. Volinsky, and Nathan D. Gallant. "Crosslinking effect on polydimethylsiloxane elastic modulus measured by custom-built compression instrument". In: *Journal of Applied Polymer Science* 131.22 (2014). DOI: https://doi.org/10.1002/app.41050. eprint: https://onlinelibrary.wiley.com/doi/pdf/10.1002/app.41050. URL: https://onlinelibrary.wiley.com/doi/abs/10.1002/app.41050.

[73] Jaemook Lim, Byeonghwa Goh, Weihao Qu, et al. "Adhesive-free bonding of PI/PDMS interface by site-selective photothermal reactions". In: *Applied Surface Science* 571 (2022), p. 151123. ISSN: 0169-4332. DOI: https://doi.org/10.1016/j.apsusc.2021.151123. URL: https://www.sciencedirect.com/science/article/pii/S0169433221021796.

[74] Shivani Joshi, R. Bagani, Lucas Beckers, et al. "Novel Method for Adhesion between PI-PDMS Using Butyl Rubber for Large Area Flexible Body Patches". English. In: *Proceedings of Eurosensors*. Proceedings 4. Eurosensors 2017 : 31st Conference ; Conference date: 03-09-2017 Through 06-09-2017. MDPI, 2017, pp. 1–5. DOI: 10.3390/proceedings1040307. URL: http://www.eurosensors2017.eu/.

[75] Michelle V Hoang, Hyun-Joong Chung, and Anastasia L Elias. "Irreversible bonding of polyimide and polydimethylsiloxane (PDMS) based on a thiol-epoxy click reaction". In: *Journal of Micromechanics and Microengineering* 26.10 (Sept. 2016), p. 105019. DOI: 10.1088/0960-1317/26/10/105019. URL: https://doi.org/10.1088/0960-1317/26/10/105019.

[76] Georges (19..-1978). Girard, Denis (1914?-2009). Gerll, and Christian. Gauthier. "Comparison of in vivo biocompatibilities between parlene-C and polydimethylsiloxane for implantable microelectronic devices". In: *Bulletin of Materials Science* 36.6 (2013).

A

Schematics & PCB design

Table A.1: List of figures for appendix A

Page	Description
1	Schematic design of the transmitter coil driver
2	Schematic design of the transmitter processor
3	Schematic design of the transmitter power distribution and USB-UART bridge
4	Schematic of the receiver
5	PCB design containing the coils

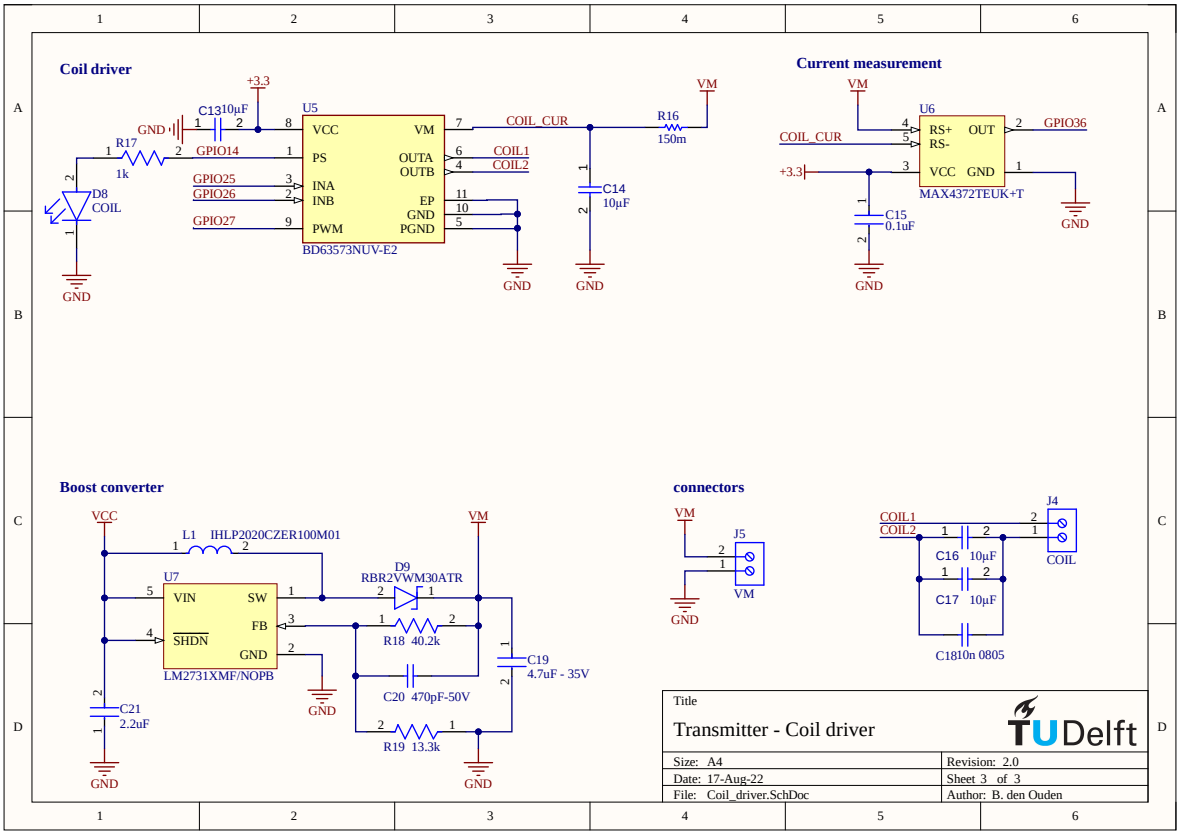

LEDs

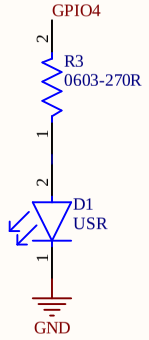

Battery voltage measurement

Programing mode

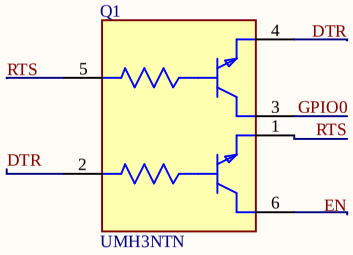

Processor

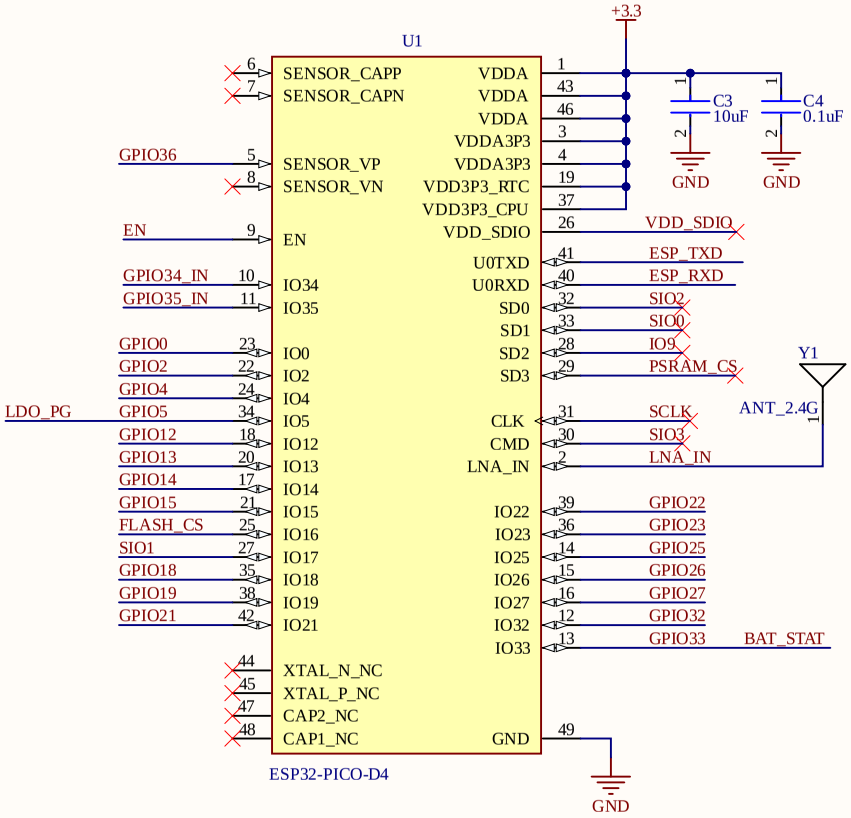

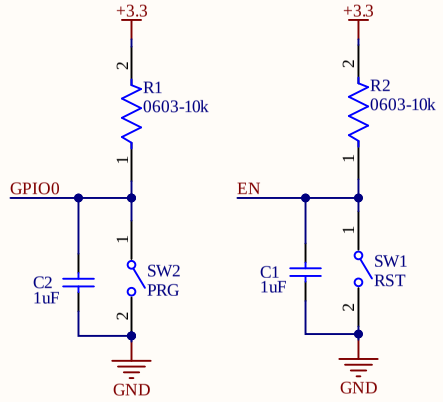

Title: Transmitter - Processor	TU Delft
Size: A4	Revision: 2.0
Date: 17-Aug-22	Sheet 1 of 3
File: processor.SchDoc	Author: B. den Ouden

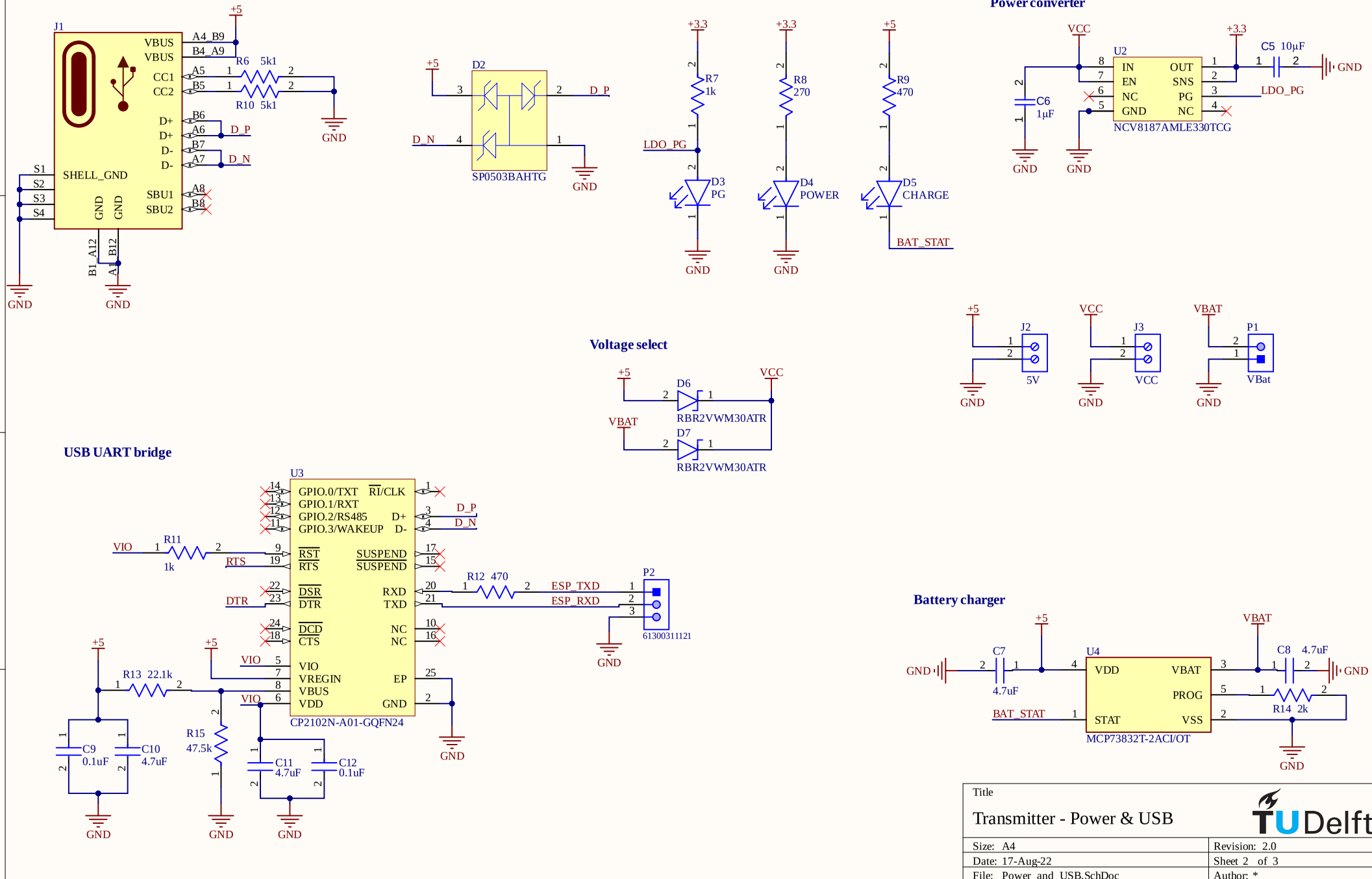
Power converter
Voltage select
USB UART bridge
Battery charger
J1
VBUS
CC1
CC2
D+
D-
SBU1
SBU2
SHELL_GND
R6 5k1
R10 5k1
D_P
D_N
D2
SP0503BAHTG
R7 1k
R8 270
R9 470
D3 PG
D4 POWER
D5 CHARGE
LDO_PG
BAT_STAT
U2
NCV8187AMLE330TCG
C5 10µF
C6 1µF
J2 5V
J3 VCC
P1 VBat
D6 RBR2VWM30ATR
D7 RBR2VWM30ATR
U3
CP2102N-A01-GQFN24
R11 1k
R12 470
R13 22.1k
R15 47.5k
C9 0.1uF
C10 4.7uF
C11 4.7uF
C12 0.1uF
P2
61300311121
ESP_TXD
ESP_RXD
U4
MCP73832T-2ACI/OT
C7 4.7uF
C8 4.7uF
R14 2k
Title
Transmitter - Power & USB
TUDelft
Size: A4
Revision: 2.0
Date: 17-Aug-22
Sheet 2 of 3
File: Power_and_USB.SchDoc
Author: *

Stimulation LED

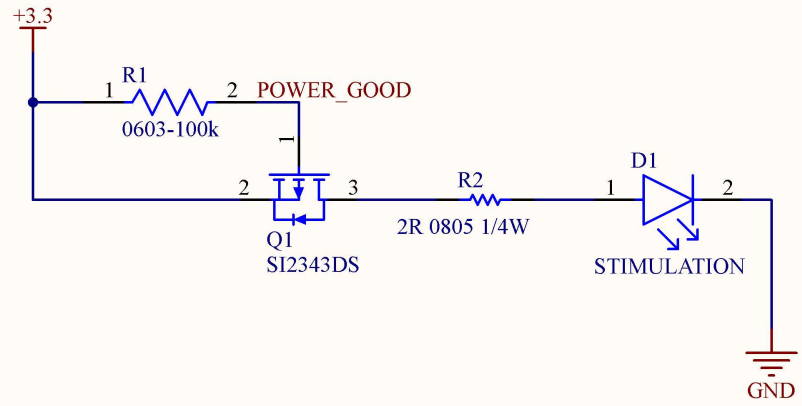

Rectifier

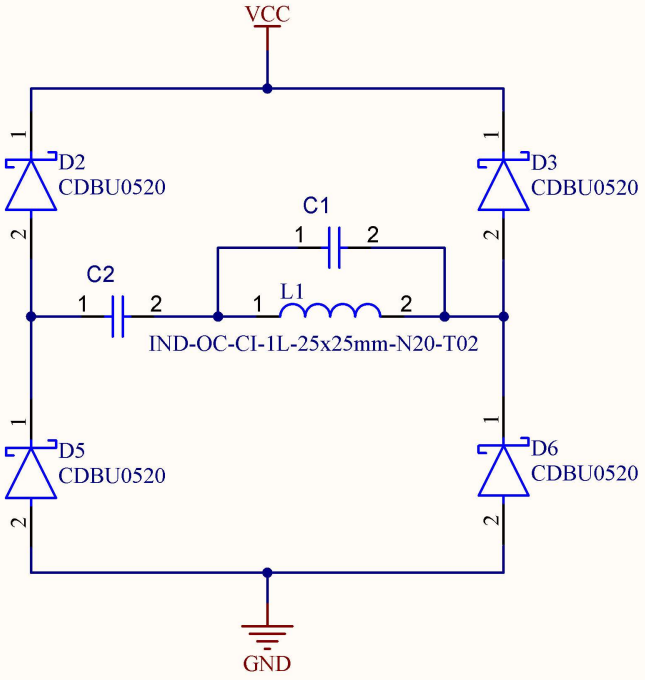

Power regulation

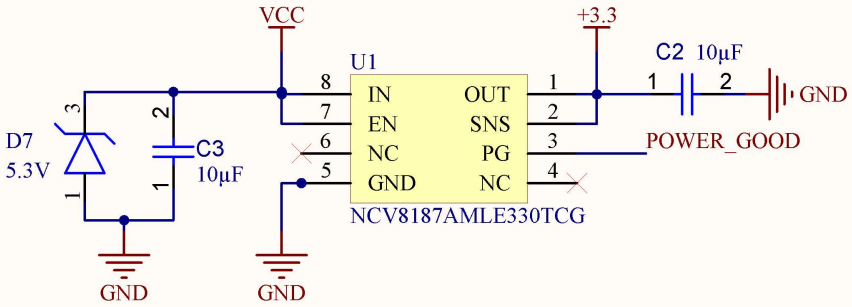

Title: OptoCoil receiver	
Size: A5	Revision: 1.1
Date: 17-Aug-22	Sheet 1 of 1
File: passive receiver.SchDoc	Author: B. den Ouden

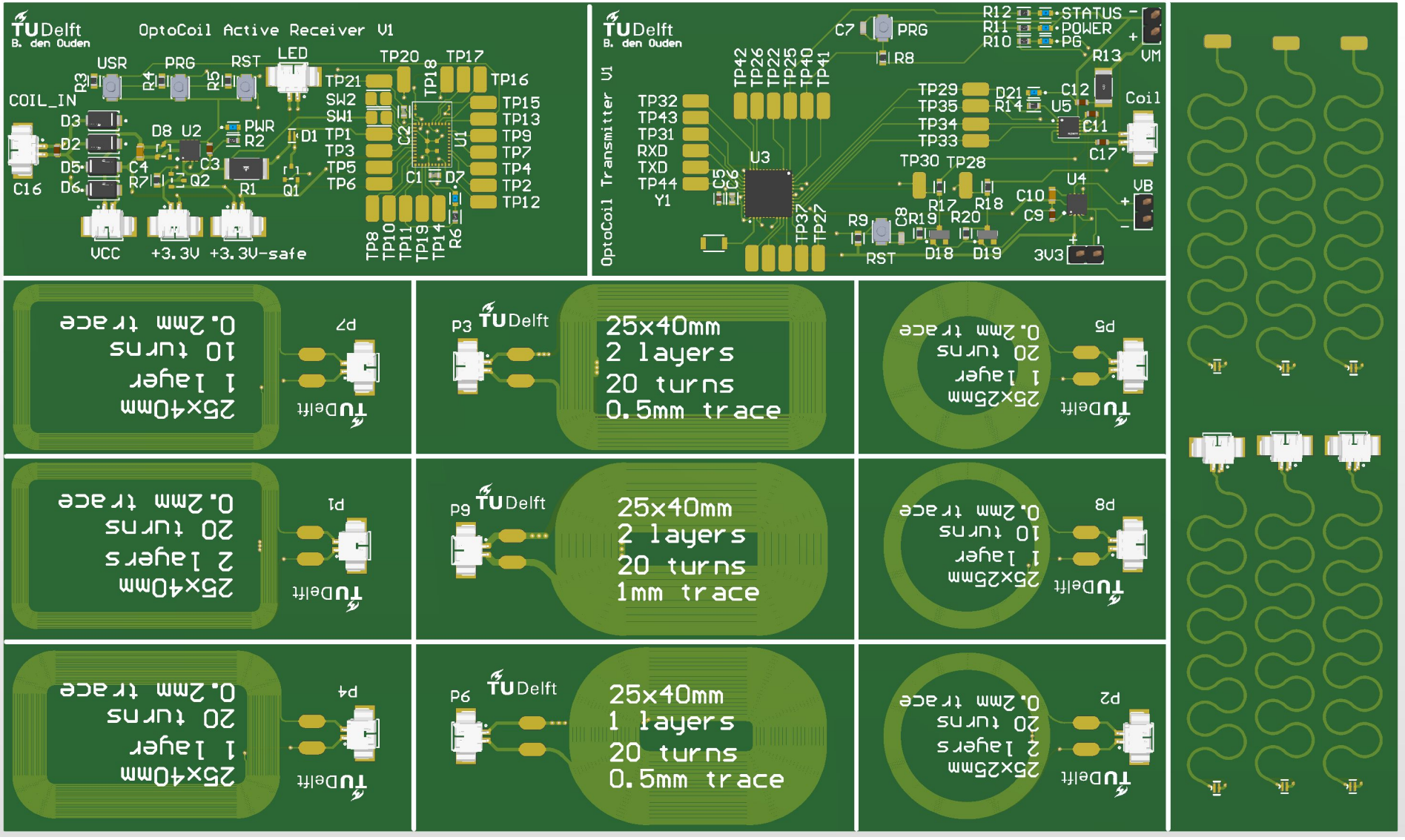
TU Delft
B. den Ouden
OptoCoil Active Receiver V1
USR
PRG
RST
LED
COIL_IN
PWR
VCC
+3.3V
+3.3V-safe
OptoCoil Transmitter V1
STATUS
POWER
PG
VM
Coil
VB
3V3
RST
25x40mm
2 layers
20 turns
0.5mm trace
25x40mm
1 layer
10 turns
0.2mm trace
25x25mm
2 layers
20 turns
0.2mm trace
25x40mm
2 layers
20 turns
0.2mm trace
25x40mm
2 layers
20 turns
1mm trace
25x25mm
1 layer
10 turns
0.2mm trace
25x40mm
1 layer
20 turns
0.2mm trace
25x40mm
1 layers
20 turns
0.5mm trace
25x25mm
2 layers
20 turns
0.2mm trace

B

Tables

Table B.1: DC-DC power transfer using different transmitter and receiver coils. P3 and P5 refer the the custom designed flexible coils. WE and C309 refer to commercially available rigid coils with comparable inductance as P3 and P5 respectively. Limits of the transmitter power supply were set to 5.9V and 0.89A.

Tx	Rx	R (Ω)	P_{tx} (W)	P_{rx} (W)	Efficiency (%)
P3	P5	10	3.13	0.15	4.637
P3	P5	5	3.13	0.14	4.477
P3	P5	2.5	3.13	0.11	3.486
P3	C309	10	2.42	0.19	7.648
P3	C309	5	2.42	0.22	8.929
P3	C309	2.5	2.42	0.26	10.583
WE	P5	10	4.48	1.03	23.015
WE	P5	5	4.01	0.83	20.588
WE	P5	2.5	3.60	0.56	15.671
WE	C309	10	2.30	0.97	42.243
WE	C309	5	2.54	0.91	35.696
WE	C309	2.5	2.42	0.74	30.632

C

Firmware

C.1. Main.cpp

```
/**
 * @file main.cpp
 * @author Bram den Ouden
 * @brief This firmware will test the basic functionality of
 * the transmitter designed for the OptoCoil project as part
 * of my MSc Thesis
 *
 * @version 0.1
 * @date 2022-02-01
 *
 * @copyright Copyright (c) 2022
 */

#include <Arduino.h>
#include <definitions_V2.h>

#ifdef WIFI_ENABLED
#include <WiFi.h>

// Replace with your network credentials
const char *ssid = "OptoCoil_AP";
const char *password = "123456789";

// Set web server port number to 80
WiFiServer server(80);

#endif // WIFI_ENABLED

#ifdef DEBUG
#define DPRINT(...) Serial.print(__VA_ARGS__)     // debug print
#define DPRINTLN(...) Serial.println(__VA_ARGS__) // debug print with new line
#define DPRINTF(...) Serial.printf(__VA_ARGS__)   // debug format string print
#else
#define DPRINT(...)   // now defines a blank line
#define DPRINTLN(...) // now defines a blank line
#define DPRINTF(...)  // now defines a blank line
#endif                // DEBUG
```

```
void setCoilFrequency(unsigned long freq)
{
    ledcSetup(COIL_PWM_CHANNEL, COIL_FREQ, COIL_PWM_RESOLUTION);
    ledcAttachPin(COIL_IN_B, COIL_PWM_CHANNEL);
    ledcWrite(COIL_PWM_CHANNEL, 64);
}

void coilSetup()
{
    pinMode(COIL_PS, OUTPUT);
    digitalWrite(COIL_PS, LOW); // coil disabled during setup

    pinMode(COIL_IN_A, OUTPUT);
    digitalWrite(COIL_IN_A, HIGH);

    pinMode(COIL_PWM, OUTPUT);
    digitalWrite(COIL_PWM, HIGH);

    setCoilFrequency(COIL_FREQ);
}

void enableCoil()
{
    digitalWrite(COIL_PS, HIGH);
}

void disableCoil()
{
    digitalWrite(COIL_PS, LOW);
}

void setup()
{
#ifdef DEBUG
    Serial.begin(115200);
#endif
    DPRINTLN("\n\nRunning setup");
    coilSetup();
    pinMode(BTN_PIN, INPUT);
    pinMode(LED_STATUS, OUTPUT);
    digitalWrite(LED_STATUS, HIGH);

    pinMode(EXT_TRIG_PIN, INPUT_PULLDOWN);

#ifdef WIFI_ENABLED
    WiFi.softAP(ssid, password);

    IPAddress IP = WiFi.softAPIP();
    DPRINT("AP IP address: ");
    DPRINTLN(IP);

    server.begin();
#endif
}
```

```
void loop()
{
    // Print channel data periodically
    static unsigned long t_print = millis();
    if (millis() - t_print > 1000)
    {
        DPRINTF(
            "Channel %d is %s, PWM Freq: %lf\n",
            COIL_PWM_CHANNEL,
            digitalRead(COIL_PS) ? "enabled" : "disabled",
            ledcReadFreq(COIL_PWM_CHANNEL)
            );

        // Analog read VM and coil current
        uint16_t VC = analogRead(COIL_CURRENT);
        DPRINTF("Coil current = %d\n", VC);
        t_print = millis();
    }

    // Read button and toggle LED
    static bool prevBtnState = digitalRead(BTN_PIN);
    static bool prevExtTrig = false;
    static unsigned long t_btn = millis();
    bool btnState = digitalRead(BTN_PIN);

    if (digitalRead(EXT_TRIG_PIN))
    {
        enableCoil();
        prevExtTrig = true;
    }
    else if (prevExtTrig)
    {
        disableCoil();
        prevExtTrig = false;
    }
    else
    {
        if (!btnState && prevBtnState && millis() - t_btn > 100)
        {
            bool ledState = digitalRead(LED_STATUS);
            digitalWrite(LED_STATUS, !ledState); // toggle led
            DPRINTLN("LED toggled");
            if (ledState){
                enableCoil();
            } else {
                disableCoil();
            }
            t_btn = millis();
        }
        else
        {
            prevBtnState = btnState;
        }
    }
}
```

C.2. Definitions_V2.h

```
/**
 * @file definitions_V2.h
 * @author Bram den Ouden
 * @brief This firmware will test the basic functionality of
 * the transmitter designed for the OptoCoil project as part
 * of my MSc Thesis
 *
 * @version 0.1
 * @date 2022-02-01
 *
 * @copyright Copyright (c) 2022
 */

#ifndef DEFINITIONS_V2_H
#define DEFINITIONS_V2_H
#include <stdint.h>

#define DEBUG
// #define WIFI_ENABLED

// Coil definitions
#define COIL_IN_A 25
#define COIL_IN_B 26
#define COIL_PWM 27
#define COIL_PS 14
#define COIL_CURRENT 36

const unsigned int COIL_FREQ = 117000; // frequency of the coil driver
const uint8_t COIL_PWM_CHANNEL = 0;
const uint8_t COIL_PWM_RESOLUTION = 7;

#define LED_STATUS 4
#define BTN_PIN 0

#define EXT_TRIG_PIN 34

#endif
```